

Notes on the 1968
Summer Study Program
in
GEOPHYSICAL FLUID DYNAMICS
at

The WOODS HOLE OCEANOGRAPHIC INSTITUTION

Reference No. 68-72

Contents of the Volumes

- Volume I Course Lectures and Abstracts of Seminars
- Volume II Participants Reports

Staff Members and Lecturers

Arakawa, Akio	University of California at Los Angeles
Broecker, Wallace S.	Lamont Geological Observatory, Palisades, New York
Bryan, Kirk	ESSA, GFD Laboratory, Princeton, New Jersey
Charnock, Henry	The University, Southampton, England
Cox, Charles S.	Scripps Institution of Oceanography, California
Craig, Harmon	Scripps Institution of Oceanography, California
Fofonoff, Nicholas P.	Woods Hole Oceanographic Institution, Massachusetts
Fuglister, Frederick C.	Woods Hole Oceanographic Institution, Massachusetts
Hansen, Donald V.	ESSA, Atlantic Oceanographic Laboratories, Miami, Florida
Hendershott, Myrl C.	Scripps Institution of Oceanography, California
Holland, William C.	ESSA, GFD Laboratory, Washington, D.C.
Howard, Louis N.	Massachusetts Institute of Technology
Hunkins, Kenneth	Lamont Geological Observatory, Palisades, New York
Kraichnan, Robert H.	Peterborough, New Hampshire
Kroll, John	Yale University
Leetmaa, Ants	Massachusetts Institute of Technology
Longuet-Higgins, Michael S.	Oregon State University
Malkus, Willem V.R.	University of California at Los Angeles
Miller, Robert L.	University of Chicago
Morton, Bruce R.	Monash University, Melbourne, Australia
Ostlund, H. Göte	Institute of Marine Sciences, University of Miami, Florida
Park, Kilho	Oregon State University
Robinson, Allan	Harvard University
Rooth, Claes	Institute of Marine Sciences, University of Miami, Florida
Spiegel, Edward A.	Institute of Mathematical Sciences, New York University
Stern, Melvin	Graduate School of Oceanography, University of Rhode Island
Stommel, Henry	Woods Hole Oceanographic Institution and Massachusetts Institute of Technology
Turekian, Karl K.	Yale University
Turner, J. Stewart	Cambridge University, England
Veronis, George	Yale University
Warren, Bruce	Woods Hole Oceanographic Institution, Massachusetts
Webster, T. Ferris	Woods Hole Oceanographic Institution, Massachusetts
Welander, Pierre	The Johns Hopkins University, Baltimore, Maryland
Worthington, L. Valentine	Woods Hole Oceanographic Institution, Massachusetts
Wunsch, Carl I.	Massachusetts Institute of Technology
Yoshida, Kozo	Geophysical Institute, University of Tokyo, Japan

Fellows

Allen, John S., Jr.	Aeronautical Engineering	Princeton University
Foster, Michael R.	Astronautics	California Institute of Technology
Gregg, Michael C.	Oceanography	University of California(San Diego)
Hazel, Philip	Geophysical Fluid Dynamics	University of Cambridge, England
Kullenberg, Gunnar E.B.	Oceanography	University of Göteborg, Sweden
Kuo, Han-hsiung	Mechanics	Yale University
Luyten, James R.	Chemical Physics	Harvard University
Mooers, Christopher N.K.	Oceanography	Oregon State University

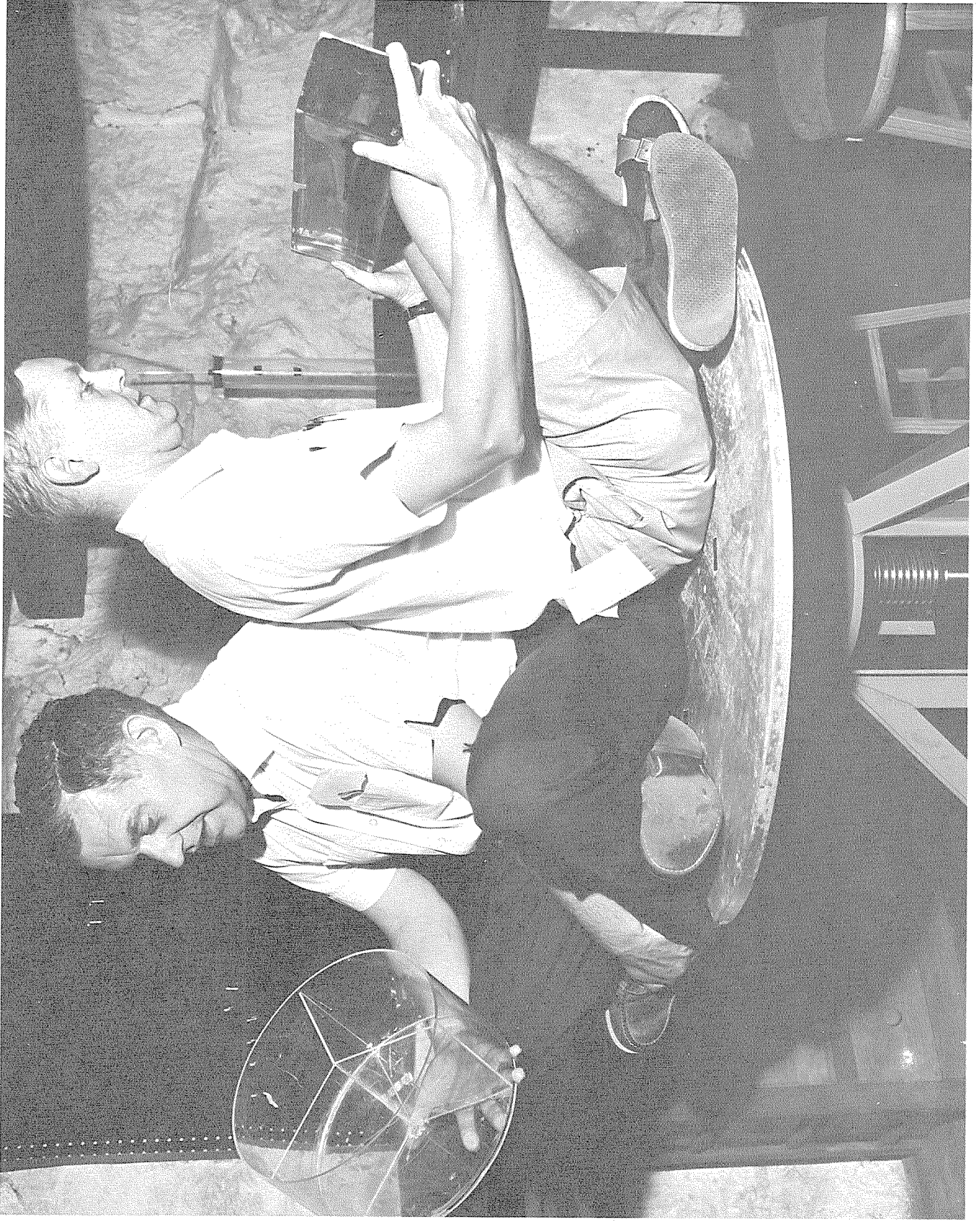
Editor's Preface

The general circulation of the oceans was the topic of concentration for the 1968 WHOI Summer Program in Geophysical Fluid Dynamics. Stommel summarized the broad range of ideas and approaches to the many problems which face the investigator of oceanographic phenomena. A series of seminars of observational studies was followed by Louis Howard's two-week course on theoretical concepts and techniques in rotating stratified fluids. An entertaining week of heated discussion on the use of chemical tracers in determining oceanic circulation emphasized the need for a much more extensive network of observations of chemical properties. The instructive function of theoretical numerical modeling of ocean circulation was clearly brought out in a series of seminars devoted to that topic. During the program various participants presented their ideas and researches on topics ranging from the micro-structure in the surface layers of the oceans to the large scale thermal circulation of the world's oceans.

The present volume contains a summary of the lectures and seminars. Some of the reports are detailed while others are brief descriptions of the talks. Perhaps the most useful purpose of the volume is the idea that it conveys of the many fascinating approaches to the understanding of our ocean environment.

We are all grateful to the National Science Foundation for its continued support and encouragement and to Paul M. Fye for making available to us the facilities of the Woods Hole Oceanographic Institution. Mary C. Thayer has again taken on the lion's share of the task of assembling and typing the reports for this and the accompanying volume. Her unique ability to keep the program functioning smoothly is a constant source of delight to all of the participants.

George Veronis



Our two principal Lecturers imported from M.I.T.

CONTENTS of VOLUME I

Course Lectures

Dr. Henry Stommel, lecturer

Woods Hole Oceanographic Institution and
Massachusetts Institute of Technology

Page No.

INTRODUCTION TO THE GENERAL OCEAN CIRCULATION

Lecture 1	General Considerations	1
I	Introduction	1
II	Vertically Integrated Transport Function	1
Surface charts	1	
Geopotential topography	7	
III	Longitudinally Integrated Transport Function and the Vertical Density Structure of the Sea Water	9
IV	The Latitudinally Integrated Transport Function	11
Lecture 2	Introduction to the Linear Viscous Theories of Sverdrup and Munk	12
I	The Vorticity Equation and Sverdrup's Interior Solution	12
II	Munk's Theory of the Wind-driven Ocean Circulation	15
Lecture 3	Inertial Theory of the Gulf Stream and a Laboratory Model for Oceanic Circulation	18
I	Hydrography of the Gulf Stream	18
II	A Model of the Gulf Stream with Uniform Potential Vorticity	19
III	Laboratory Model for Oceanic Circulation	22
IV	Abyssal Circulation of the World	26
Lecture 4	The Use of Tracers in Studying the Abyssal Circulation and the T-S Fine Structure in the Thermocline	27
I	The Use of Tracers in Determining the Deep Circulation	27
Bolin and Stommel Box Model	27	
Munk's Abyssal Recipes	29	
II	Temperature-Salinity Fine Structure in the Thermocline	30
Lecture 5	The Thermohaline Circulation and the Action of Variable Wind Stress on a Stratified Ocean	32
I	Blandford's Model of the Thermohaline Circulation	32
II	The Action of Variable Wind Stresses on a Stratified Ocean	35

Dr. Louis N. Howard, lecturer
Massachusetts Institute of Technology

ROTATING AND STRATIFIED FLUIDS

	Page No.
Lecture 1 Rotating Homogeneous Fluids	41
Introduction	41
Problems where	43
Fundamental Theorem of Weather Maps	44
Non-horizontal Boundaries	45
Time-dependent Flows	46
Lecture 2 Mean Circulation Theorem	47
Uniqueness of a Steady Solution	50
The Initial Value Problem	52
The Normal Modes	55
Lecture 3 The Effects of Viscosity	59
Lecture 4 Boundary Layer Solutions for a Rotating Cylinder	66
Lecture 5 Rotating Homogeneous Fluids with Free Surfaces	71
Lecture 6 Rotating and Continuously Stratified Fluids - Inviscid Flows	80
and 7 Ertel's Theorem	80
Flows with Strong Rotation and Stratification	82
The Initial-Boundary-Value Problem	85
Uniqueness of the Steady Solution	90
Oscillations in a Stratified Rotating Fluid	92
Lecture 8 Rotating and Stratified Fluids - Viscous Flows	98
Spin-up Problem	99
Lecture 9 Dissipative Effects on the Normal Modes of a Rotating Stratified Fluid	105
Time-dependent Modes in a Cylinder	107
Lecture 10 Initial Phase of the Spin-up Problem	110

Lectures

T. Ferris Webster, "Observation of Time Dependent Ocean Currents"	115
Nicholas P. Fofonoff, "Measurements of Internal Waves from Moored Buoys"	123
L. Valentine Worthington, "A Discussion of the Sources and Circulation of North Atlantic Deep Water"	133
Frederick C. Fuglister, "Gulf Stream Rings"	142

CONTENTS of VOLUME I (continued)

Page No.

ABSTRACTS

Summary of Discussions on Chemical Tracers in the Oceans - Wallace S. Broecker, Harmon Craig, H. Göte Ostlund, Kilho Park and Karl K. Turekian	153
Abyssal Radiocarbon - CO ₂ - Oxygen - Harmon Craig	156
Air-Sea Exchange of Water in Hurricanes - H. Göte Ostlund	160
A Non-linear Model of an Ocean Driven by Wind and Differential Heating - Kirk Bryan	161
Boundary Layers and Large Scale Numerical Models - Henry Charnock	162
Thermal Microstructure in the Sea - Charles S. Cox	164
Observational Evaluation of Topographic Effects on the Gulf Stream - Donald V. Hansen	166
The Numerical Solution of Vibration Problems - Myrl C. Hendershott	167
A Numerical Solution of Laplace's Tidal Equations - Myrl C. Hendershott	168
On the Distribution of Some Tracers in the Ocean - William C. Holland	169
Some Effects of Stratification on Rotating Fluids - Ants Leetmaa	170
Double Kelvin Waves - Michael S. Longuet-Higgins	171
On Wave Breaking and the Equilibrium Spectrum of Wind-generated Waves - Michael S. Longuet-Higgins	174
The Effect of Surface Tension on the Limit Form of Waves - Robert L. Miller	175
Modelling Thermals with Vortex Rings - Bruce R. Morton	179
Non-similar Turbulent Plumes - Bruce R. Morton	180
Finite Amplitude Internal Gravity Waves in a Continuously Stratified Fluid - Isidoro Orlanski and Kirk Bryan	182
Energetics of the General Circulation - Melvin E. Stern	184

CONTENTS of VOLUME I (continued)

	Page No.
A Stable Salinity Gradient Heated from Below - J. Stewart Turner	185
Effects of Bottom Topography on Large-scale Oceanic Flow - Pierre Welander	186
Sea Level Fluctuations Across the Straits of Florida - Carl I. Wunsch and Donald V. Hansen	189
Subtropical Countercurrent - Kozo Yoshida	190
On Theoretical Models of the Thermohaline Circulation - George Veronis	192

INTRODUCTION TO THE GENERAL OCEAN CIRCULATION

Henry Stommel

Lecture 1. General Considerations

June 26, 1968

1. Introduction:

A selected list of references is given in Appendix 1.

The topics which will be discussed are:

- (1) general ocean circulation, and
- (2) special related subjects such as Gulf Stream, equatorial currents, thermohaline circulation, etc.

General partial description of oceans will be found in books such as "The Oceans" by Sverdrup, Johnson and Fleming. We are going to study the dynamical theories governing these phenomena.

One way of describing the general circulation can be obtained by considering the transport function obtained by integrating over the three different coordinates. Each will reveal some feature of the general circulation. The result is summarized in the following diagram. (Fig. 1)

II. Vertically Integrated Transport Function

1. Surface Charts (Chart 1.)

The most basic information on the circulation comes from records of surface currents compiled by hydrographic offices from thousands of individual observations of ship drift. The charts compiled from these observations give the general picture of the mean surface circulation and comprise the main evidence for features such as the Equatorial Counter-currents. Some of the principal features shown by these charts are:

Latitude

Longitude

Vertical

Direction of integration

Geostrophic calculations off Cape Horn, Cape of Good Hope, Australia

Vertical density structure charts
North-South cross section of density structure charts, etc.

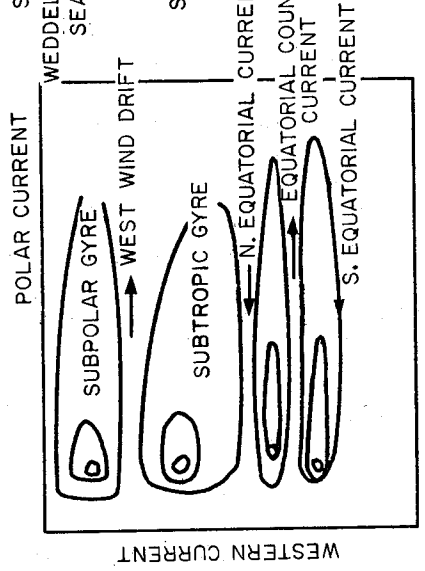
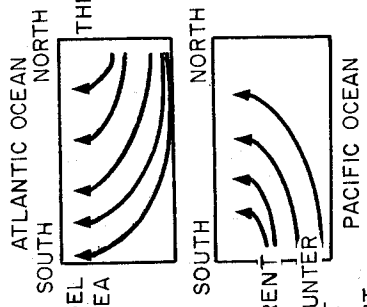
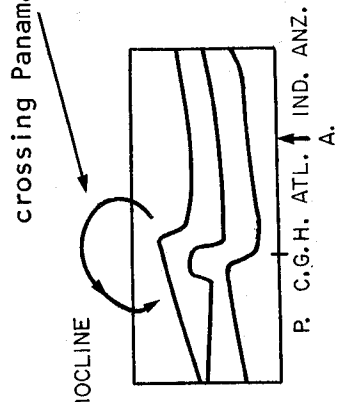
Surface current charts (Geopotential topography)

Observational materials

(Abyssal circulation)

(Wind driven ocean circulation)

Moist trade winds crossing Panama



Revealed feature

Note each stream line represents $30 \times 10^6 \text{ m}^3/\text{sec}$.

Figure 1.

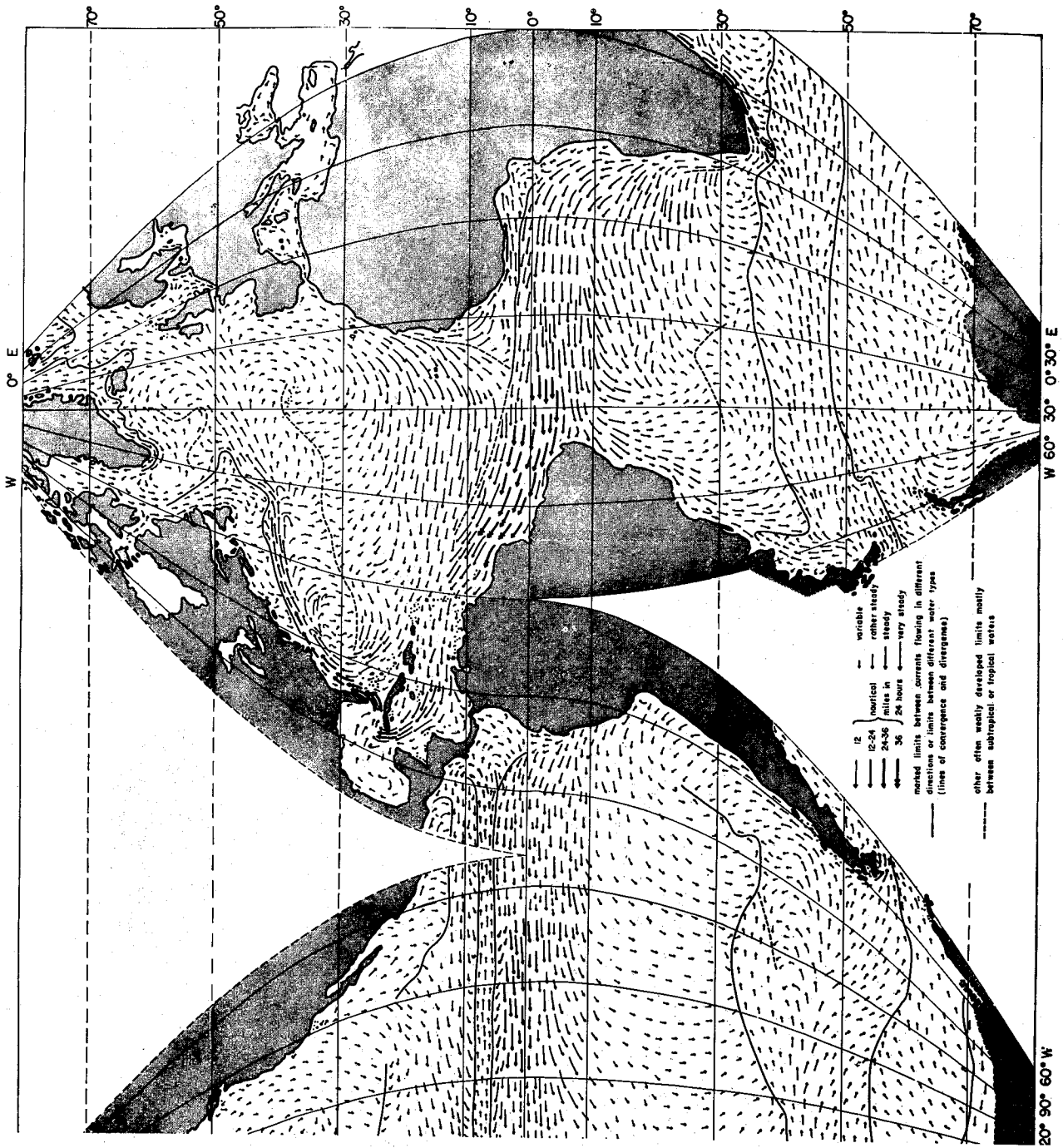


Chart 1a. Surface currents. Northern hemisphere winter.

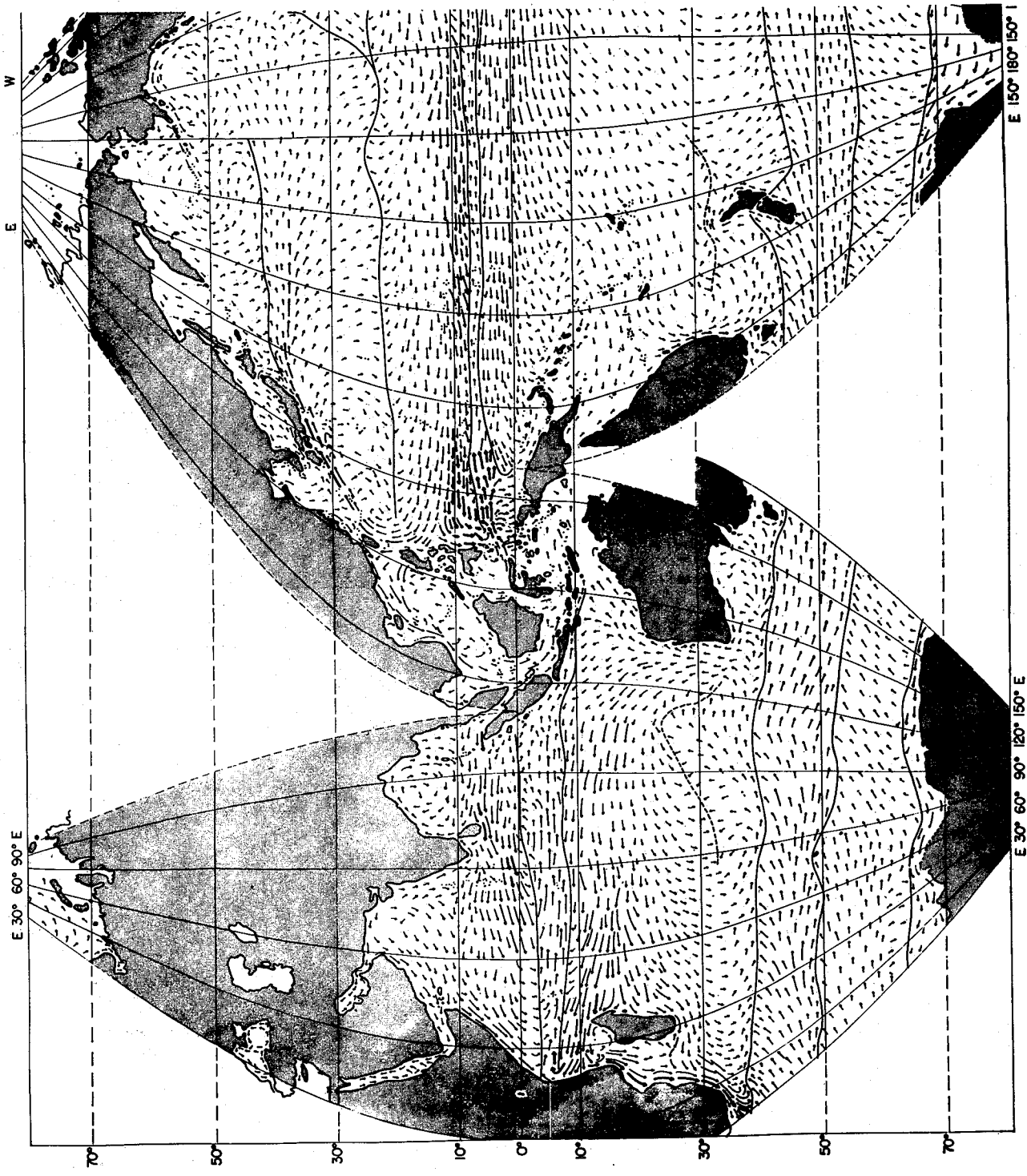


Chart 1b. Surface currents. Northern hemisphere winter.

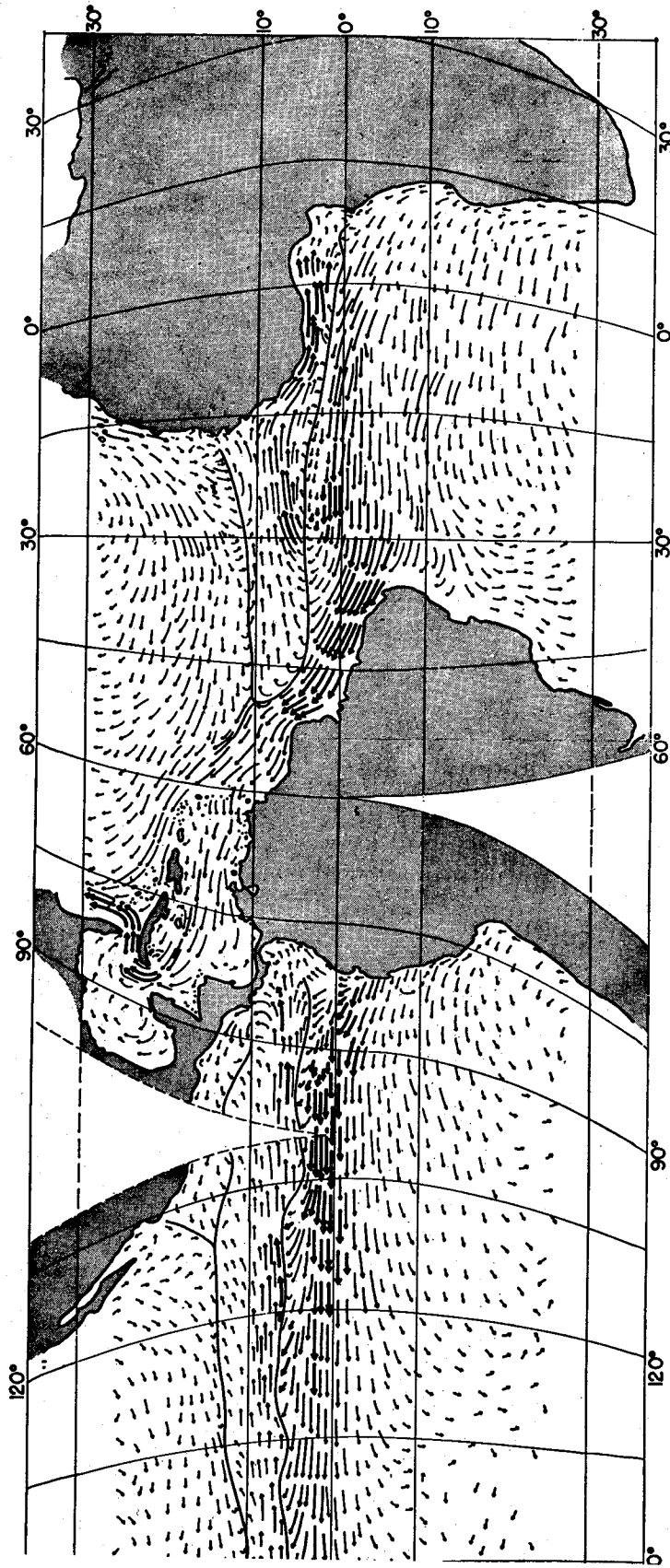


Chart 1c. Surface currents. Northern hemisphere summer.

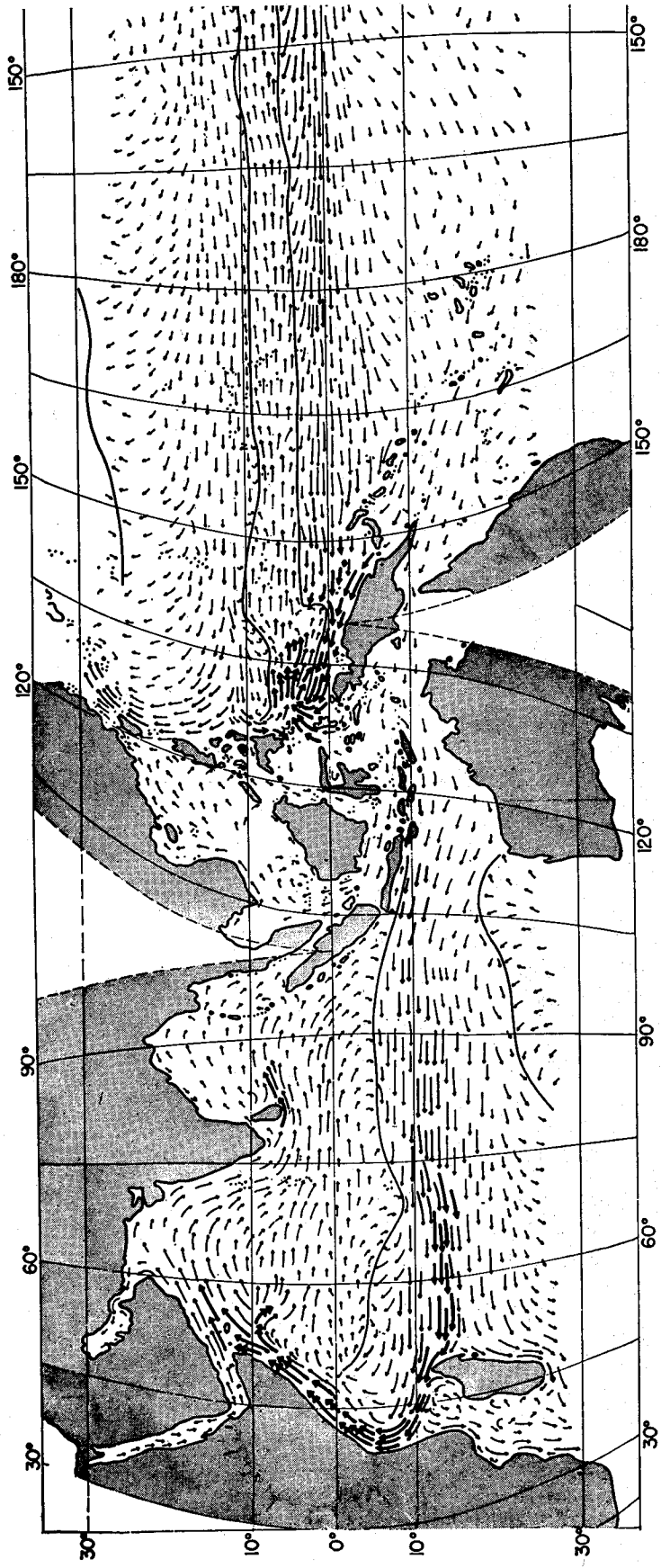


Chart 1d. Surface currents. Northern hemisphere summer.



a. In mid-latitudes of the oceans there are intense, narrow, poleward currents on the western boundaries and slow, broad, equatorward drifts over the eastern parts of the oceans. These large features have been called subtropical gyres by Munk. The intense western boundary current occurs in the North Atlantic as the Gulf Stream and in the North Pacific as the Kuroshio Current. The situation in the Indian Ocean is complicated by the monsoon winds.

b. In northern latitudes there seem to be cyclonic gyres of smaller scale called subpolar gyres.

c. There is an eastward-flowing current usually lying a few degrees north of the equator in the Pacific called the Equatorial Counter-current.

This circulation seems to be driven by the mean winds over the oceans. However, the winds do not show the narrow asymmetry found in the surface currents. This paradox will be discussed in the next lecture.

Ekman did the first important study of the effect of wind on the ocean. He found that the effect of a steady uniform wind was confined to a shallow surface layer. The actual non-uniformity of the wind results in convergences and divergences in the Ekman layer. The resulting vertical motions act as an important input for the geostrophic current below.

2. Geopotential Topography (Chart 2.)

The vertical balance of forces in the ocean is basically hydrostatic. Consequently surfaces of equal pressure are farther apart where the density is low than where it is large. Complicating this are spatial variations in the earth's gravity field which requires the use of geopotential rather than distance. The customary oceanographic units of

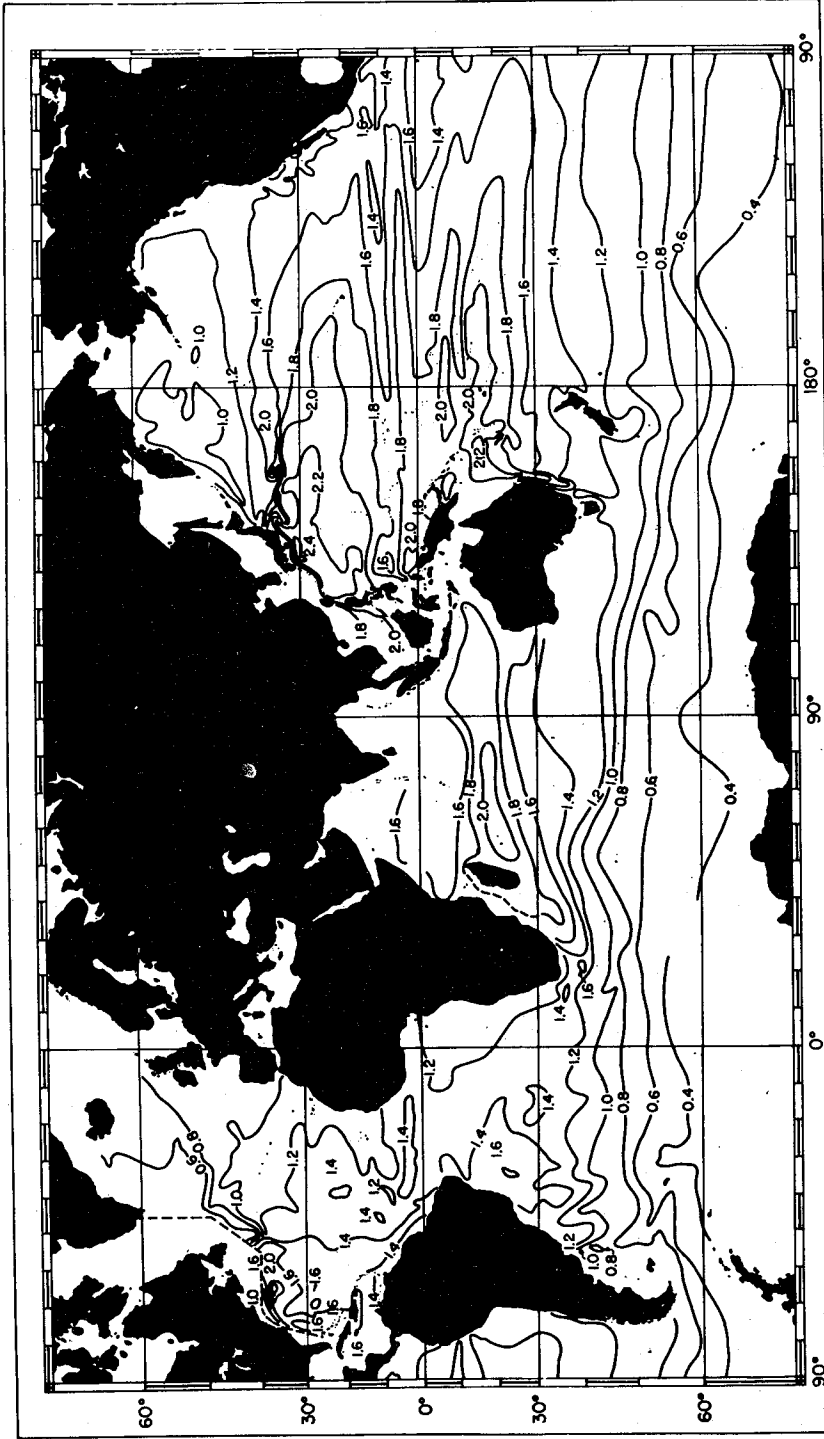


Chart 2. Contours of topography of dynamic height (in meters) of sea-surface relative to 1000 meters.

geopotential distance, and pressure correspond closely in numerical values. Thus a separation of one meter in distance corresponds to one dynamic meter in geopotential and one decibar in pressure.

The data from standard hydrographic stations gives the density field in the ocean. This data provides the basis for computing the vertical gradient of horizontal velocity between two stations. By assuming that the deep pressure surfaces are nearly horizontal, with zero geostrophic velocities, it is possible to determine geostrophic velocity as a function of depth by numerical integration. The 1000-decibar surface will be used as the level of no motion in these lectures.

It is instructive to look at the topography of the sea surface relative to the 1000-decibar surface. The total range of variation is about two meters. The main features of the dynamic topography do not seem to be subject to significant seasonal variations. The seasonal distribution of data is barely good enough to show seasonal variation. Sea-level data for mid-ocean stations such as Bermuda, show an apparent rise and fall of the free surface with seasonal density changes once high frequency tides and atmospheric pressure fluctuations have been filtered out. This means that the light surface waters simply expand and contract with seasonal changes resulting in negligible pressure changes at the 1000-decibar surface, the range is less than 20 cm, the contour interval of Chart 2.

III. Longitudinally Integrated Transport Function and the Vertical Density Structure of the Sea Water

(A) The vertical structure of the specific volume of the sea water may be indicated in the following diagrams. (Chart 3.)

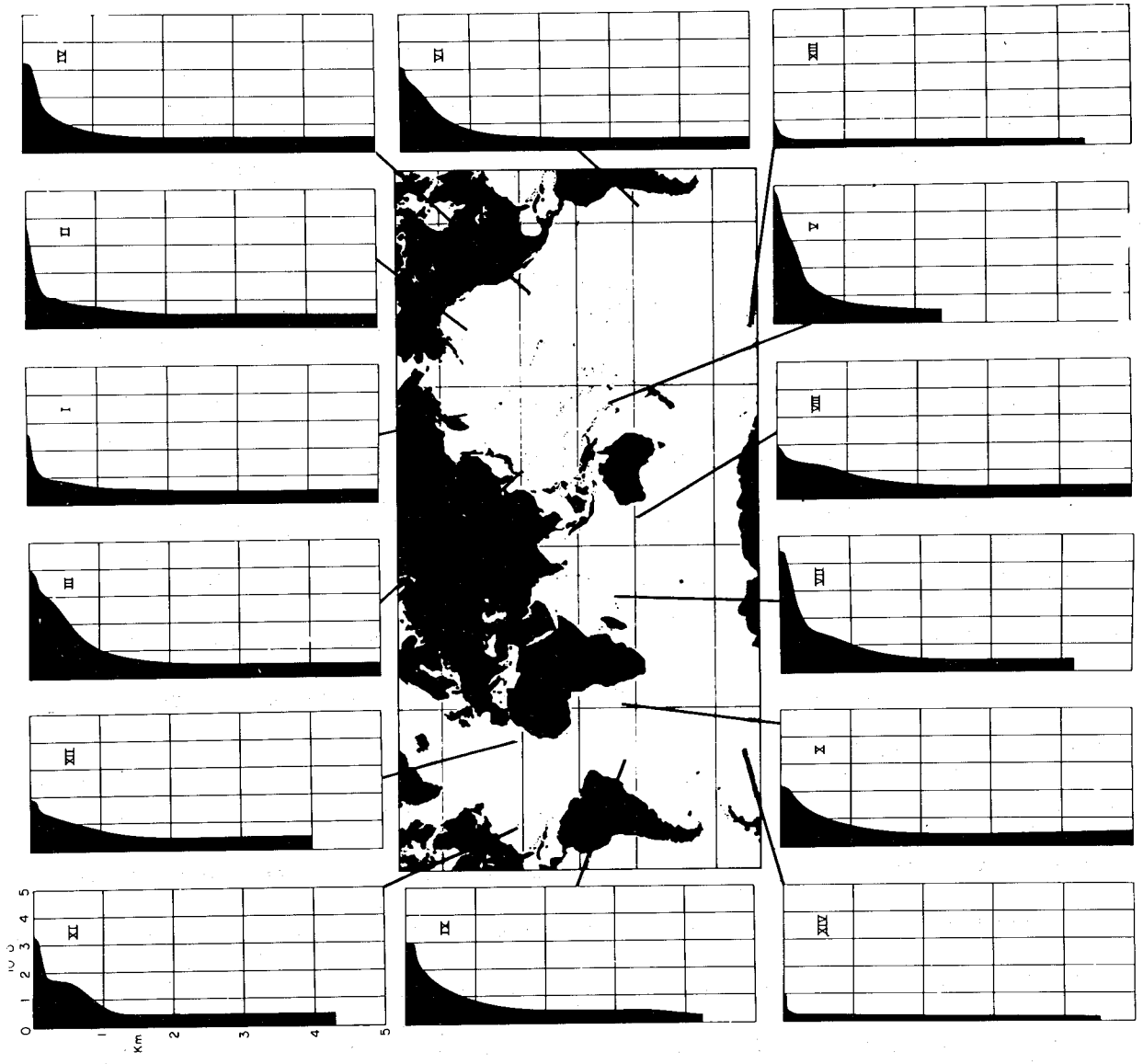


Chart 3. Vertical distribution of specific volume anomaly $10^{-5} \text{ cm}^3/\text{gm}$ at selected stations.

(B) Meridional sections of water properties reveal some features of the abyssal circulations.

1. There must be slow (1 cm/day) general upward flow of cold deep water to balance the loss of heat by diffusion from the warm light water above the main thermocline.

2. There is an indication of a slow poleward drift of deep water over much of the ocean basins with an intense deep western boundary current to provide the return flow.

3. There are two source regions for deep water: the North Atlantic in the vicinity of Greenland, and the Weddell Sea. The source regions are much smaller than the wider-spread upward regions underlying the whole thermocline.

4. From salinity profiles there is an indication of a net flow of North Atlantic deep water into the Pacific via the Antarctic Circumpolar Current.

IV. The Latitudinally Integrated Transport Function

The general feature is summarized in the diagram indicated in the introduction to this lecture. An interesting thing to notice is that there seems to exist a fresh-water transport of about $1 \times 10^6 \text{ m}^3/\text{sec}$ over Panama from Atlantic Ocean to Pacific Ocean by the moist trade winds, and this is related to a bimodal distribution of volume vs. salinity for the whole ocean water mass.

Notes submitted by
Michael C. Gregg and
Han-Hsiung Kuo

INTRODUCTION TO THE LINEAR VISCOUS THEORIES OF SVERDRUP AND MUNK

Henry Stommel

Lecture #2

June 24, 1968

1. The Vorticity Equation and Sverdrup's Interior Solution

Consider the steady linearized equations of motion in the form

$$\begin{aligned} -f\rho v &= -\frac{\partial p}{\partial x} + \frac{\partial \tau_x}{\partial z} \\ f\rho u &= -\frac{\partial p}{\partial y} + \frac{\partial \tau_y}{\partial z} \end{aligned} \quad \begin{array}{c} z \\ \nearrow Y \\ \text{north} \\ \searrow \\ X \\ \text{east} \end{array} \quad (1)$$

where $f = f_\sigma + \beta y$. . . the coriolis parameter
 τ_x, τ_y . . . vertical wind-stress component
 p . . . pressure
 ρ . . . density.

Assume at $z = -h$ the horizontal pressure gradients and motion vanish, and $z = z_0$ is the sea surface ($z = 0$, is the mean sea surface). Besides, one assumes that the depth of h is far less than the depth of the ocean. Thus bottom friction is negligible.

The vertically integrated mass transports per unit width are defined as follows:

$$M_x = \int_{-h}^{z_0} \rho u dz, \quad M_y = \int_{-h}^{z_0} \rho v dz \quad (2)$$

and a function P is defined as:

$$P = \int_{-h}^{z_0} p dz \quad (3)$$

Thus the equations (1) in integrated form are

$$\begin{aligned} -\int M_y &= -\frac{\partial P}{\partial x} + \tau_x / z = z_0 \\ \int M_x &= -\frac{\partial P}{\partial y} + \tau_y / z = z_0 \end{aligned} \quad (4)$$

In the above equations differentiation and integration have been interchanged in the pressure term. No additional terms are added because z_0 is chosen at zero horizontal pressure gradients and terms introduced by the variation in surface elevation are negligible.

The integrated form of the continuity equation is

$$\frac{\partial M_x}{\partial x} + \frac{\partial M_y}{\partial y} = 0 \quad (5)$$

Cross-differentiation of equations (4) with equation (5) yields the vorticity equation first developed by Sverdrup

$$\beta M_y = \text{curl } \vec{\tau} \Big|_{z=z_0} \quad (6)$$

If M_x is taken as zero at one meridional coast, M_x can be obtained using equation (5). However, the solution cannot satisfy a boundary condition at the other coast. The dynamics of this model are not of high enough order to permit a solution of the closed ocean basin problem.

In order to seek a more physical meaning of equation (6) let us break each transport component into two parts: one set to represent the Ekman wind-drift transport components M_{xe} , M_{ye} , largely confined to the upper hundred meters, and the other the geostrophic transport components M_{xg} , M_{yg} , extending deeper into the main thermocline:

$$M_x = M_{xe} + M_{xg}, \quad M_y = M_{ye} + M_{yg} \quad (7)$$

and
$$-f M_{ye} = \tau_x \Big|_{z-z_0} \qquad f M_{xe} = \tau_y \Big|_{z-z_0} \qquad (8)$$

$$-f M_{yg} = - \frac{\partial p}{\partial x} \qquad f M_{xg} = - \frac{\partial p}{\partial y} \qquad (9)$$

The horizontal divergence of the Ekman wind drift, $\text{div}_H \vec{M}_e$ is obtained from (8)

$$\text{div}_H \vec{M}_e = - \frac{-\beta M_{ye} + \text{curl } \vec{\tau}}{f} \qquad (10)$$

Because of the variation of the Coriolis parameter with latitude, all northward or southward geostrophic motions exhibit a horizontal divergence, $\text{div}_H \vec{M}_g$, which can be obtained from (9)

$$\text{div}_H \vec{M}_g = - \frac{\beta M_{yg}}{f} \qquad (11)$$

In steady state, the total horizontal divergence $\text{div}_H \vec{M}_g$ must vanish. Thus the sum of equations (10) and (11) leads to equation (6). Then it is clear that the equation (6) indicates that the divergence of the Ekman wind drift, produced by wind, is compensated for by the divergence of the geostrophic flow. Thus the picture presented is a coupled flow comprised of the Ekman layer responding to the wind and the underlying geostrophic layer which adjusts itself to the upward or downward flow from the Ekman layer.

A serious difficulty in relating the above approach to the real ocean is determining the actual mean wind stress over the ocean. Using the mean wind stresses over the central North Atlantic as obtained from pilot charts, M_y can be computed using equation (6). Assuming a zero velocity at great depth and using density data geostrophically along 32°N to compute $v_g(z)$,

we get figure (1)

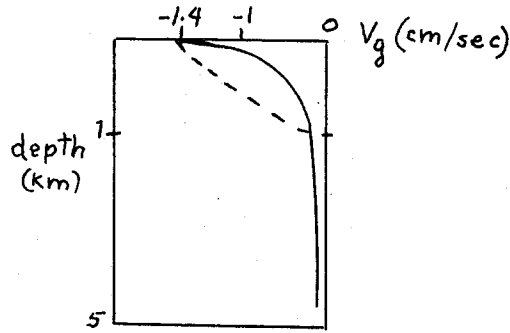


(Figure 1)

Thus, M_y is given by the area of the triangle in the upper right-hand corner of the figure.

$$\begin{aligned} M_y &= -1/2 \times 10^3 \text{ m} \times 1.4 \times 10^{-2} \text{ m/sec} \\ &= -7 \text{ m}^2/\text{sec} \end{aligned}$$

Taking the width of the North Atlantic as 5000 km ($5 \times 10^6 \text{ m}$) we get a net interior transport to the south of $35 \times 10^6 \text{ m}^3/\text{sec}$.

Measurements of deep currents in the vicinity of Bermuda by Swallow and Crease showed much larger velocities than indicated above. They found what appears to be large (50 miles) scale eddy motion with large amplitude (10 cm/sec) and low frequency (1 cycle/2 months). This raises a question about the lateral processes which has been neglected in the Sverdrup model and points out that it is not possible to infer that geostrophic velocities necessarily vanish at great depths.

II. Munk's Theory of the Wind-driven Ocean Circulation

By introducing a higher order term in the form of a horizontal shear stress Munk was able to obtain solutions for the closed oceanic circulation.

Thus equations (1) become:

$$\begin{aligned} -f\rho v &= -\frac{\partial p}{\partial x} + \frac{\partial \tau_x}{\partial z} + K_H \left(\frac{\partial^2}{\partial x^2} + \frac{\partial^2}{\partial y^2} \right) u \\ f\rho u &= -\frac{\partial p}{\partial y} + \frac{\partial \tau_y}{\partial z} + K_H \left(\frac{\partial^2}{\partial x^2} + \frac{\partial^2}{\partial y^2} \right) v \end{aligned} \tag{12}$$

where K_H is the horizontal eddy viscosity.

Let us assume that:

$$A \left(\frac{\partial^2}{\partial x^2} + \frac{\partial^2}{\partial y^2} \right) M_x = \int_{-h}^{z_0} K_H \left(\frac{\partial^2}{\partial x^2} + \frac{\partial^2}{\partial y^2} \right) U dz \quad (13)$$

$$A \left(\frac{\partial^2}{\partial x^2} + \frac{\partial^2}{\partial y^2} \right) M_y = \int_{-h}^{z_0} K_H \left(\frac{\partial^2}{\partial x^2} + \frac{\partial^2}{\partial y^2} \right) V dz$$

where $A \approx K_H$. Introducing a transport function ψ , defined by the following equation

$$M_x = - \frac{\partial \psi}{\partial y}, \quad M_y = \frac{\partial \psi}{\partial x} \quad (14)$$

Thus from equations (12), (13) and (14), we obtain

$$\left[A \left(\frac{\partial^2 \psi}{\partial x^2} + 2 \frac{\partial^2 \psi}{\partial x^2 \partial y^2} + \frac{\partial^2 \psi}{\partial y^2} \right) - \beta \frac{\partial}{\partial x} \right] \psi = \frac{\partial \tau_x}{\partial y} - \frac{\partial \tau_y}{\partial x} \quad (15)$$

Eqn. for singular boundary region

Eqn. for interior region

The boundary conditions for ψ are that both ψ and its derivative normal to the boundary shall vanish.

If the boundaries are taken as forming a simple rectangle $x = 0, r$, and $y = \pm S$, and only an east-west wind system is assumed, $\tau_y = 0$, then an approximate solution is of the form

$$\psi = r X \beta^{-1} \frac{\partial \tau_x}{\partial y}$$

where

$$X = -\beta e^{-(\frac{1}{2})Kx} \cos\left(\frac{\sqrt{3}}{2}Kx + \frac{\sqrt{3}}{2Kr} - \frac{\pi}{6}\right) + 1 - \frac{1}{Kr} \left(Kx - e^{-K(n-x)} - 1 \right)$$

and

$$\beta = \left(\frac{2}{\sqrt{3}} \right) - (\sqrt{3}/Kr), \quad K = 3\sqrt{\beta/A}$$

A rough plot of $X(x)$ is given by Figure (2).

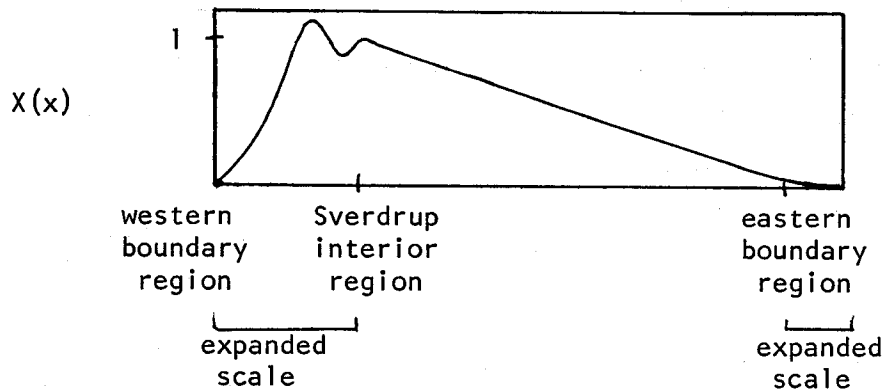


Figure (2)

Using the mean annual zonal winds only, the solution shows that the integrated oceanic wind-driven circulation is divided into closed circulatory systems or "gyres". The gyres are bounded at latitudes where $\text{curl } \vec{\tau} = 0$ and are centered at latitudes where $\text{curl } \vec{\tau}$ is an extremum.

The Munk solution of the theoretical vertically integrated transport is about the limit to which one can go in the physical geography of currents using linear vertically integrated models.

Notes submitted by

Han-Hsiung Kuo and

Michael C. Gregg

INERTIAL THEORY OF THE GULF STREAM
AND A LABORATORY MODEL FOR OCEANIC CIRCULATION

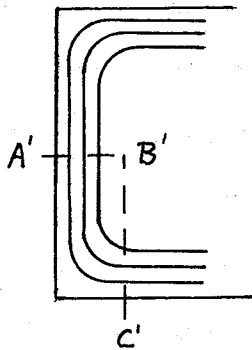
Henry Stommel

Lecture #3

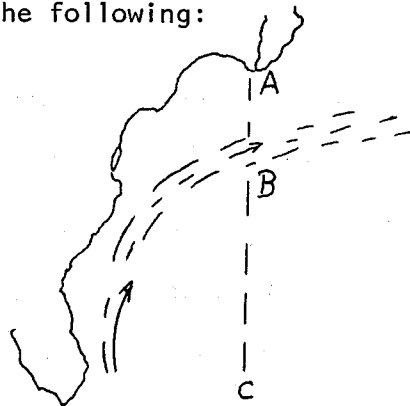
June 26, 1968

1. Hydrography of the Gulf Stream

In comparing temperature and salinity profiles across the Gulf Stream with theoretical ideas, we distinguish the following:



schematic location of section in theoretical gyre



actual geographical location of corresponding section in Atlantic Ocean

a. The observed section AB corresponds to the western boundary region A'B' of Munk's or Stommel's model. The observed section BC corresponds to the Sverdrup interior region.

b. From A to B the isotherms have a large downward slope toward south under the Gulf Stream. From B to C, the region where the Gulf Stream is being fed, the isotherms seem to slope linearly upward with decreasing latitude.

c. The major hydrographic difference in section ABC is the change in thickness of the water lying between the 16°C and 20°C isotherms - called 18° water. There is a very marked decrease in thickness of the layer going from mid-ocean to the Gulf Stream. It seems dynamically significant that this vertical shrinking is just about the amount required for the potential vorticity of the layer to be conserved across the Stream.

d. The "18° water" seems quite homogeneous in temperature and salinity throughout the western North Atlantic. It is not yet known where this water comes from and what maintains it. One would expect theoretically that it is being fed by the Ekman layer over the whole year. However, this should result in greater temporal and spatial variations under the Ekman layer than seem to be observed. At first glance the homogeneity of the water suggests formation in a small region during winter months only and this seems inconsistent with the Ekman idea.

II. A Model of the Gulf Stream with Uniform Potential Vorticity

Now let us consider a two-layer model as indicated below. Layer 2 is at rest.

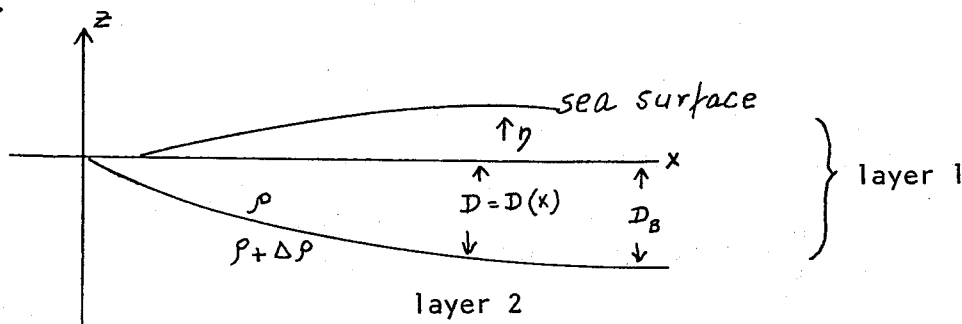


Figure 1.

The conservation of potential vorticity is:

$$\frac{d}{dt} \left(\frac{f+J}{D} \right) = 0 \quad (1)$$

where $f = \beta y$ and ρ is relative vorticity, $J = \frac{\partial v}{\partial x} - \frac{\partial u}{\partial y}$.

u, v are velocities in layer 1.

In the middle of the ocean $J \ll f$. From the observed variation of thermocline depth with latitude it seems that in the interior $\frac{f}{D}$ is the same for all transport lines. Therefore, the potential vorticity along streamlines in the interior is f_B/D_B . In the Gulf Stream region J is comparable to f , and u is negligible. Hence, the potential vorticity in the western boundary is $\frac{f + \frac{\partial v}{\partial x}}{D}$. From equation (1) we have,

$$\frac{f + \frac{\partial v}{\partial x}}{D} = \frac{f}{D_B} \quad (2)$$

Flow in the Gulf Stream may be taken as geostrophic

$$-fv = -\frac{1}{\rho} \frac{\partial p}{\partial x} \quad (3)$$

Noting that the pressure in the 2nd layer is

$$p_2(z) = g \int_z^\eta \rho dz = g \int_{-D}^\eta \rho dz + g \int_z^{-D} (\rho + \Delta\rho) dz \quad (4)$$

and the layer is at rest, we have

$$0 = g\rho \frac{\partial \eta}{\partial x} + g\rho \frac{\partial D}{\partial x} - g(\rho + \Delta\rho) \frac{\partial D}{\partial x} \quad (5)$$

$$\frac{\partial \eta}{\partial x} = \frac{\Delta\rho}{\rho} \frac{\partial D}{\partial x}$$

Since $\frac{\partial p}{\partial x} = -g\rho \frac{\partial \eta}{\partial x}$, equation (3) may now be written as

$$fv = g' \frac{\partial D}{\partial x} \quad (6)$$

where $g' = g \frac{\Delta \rho}{\rho}$

From equations (6) and (2), we have, by eliminating V

$$\frac{\partial^2 D}{\partial x^2} = \frac{1}{\lambda_B^2} (D - D_B) \quad (7)$$

where

$$\lambda_B = \frac{\sqrt{g' D_B}}{f}$$

The solution of equation (7) under the boundary conditions $D=0$ at $X=0$ and $D=D_B$ for large X , completely determines the cross-stream profile of depth and velocity.

$$\begin{aligned} D &= D_B (1 - e^{-x/\lambda_B}) \\ V &= V \sqrt{g' D_B} e^{-x/\lambda_B} \end{aligned} \quad (8)$$

if we introduce the numerical values as

$$\begin{aligned} D_B &= 8 \times 10^4 \text{ cm}, \quad \frac{\Delta \rho}{\rho} \sim 2 \times 10^{-3} \\ g &\sim 10^3 \text{ cm sec}^{-2} \quad f \sim 10^{-4} \text{ sec}^{-1} \end{aligned}$$

it is obtained,

$$\lambda = 40 \text{ km} = \frac{1}{e} \quad \text{width of the Gulf Stream}$$

$$V_{\max} = 4 \text{ m/sec}$$

The value of 40 km for the width of the Stream seems reasonable compared to Fuglister's Gulf Stream '60 data. Charney's (1956) paper treats the formation of an inertial Gulf Stream where a more general, non-uniform, law of potential vorticity with latitude holds in the interior.

III. Laboratory Model for Oceanic Circulation

We are going to study a laboratory model to simulate some aspects of oceanic circulation such as the intense western boundary current. Consider a rotating sector with dimensions indicated as below. In this experiment the change in height of a column with radial movement is used to simulate the variation of the Coriolis parameter with latitude on the earth.

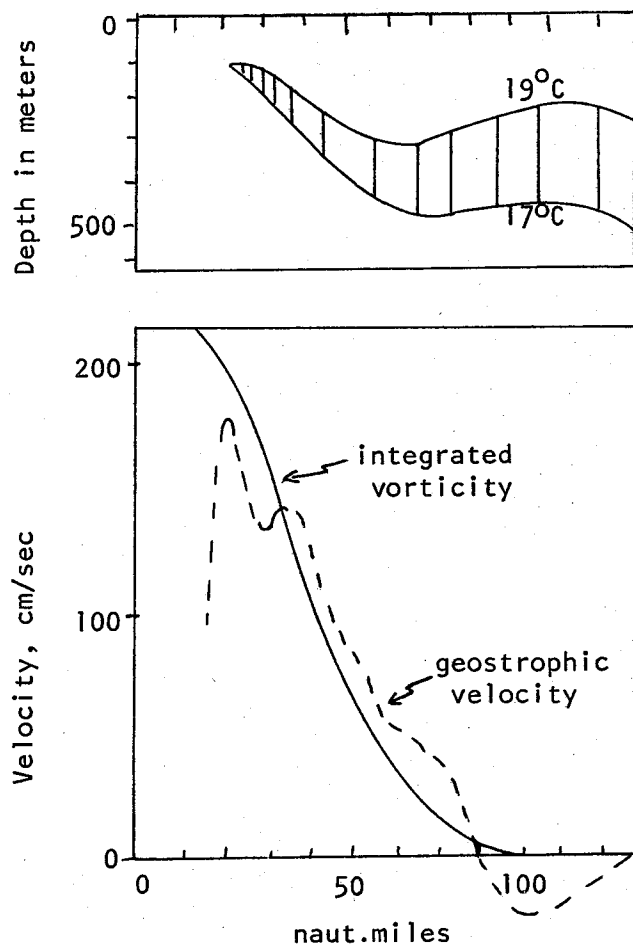


Figure 2.

The lower figure is a potential vorticity analysis of the upper figure. The solid line shows velocity computed by vorticity formula obtained by integrating equation (2) with respect to x from x to ∞ . The dotted line shows geostrophic velocity computed from the section.

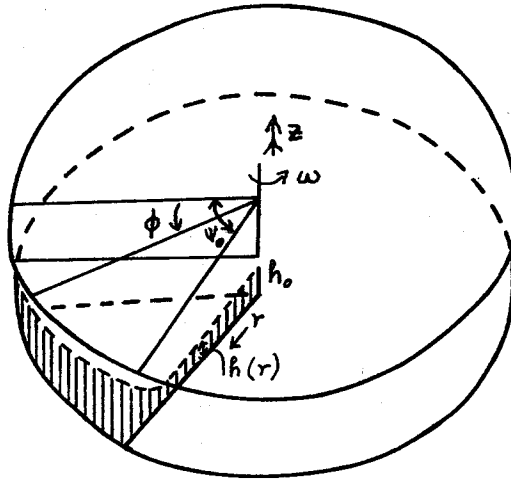


Figure 3

We will put point sources in various locations and consider the rising of the free surface as a uniformly distributed sink.

The unperturbed paraboloidal surface h associated with the radial pressure gradient balances the centripetal acceleration term. We take the level h in the basic state of relative rest as

$$h = h_0 \left(1 + l \frac{r^2}{a^2} \right) \quad (1)$$

where
$$l = \frac{\omega^2 a^2}{2g h_0} .$$

Assuming hydrostatic equilibrium in the vertical and denoting by ζ the vertical displacement from the paraboloid surface, associated with steady geostrophic flow, the equations of motion governing interior flow read

$$2a V_\phi = g \frac{\partial \zeta}{\partial r} \quad (2)$$

$$-\partial \omega V_r = \frac{g}{r} \frac{\partial \zeta}{\partial \phi} \quad (3)$$

Neglecting ζ relative to h , equation of continuity is

$$\frac{\partial}{\partial r} (h r v_r) + \frac{\partial}{\partial \phi} (h v_\phi) = -r \dot{\zeta} \quad (4)$$

$$\text{where } \dot{\zeta} = \frac{\partial \zeta}{\partial t}$$

From equations (1), (2), (3), and (4), we can solve for

$$V_r = - \frac{\dot{\zeta} a^2}{2 h_0 l r} \quad (5)$$

Thus the interior geostrophic flow which arises when a source adds water to the basin, producing a positive $\dot{\zeta}$, is directed radially inward and has no ϕ component.

If sources S (rate of addition of volume) are assumed to produce a uniform vertical rising surface throughout the basin, geometry requirements give the relation

$$\dot{\zeta} = + \frac{2S}{\phi_0 a^2} \quad (6)$$

and equation (5) becomes

$$V_r = \frac{S}{\phi_0 h_0 l r} \quad (7)$$

Consider the water budget of the shaded sector defined by $r = r$ in the figure below.

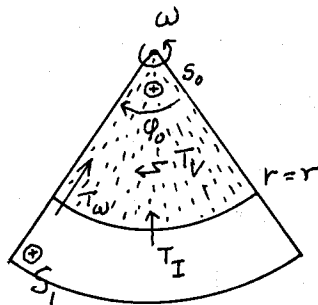


Figure 4

T_I represents the transport into the sector by the interior geostrophic flow; T_V represents the vertical transport associated with \dot{j} ; S_o denotes the source transport. We postulate the existence of T_w as one of the elements of the regime, and we solve for it on the basis of the mass conservation requirement

$$T_w + T_I + S_o + T_V = 0 \quad (8)$$

From equations (6), (7), and the geometry of the system:

$$T_I = -hr\phi_o V_r = \frac{S}{\ell} \left(1 + \frac{\ell r^2}{a^2}\right) \quad (9)$$

$$T_V = -\frac{\phi_o r^2}{2} \dot{j} = -S \frac{r^2}{a^2} \quad (10)$$

Solving for T_w :

$$T_w = -\frac{S}{\ell} \left(1 + \frac{\ell r^2}{a^2}\right) - S_o + \frac{S r^2}{a^2} = -S_o - \frac{S}{\ell} \quad (11)$$

where, for the general case depicted in above figure

$$S = S_o + S_1 \quad (12)$$

If S_o is positive and $S_1 = 0$, we have

$$T_w = -S_o \left(1 + \frac{1}{\ell}\right) \quad (13)$$

where ℓ is the parameter characterizing the slope of the equilibrium surface. Note that the transport is larger than the source input.

If $S_o = 0$ and S_1 is positive we have

$$T_w = -\frac{S_1}{\ell} \quad (14)$$

The actual experiments we are going to perform do show the internal western boundary current and show interior flow.

(The actual demonstration did not give as narrow western boundary currents as it usually does. No explanation is offered.)

IV. Abyssal Circulation of the World.

A model of the abyssal circulation can be constructed by using the following:

- 1) An areal upwelling flow of 1 cm/day everywhere just beneath the main thermocline
- 2) Point source regions in the North Atlantic and Weddell Sea
- 3) Geostrophic flow in the interior
- 4) Western boundary currents

The resulting flow patterns are shown in Figure 5.

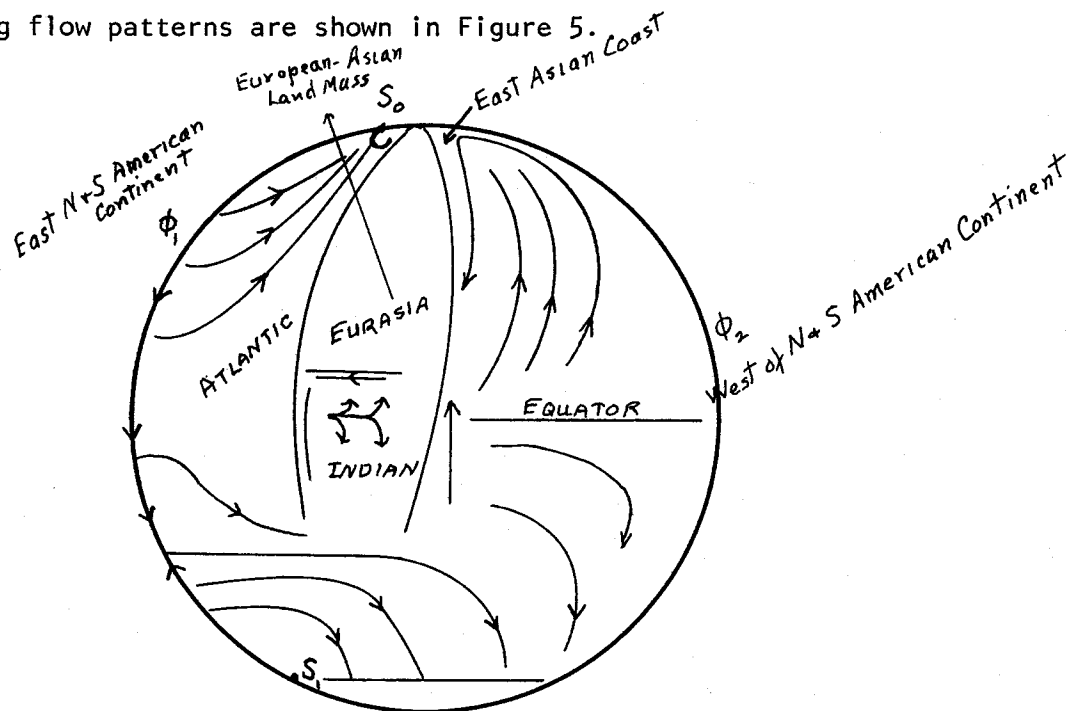


Figure 5.

Reference: Stommel, H., A. Arons, and A. Faller, 1958. Tellus X: 179-184. "Stationary Planetary Flow Patterns".

Notes submitted by
Michael C. Gregg and
Han-Hsiung Kuo

THE USE OF TRACERS IN STUDYING THE ABYSSAL CIRCULATION
AND THE T-S FINE STRUCTURE IN THE THERMOCLINE

Henry Stommel

Lecture #4

June 27, 1968

I. The Use of Tracers in Determining the Deep Circulation

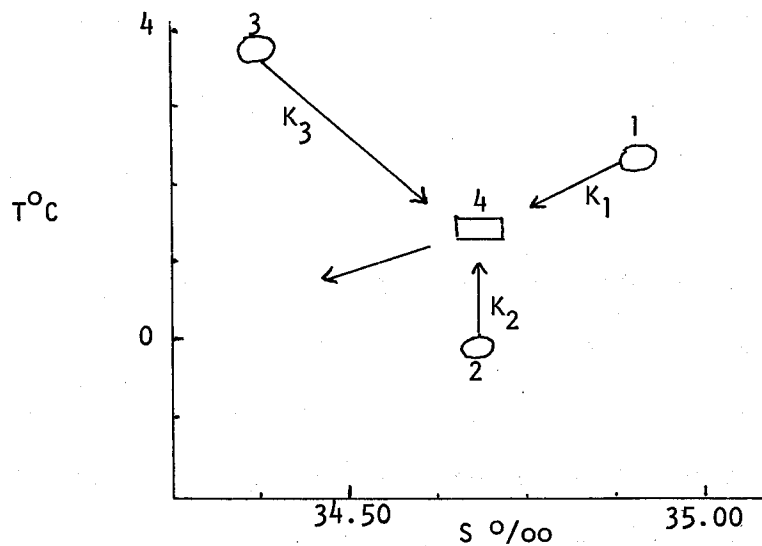
A. Bolin and Stommel Box Model

The observed distributions of tracers in the ocean can be used to deduce the deep circulation. In Longitudinal Profiles 1 and 2 the distribution of temperature, salinity, and dissolved oxygen are portrayed. They exhibit tongues presumably associated with direction of flow. Insufficient geochemical measurements are available for this purpose, however. A box model of the deep circulation was constructed by Bolin and Stommel using the observed distributions of temperature, salinity and very limited data on carbon. It was possible to obtain estimates of the origins and rate of flow of waters that make up the Common Water in the Pacific and Indian Oceans.

The most voluminous water mass in the world ocean is the deep water of the Indian and Pacific Oceans, called Common Water. (See T-S diagram, page 28.)

If we assume that the Common Water is pure Antarctic Bottom Water and the small geothermal heat flux warms the Antarctic Bottom Water slowly as it travels, a calculation shows that about 6000 years would be required to warm the Antarctic Water 1.5°C . This is too long in comparison with qualitative indications derived from radiocarbon data.

Now we try another box model. Assume the Common Water is a mixture of North Atlantic Deep Water, Antarctic Bottom Water and Intermediate Water. The flux of various water masses is indicated as K_i (for example K_1 to be the flux



T-S diagram showing characteristics of the water masses being mixed to form Common Water

where

- 1 represents North Atlantic Deep Water
- 2 represents Antarctic Bottom Water
- 3 represents Intermediate Water
- 4 represents Common Water.

of North Atlantic Deep Water to Common Water, K_4 the flux of water out of Common Water). The conservation laws of mass, heat, salt, and radiocarbon in Common Water may be written as:

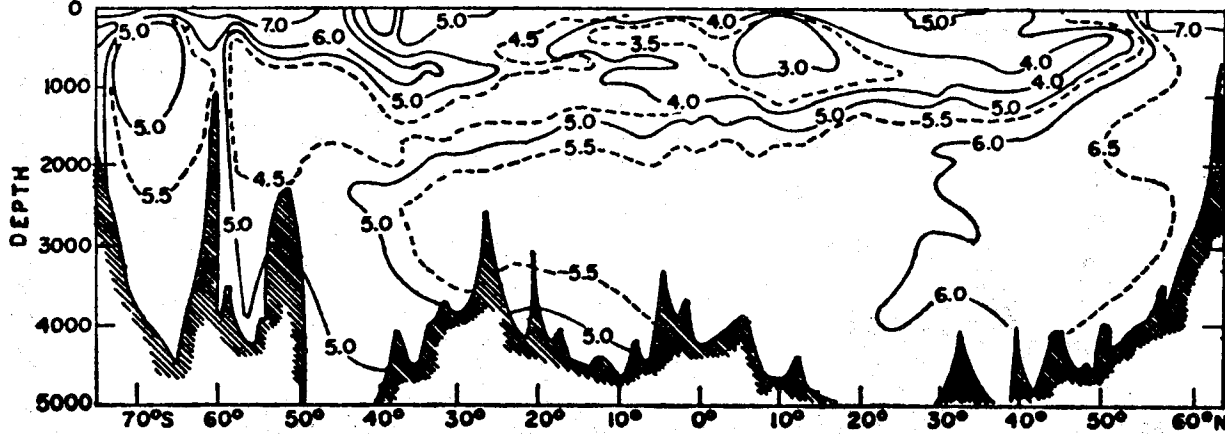
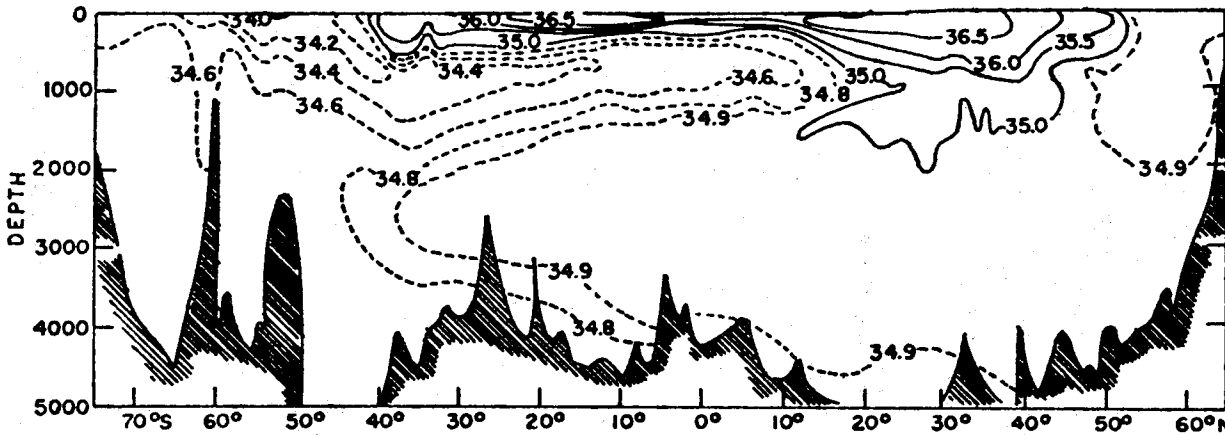
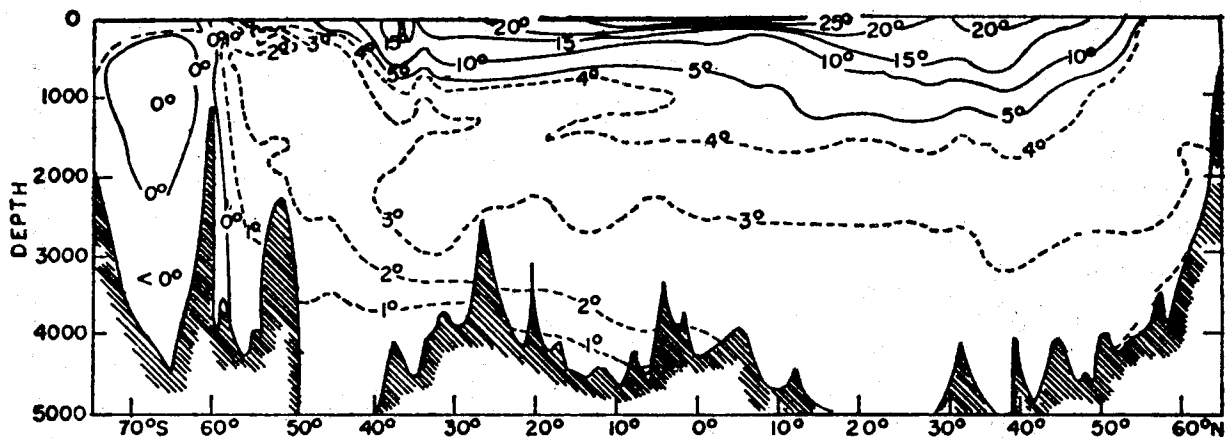
$$K_1 + K_2 + K_3 - K_4 = 0$$

$$K_1 S_1 + K_2 S_2 + K_3 S_3 - K_4 S_4 = 0$$

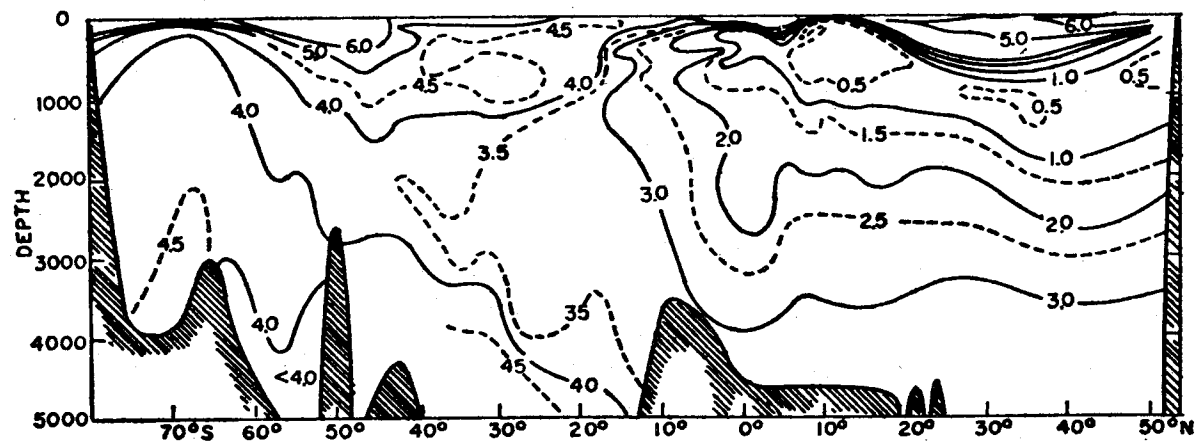
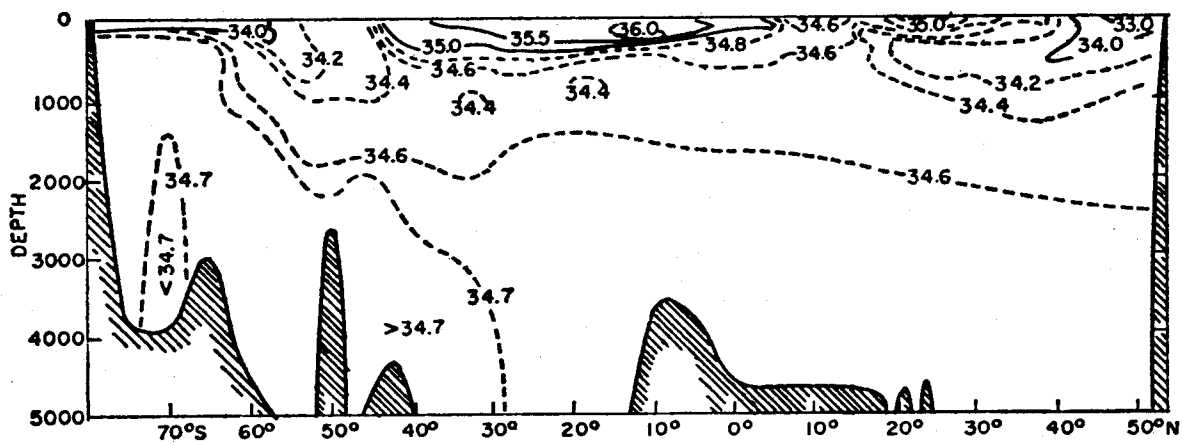
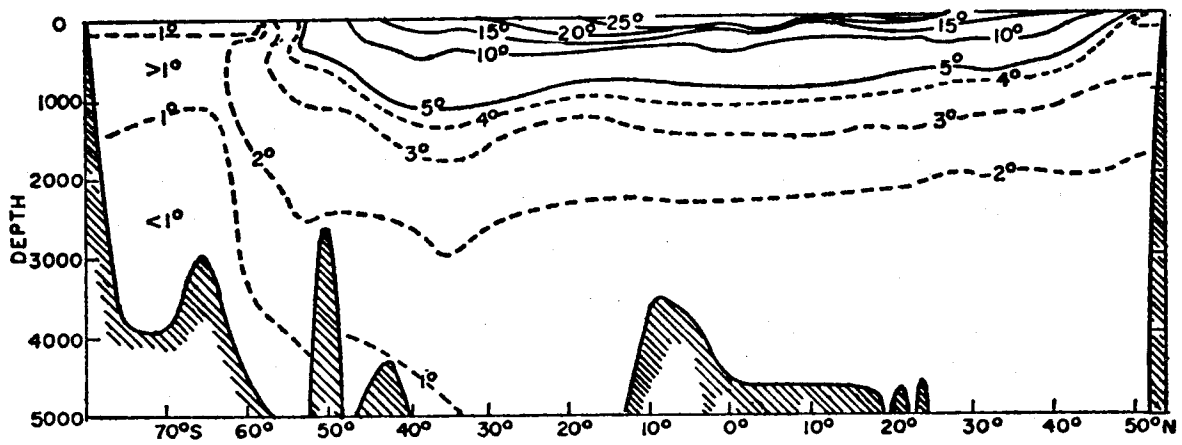
$$K_1 T_1 + K_2 T_2 + K_3 T_3 - K_4 T_4 = -HM_4$$

$$K_1 C_1 + K_2 C_2 + K_3 C_3 - K_4 C_4 = \lambda M_4 C_4$$

where HM_4 represents the rate of gain of heat due to geothermal flux through the bottom, $\lambda M_4 C_4$ denotes the radio carbon decay and $\lambda = 1.2 \times 10^{-4} \text{ yr}^{-1}$ and M_4 is the total mass of Common Water.



Longitudinal Profile #1. Atlantic N-S Section of Temperature, Salinity, and Dissolved Oxygen



Longitudinal profile #2. Pacific N-S Section of Temperature, Salinity, and Dissolved Oxygen.

The solutions are:

$$K_1 = 3.9 \times 10^6 \text{ m}^3/\text{sec}$$

$$K_2 = 9.6 \times 10^6 \text{ m}^3/\text{sec}$$

$$K_3 = 0.6 \times 10^6 \text{ m}^3/\text{sec}$$

$$K_4 = 16.2 \times 10^6 \text{ m}^3/\text{sec}$$

The K values are believed accurate within 50%. A principal source of uncertainty is the C^{14} values. The residence time for Common Water is determined to be about 1200 years. Hence, the mixing is rapid enough that geothermal heating is of minor consequence. The solutions are consistent with an upwelling velocity of 1 cm/day beneath the thermocline.

B. Munk's Abyssal Recipes

Munk (1966) looked at the vertical distributions of temperature, salinity, and radiocarbon in the interior Pacific (excluding the top and bottom kilometer) and considered a balance between vertical advection and mixing. He obtained an upwelling velocity of 1.3 cm/day and an eddy diffusivity of $1.3 \text{ cm}^2/\text{sec}$.

The physical explanations for vertical mixing may be:

- (1) biological mixing
- (2) boundary mixing
- (3) shear mixing (internal Väisälä frequency, internal tide wave; interior planetary wave, etc.)
- (4) thermodynamical mixing (salt fingers)

II. Temperature-Salinity Fine Structure in the Thermocline

An STD trace shows many small wiggles in the thermocline. Although some may be caused by instrumental effects, such as the pen sticking on the chart paper, some of the wiggles seem to represent real features in salinity and temperature. Repeated lowerings taken by Cooper and Stommel off Bermuda (in 1967) show the same type of jumps at the same temperatures. There are jumps in salinity coincident with the temperature jumps. In the Sargasso Sea, the main thermocline seems to be filled with layers less than 10 m in height (Figure 1).

The ocean can be crudely represented in the laboratory by a two-layer model with warm salty water representing the mixed layer above the thermocline and cold fresh water representing the deep water. An experiment of this type, described by Turner and Stommel, shows that an interchange of water takes place across the interface. High salinity columns, called salt fingers, descend from the upper layer and low salinity columns rise from the lower layer. Malkus has examined the problem in an unpublished manuscript and is able to predict many of the observed features. Stern has carried out many theoretical studies of this phenomenon and will discuss them later this summer.

From this it seems reasonable that salt fingers could fall through one of the Cooper-Stommel layers in less than a day. A time scale of one layer overturn per day would give a result resembling the eddy coefficient obtained by Munk.

At this point there was some general discussion concerning the possible ways in which salt-convection may be operating in the main thermocline.

References

- Bolin, B. and H. Stommel, 1961. Deep-Sea Research 8: 95-110. "On the Abyssal Circulation of the World Ocean - IV".
- Munk, W. H., 1966. Deep-Sea Research 13: 707-730. "Abyssal Recipes".
- Turner, J. S. and H. Stommel, 1964. Proc.Nat.Acad.Sci., 52: 49-53.
"A New Case of Convection in the Presence of Combined Vertical Salinity and Temperature Gradients".

Notes submitted by
Han-Hsiung Kuo and
Michael C. Gregg

THE THERMOHALINE CIRCULATION AND THE ACTION OF VARIABLE WIND-STRESS
ON A STRATIFIED OCEAN

Lecture #5

Henry Stommel

June 28, 1968

I. Blandford's Model of the Thermohaline Circulation

This model of the deep interior circulation of the ocean assumes that advection is balanced by vertical diffusion. The dynamics of the Ekman layer is replaced by an imposed distribution of surface temperature and vertical velocity specified at the bottom of the Ekman layer. Purely geostrophic dynamics will be used, together with the Boussinesq approximation.

$$\left. \begin{aligned} -v \sin \theta &= -\frac{1}{\cos \theta} p_{\varphi} \\ u \sin \theta &= -p_{\theta} \end{aligned} \right\} \text{geostrophic equations} \quad (1)$$

$$-p_z + T = 0 \quad \text{hydrostatic equation} \quad (2)$$

$$\frac{1}{\cos \theta} u_{\varphi} + \frac{1}{\cos \theta} (v \cos \theta)_{\theta} + w_z = 0 \quad \text{continuity equation} \quad (3)$$

$$-\chi T_{zz} + \frac{u}{\cos \theta} T_{\varphi} + v T_{\theta} + w T_z = 0 \quad \text{heat equation} \quad (4)$$

All the variables have been non-dimensionalized and scaled, subscripts indicate differentiation with respect to the subscripted variables: (u, v, w) are the horizontal and vertical velocity components; (φ , θ , z) are longitude, latitude, and vertical distance, respectively; T the temperature, p the pressure, and χ is the non-dimensional (turbulent) thermometric conductivity. The following list gives the expressions by which the corresponding fields have been non-dimensionalized and scaled.

$$(u, v), [\alpha^2 T_s^2 g^2 / 4 \Omega^2 R]^{\frac{1}{3}}; w, [\alpha T_s g / 2 \Omega R^2]^{\frac{1}{3}}$$

$$z, [2 \Omega R^2 K_0 / \alpha T_s g]^{\frac{1}{3}}; P, [2 \Omega K_0 \alpha^2 R^2 T_s^2 g]^{\frac{1}{3}}$$

$$T, T_s; K, K_0$$

If we work with the density field, T may be regarded as effective temperature.

Following Robinson and Welander, we define the potential function

$$M = - \int_{-\infty}^z \int_{-\infty}^{z_1} T dz_1 dz_2 + c(\theta, \varphi) \quad (6)$$

We can obtain the equation governing M

$$-\frac{K}{2} M_{zzzz} \sin 2\theta + M_{\theta z} M_{zz\varphi} - M_{z\varphi} M_{zz\theta} - \cot \theta M_{\varphi} M_{zzz} = 0 \quad (7)$$

A similarity variable for this problem is

$$\eta = (\sin \theta)^m (\varphi + E(\theta))^n z \quad (8)$$

The similarity function is defined as

$$M = \frac{1}{2} (\sin \theta)^{m+2} (\varphi + E)^{n+1} G(\eta) \quad (9)$$

The governing equation for G(η) is derived from (8) as

$$\chi G^{IV} - (n-m)\eta G'G''' + (n+1)G''G'' + (2n-m)\eta G''G'' - (2n-m)G''G' = 0 \quad (10)$$

An exact solution to (10) is given by

$$G = -a + b e^{(a/\chi)\eta} (\sin^{-1} \theta)$$

for the case $n = 0, m = -1$.

The expressions for the fields of the exact solution are

$$T = -\frac{1}{2} (\sin^{-1} \theta) (\varphi + E) b (a^2/k^2) e^{(a/k)\eta}$$

$$W = -\frac{1}{2} (\sin^{-1} \theta) (-a + b e^{(a/k)\eta})$$

$$\eta = z (\sin^{-1} \theta)$$

$$u = \frac{1}{2} \sin^{-2} \theta \left[-\cos \theta (\varphi + E) (b a^2 / \kappa^2) \eta e^{(a/\kappa) \eta} + (\sin \theta) (z_0 b a / \kappa) e^{(a/\kappa) \eta} \right]$$

$$v = -\frac{1}{2} \sin^{-1} \theta (\cos^{-1} \theta) (b a / \kappa) e^{(a/\kappa) \eta}$$

The exact solution must satisfy the boundary condition at $\phi = 0$ if we let $E = 0$. A choice $\varphi = -1$ corresponds to the western North Atlantic, and we may then assume $T = T_0 / w = w_0$. At $z = 0$, $\theta = 30^\circ \text{N}$ the surface of a subtropical region then

$$T_0 = b a^2 / \kappa^2, \quad w_0 = a - b$$

Eliminating b , the resulting cubic is

$$(a/w_0)^3 - (a/w_0)^2 - (T_0 \kappa^2) / w_0^3 = 0$$

It is necessary to solve for $a > 0$, because the deep vertical velocity component must be positive.

Figure 1 shows the graph of a/w_0 as a function of $(T_0 \kappa^2) / w_0^3$ for those solutions for which $a > 0$.

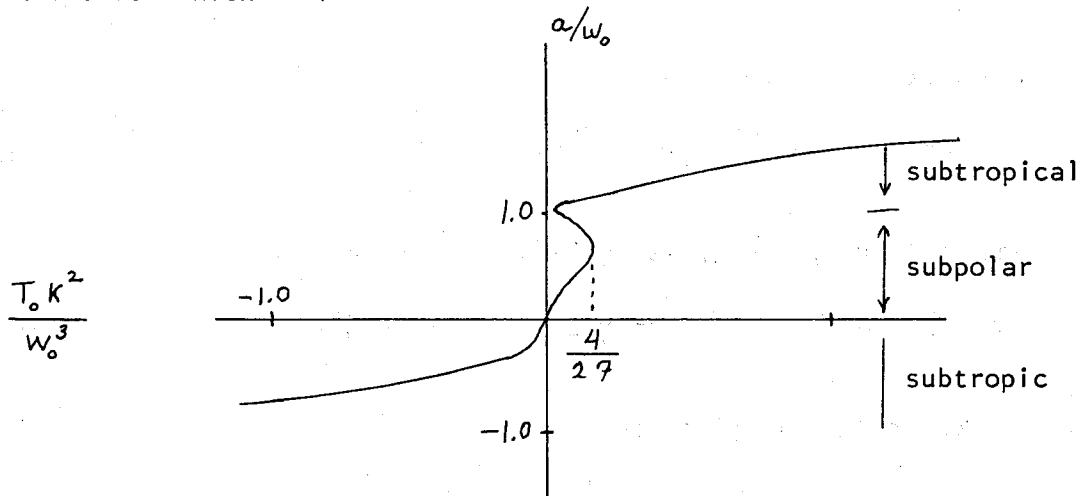
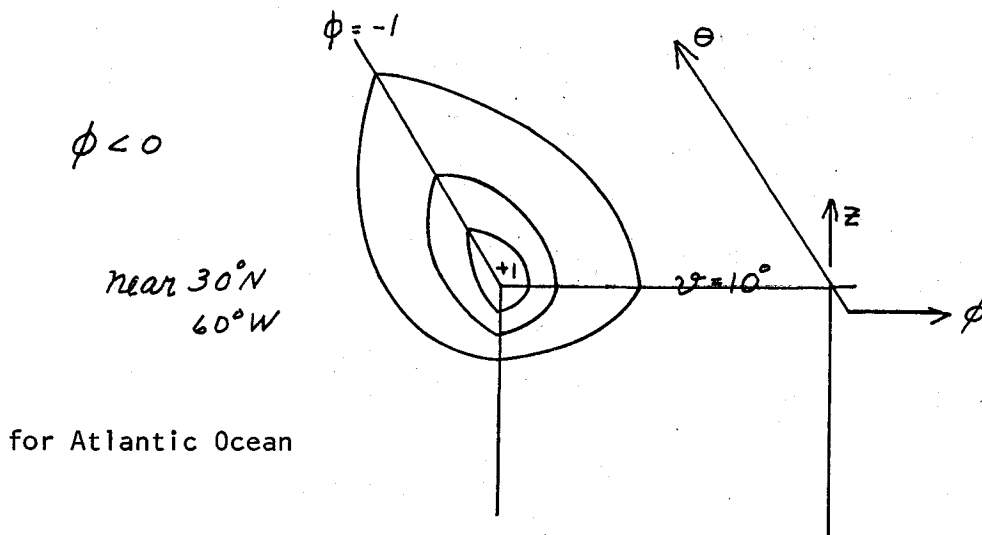


Figure 1.

Asymptotic vertical velocity \underline{a} , as function of surface temperature, T , eddy diffusion coefficient κ , and Ekman velocity w_0 , for subtropical and subpolar gyres.

The temperature field for the ocean basin is



Now we examine the scaling for $W \sim [\alpha T_s g / 2 \Omega R^2]^{1/3}$

and $z \sim [2 \Omega R^2 \chi_0 / \alpha T_s g]^{1/3}$. If we let $\alpha \sim 2 \times 10^{-4}$

$T_s \sim 10^\circ\text{C}$, $g \sim 10^3 \text{ cm/sec}^2$, $\Omega \sim 0.7 \times 10^{-4} \text{ sec}^{-1}$, $R \sim 6.3 \times 10^4$

and $z = 800 \text{ M}$, and

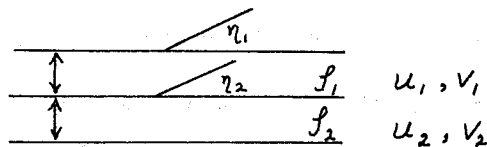
choosing $W_0 \sim 3 \times 10^{-5} \text{ cm/sec}$

$\chi_0 \sim 1.1 \text{ cm}^2/\text{sec}$

$Q = 1.5 \times 10^{-5} \text{ cm/sec}$

This is consistent with results previously obtained with radiocarbon but no dynamics.

II. The Action of Variable Wind Stresses on a Stratified Ocean



Consider a model of a two-layer ocean basin in which it is assumed that the motions are quasi-hydrostatic and that no momentum is transmitted across the interface by friction. If the motions are small the equations may be linearized. Thus

$$\text{Linearized equations in upper layer } \frac{\partial u_1}{\partial t} - f v_1 = -g \frac{\partial \eta}{\partial x} + \frac{\tau'}{D_1} \quad (1)$$

$$\frac{\partial v_1}{\partial t} + f u_1 = -g \frac{\partial \eta}{\partial y} + \frac{\tau}{D_1} \quad (2)$$

$$\text{Continuity equation in upper layer } \frac{\partial}{\partial t} \phi + D_1 \left(\frac{\partial \eta}{\partial x} + \frac{\partial v_1}{\partial y} \right) = 0 \quad (3)$$

$$\text{Linearized equations in lower layer } \frac{\partial u_2}{\partial t} - f v_2 = -g \left(a \frac{\partial \eta}{\partial x} + b \frac{\partial \eta_2}{\partial x} \right) \quad (4)$$

$$\frac{\partial v_2}{\partial t} + f u_2 = -g \left(a \frac{\partial \eta}{\partial y} + b \frac{\partial \eta_2}{\partial y} \right) \quad (5)$$

$$\text{Continuity equation in lower layer } \frac{\partial}{\partial t} (\eta - \phi) + D_2 \left(\frac{\partial u_2}{\partial x} + \frac{\partial v_2}{\partial y} \right) = 0 \quad (6)$$

where $\eta = \eta_1$, $\phi = \eta_1 - \eta_2$; and x (directed eastward) and y (directed northward) are the horizontal coordinates; t is time; u_i and v_i ($i = 1, 2$) are the velocities in x and y directions respectively; D_1 is the equilibrium thickness of the upper layer; η_1 is the deviation of the free surface from its equilibrium position; g is gravity; $f = 2\Omega \sin$ (latitude) is the Coriolis parameter; Ω is the angular speed of the earth's rotation; $a = \rho_1 / \rho_2$; $b = (\rho_2 - \rho_1) / \rho_2$, ρ_1 is the density of the upper layer; τ' and τ are stresses in the x and y directions, respectively, exerted on the ocean surface by wind. The terms with subscripts "2" define similar quantities in the lower layer; the variability of the Coriolis parameter is taken into account by writing $df/dy = \beta = \text{constant}$ wherever f appears in differentiated form. Otherwise f is assumed constant. Cross-differentiating equations (1) and (2) and (4) and (5) we obtain the vorticity equations:

$$\frac{\partial J_1}{\partial t} - \frac{f}{D_1} \frac{\partial \phi}{\partial t} + \beta v_1 = \frac{1}{D_1} \left(\frac{\partial \tau'}{\partial x} - \frac{\partial \tau}{\partial y} \right) \quad (7)$$

$$\frac{\partial J_2}{\partial t} - \frac{f}{D_2} \frac{\partial}{\partial t} (y - \phi) + \beta v_2 = 0 \quad (8)$$

where $J_1 = \partial v_1 / \partial x - \partial u_1 / \partial y$ and $J_2 = \partial v_2 / \partial x - \partial u_2 / \partial y$

Assuming at this point that motions are independent of y , we may obtain for the upper layer from (7), (8), (2), (3), (5) and (6),

$$r\lambda^2 \eta_{xxxt} - \frac{\phi_{xttt}}{f_2} - \phi_{xt} + r\beta\lambda^2 \eta_{xx} - \frac{\beta}{f_2} \phi_{tt} = \tau_{xy}/f \quad (9)$$

where $r = D_1/D_2$ and $\lambda^2 = gD_2/f_2$

and, for the lower layer

$$\lambda^2 (\eta - b\phi)_{xxxt} - \frac{(\eta - \phi)}{f_2} x_{ttt} - (\eta - \phi)_{xt} + \beta\lambda^2 (\eta - b\phi)_{xx} - \frac{\beta}{f} (\eta - \phi)_{tt} = 0 \quad (10)$$

Introducing normal modes by multiplying (8) by the arbitrary constant α and adding to (10), we obtain

$$\lambda^2 [(r+\alpha)\eta - \alpha b\phi]_{xxxt} - \frac{1}{f^2} [(1-\alpha)\phi + \alpha\eta]_{xttt} - [(1-\alpha)\phi + \alpha\eta]_{xt} + \beta\lambda^2 [(r+\alpha)\eta - \alpha b\phi]_{xx} - \frac{\beta}{f^2} [(1-\alpha)\phi + \alpha\eta]_{tt} = \frac{\tau_{xx}}{f} \quad (11)$$

The conditions $(1-\alpha)\phi + \alpha\eta = R$ and $(r+\alpha)\eta - \alpha b\phi = kR$ where k is a constant of proportionality, are sufficient to reduce the equations to a single variable. Thus we have

$$k = -\frac{\alpha b}{1-\alpha} = \frac{r+\alpha}{\alpha}$$

and

$$\alpha = \frac{1-r \pm \sqrt{(1+r)^2 - 4rb}}{2(1-b)}$$

Consequently,

$$\alpha_1 \sim \frac{1+r-rb}{(1+r)(1-b)} \quad \alpha_2 \sim \frac{-r(1+r-b)}{(1+r)(1-b)}$$

$$k_1 \sim 1+r \quad k_2 \sim rb/1+r$$

The two values of R (two normal modes corresponding to the two values of α) are

$$R_i = (1-\alpha_i)\phi_i + \alpha_i\eta \quad (i=1,2)$$

Thus (11) may be written

$$\lambda^2 k_i R_{ixxt} - \frac{1}{f^2} R_{ixttt} - R_{ix} + \beta \lambda^2 k_i R_{ixx} - \frac{\beta}{f^2} R_{itt} = \frac{T_{xx}}{f} \quad (12)$$

Consider a free wave solution of the normal modes

$$R_i = S_i \sin(\ell x + \omega_i t)$$

where $S_i = \text{constant}$ and where ℓ is the wave number associated with the wave length L . i.e. $\ell = 2\pi/L$.

Substituting into (12) we obtain a pair of frequency equations of the form

$$\left(\frac{\omega_i}{f}\right)^3 - \frac{\beta}{f\ell} \left(\frac{\omega_i}{f}\right)^2 + (1 + \mu_i^2) \frac{\omega_i}{f} + \frac{\beta \mu_i^2}{\ell f} = 0 \quad (i=1,2)$$

where $\mu_i^2 = k_i \ell^2 \lambda^2$.

From an oceanographic point of view, only a limited range of values of ℓ is of interest and the approximate roots of the cubic equation within this range of value ℓ are

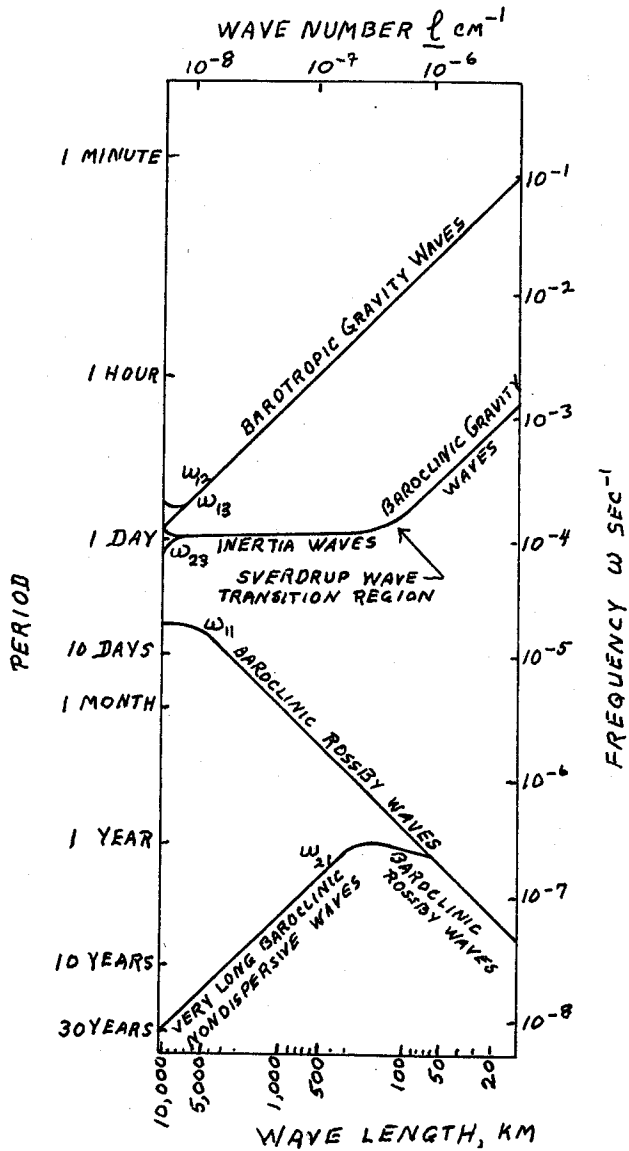
$$\begin{aligned} \omega_{i1} &= \frac{\beta}{\ell} \frac{\mu_i^2}{r_i} \\ \omega_{i2} &= \frac{\beta}{2\ell r_i} + \sqrt{\left(\frac{\beta}{2r_i \ell}\right)^2 + \frac{4\beta \mu_i^2}{\ell^2 r_i^2} + 4f^2 r_i} \\ \omega_{i3} &= \frac{\beta}{2\ell r_i} - \sqrt{\left(\frac{\beta}{2r_i \ell}\right)^2 + \frac{4\beta \mu_i^2}{\ell^2 r_i^2} + 4f^2 r_i} \end{aligned}$$

The phase velocity and frequency of various waves of interest are shown in the following figure for the range of wave lengths $10 \text{ km} \leq L \leq 12,000 \text{ km}$.

References

Blandford, R., 1965. J.Mar.Res. 23(1): 18-29. "Notes on the Theory of the Thermocline".

Veronis, G. and H. Stommel, 1956. J.Mar.Res. 15(1): 43-75. "The Action of Variable Wind Stresses on a Stratified Ocean".



Notes submitted by
Han-Hsiung Kuo and
Michael C. Gregg



ROTATING AND STRATIFIED FLUIDS

Louis N. Howard

Lecture #1

I. Rotating Homogeneous Fluids

1. Introduction:

We consider a mathematical model which can be described by the Euler equations, bearing in mind that this is a simplification. Also, we are interested in problems in which the flow is near to rigid rotation, in some sense, so that it helps to introduce a rotating coordinate system. We take the axis of rotation to be the z-axis, and parallel to the gravitational vector. Thus the governing equations, in dimensional variables, are:

$$\left\{ \begin{array}{l} \frac{\partial \underline{u}^*}{\partial t} + \underline{u}^* \cdot \nabla \underline{u}^* + \underbrace{2 \underline{\Omega} \times \underline{u}^*}_{\text{Coriolis term}} + \frac{1}{\rho} \nabla P^* + \underbrace{\nabla (gz - \frac{1}{2} (\underline{\Omega} \times \underline{r})^2)}_{\substack{\text{gravitational term} \\ \text{centrifugal term}}} = 0 \\ \nabla \cdot \underline{u}^* = 0 \end{array} \right. \quad (1.1.1)$$

In order to non-dimensionalize the equations we choose a time scale Ω^{-1} , length scale L , velocity scale U (relative to rotating axes).

The non-dimensional number $\epsilon = \frac{U}{\Omega L}$ is a measure of the departure of the flow from rigid rotation, and is the Rossby number. We are considering problems in which ϵ is small.

The equations, when expressed in dimensionless variables, are

$$\left\{ \begin{array}{l} \underline{u} \Omega \underline{u} t + \frac{U}{L} \underline{u} \cdot \nabla \underline{u} + 2 \Omega U \underline{k} \times \underline{u} + \frac{1}{L} \nabla \left[\frac{P^*}{\rho} + gLz - \frac{1}{2} \Omega^2 L^2 (\underline{k} \times \underline{r})^2 \right] = 0 \\ \nabla \cdot \underline{u} = 0 \end{array} \right. \quad (1.1.2)$$

$$\Rightarrow \left\{ \begin{array}{l} \underline{u}_t + \epsilon \underline{u} \cdot \nabla \underline{u} + 2 \underline{k} \times \underline{u} + \nabla \left[\frac{P^*}{LU\Omega\rho} + \frac{g}{U\Omega} z - \frac{1}{2} \frac{\Omega L}{U} (\underline{k} \times \underline{r})^2 \right] = 0 \\ \nabla \cdot \underline{u} = 0 \end{array} \right. \quad (1.1.3)$$

The zeroth order approximation for $\epsilon \ll 1$ is a balance given by the terms in the square bracket, which is the case of rigid rotation.

If there is a free surface, it takes the form of a paraboloid

$$z = \left(\frac{\Omega^2 L}{g}\right)(x^2 + y^2)$$

$\frac{\Omega^2 L}{g}$ is associated with a "rotational Froude number"

If there is no free surface, (or Froude number small) we can lump all of the last three terms into an "effective pressure", thus suppressing the true zeroth order solution:

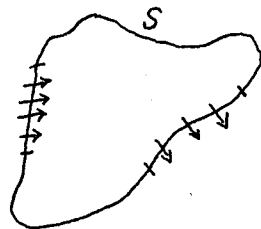
$$\underline{u}_t + \epsilon \underline{u} \cdot \nabla \underline{u} + 2 \underline{k} \times \underline{u} + \nabla p = 0$$

$$\nabla \cdot \underline{u} = 0 \tag{1.1.4}$$

We can treat $\epsilon \underline{u} \cdot \nabla \underline{u}$ as a perturbation term on the equations, but it is a singular perturbation, as we are dropping the highest order spatial derivative. This can lead to non-uniformities in the convergence of the perturbation solution to the solution of the general equation, so we must be careful. (N.B. We have already made another singular perturbation by throwing away $\nu \nabla^2 \underline{u}$).

The lower order equation cannot satisfy as many boundary conditions as the full equation. The initial value problem is a sensible one for the Navier-Stokes equations, but for the Euler equations, which conditions must we drop? Usually we specify $\underline{u} \cdot \underline{n}$ on the boundary, but this is not always so.

Example: Non-rotating problem in closed region:



<u>Conditions for N.S. Eqns.</u>	<u>Possible conditions for Euler Eqns.</u>	<u>Remarks</u>
$\underline{u} = 0$ on S $\underline{u} = \underline{u}_I$ at $t=0$	$\underline{u} \cdot \underline{n} = 0$ on S $\underline{u} = \underline{u}_I$ at $t=0$	This problem is well posed.
$\underline{u} = \underline{u}_B$ on S (such that $\int \underline{u}_B \cdot \underline{n} ds = 0$ for continuity) $\underline{u} = \underline{u}_I$ at $t=0$	$\underline{u} \cdot \underline{n} = \underline{u}_B \cdot \underline{n}$ on S $\underline{u} = \underline{u}_I$ at $t=0$	This is not well posed, can have more than one solution.
ditto	$\underline{u} \cdot \underline{n} = \underline{u}_B \cdot \underline{n}$ on S $\underline{u} \cdot \underline{t} = \underline{u}_B \cdot \underline{t}$ on parts of S where $\underline{u}_B \cdot \underline{n} < 0$ (inflow) $\underline{u} = \underline{u}_I$ at $t=0$	Now the problem is well posed.

An alternative to this last problem is to give the tangential components of vorticity, rather than of velocity, at points of inflow. In two dimensions the relevance of this condition is particularly clear. Physically, it means that we must "tell" the fluid about any vorticity that is entering the region.

2. Problems where $\epsilon = 0$

We consider:

$$\begin{aligned} \underline{u}_t + 2 \underline{k} \times \underline{u} + \nabla P &= 0 \\ \nabla \cdot \underline{u} &= 0 \end{aligned} \tag{1.2.1}$$

Taking the curl of the former gives the vorticity equation:

$$\left(\nabla \times \underline{u} \right)_t - 2 \frac{\partial \underline{u}}{\partial z} = 0 \tag{1.2.2}$$

(If we consider a particular component of the vorticity, say the z component,

it increases in time if $\frac{\partial \omega}{\partial z} > 0$. This implies a "vertical divergence" or a stretching of vortex lines.)

For steady flow we have

$$\frac{\partial u}{\partial z} = 0, \tag{1.2.3}$$

i.e. the velocity is independent of z - the Taylor-Proudman Theorem. An experiment to illustrate this theorem was performed. A fishing float, suitably weighted so that it was only slightly positively buoyant, was allowed to rise from the bottom to the top of a vessel of water, firstly when it was not rotating, and then after the vessel had been spun up to about 25 r.p.m. The time of rise in the second case was seen to be noticeably longer than in the first - a ratio of 8:1 was obtained in one run.

For the ball to rise at all, the velocity field must be z -dependent, hence the phenomenon must depend on the small effects that we have neglected in deriving the Taylor-Proudman theorem, namely time dependence, zero Rossby number, and zero viscosity. Probably all three are involved.

Flows for which $\epsilon = 0$, $\frac{\partial}{\partial t} = 0$ are called geostrophic.

Fundamental Theorem of Weather Maps:

Consider a flow region $z_B \leq z \leq z_T$; (x, y) in a two-dimensional region R .

We have then

$$\begin{aligned} -2v + P_x &= 0 \\ 2u + P_y &= 0 \end{aligned} \tag{1.2.4}$$

In the case z_B, z_T constant we can give a general solution:

$$\left. \begin{aligned} u &= -\frac{1}{2} P_y \\ v &= \frac{1}{2} P_x \\ w &= 0 \end{aligned} \right\} \text{ where } P(x, y) \text{ is any single valued function.} \tag{1.2.5}$$

Thus $\frac{1}{2} P$ is a stream function for this two-dimensional flow, and the streamlines coincide with the lines of constant pressure. Any incompressible two-dimensional flow where stream function can be interpreted as a pressure is a possible geostrophic flow. The interpretation as a pressure (i.e. single valuedness) is important with multiply-connected regions, particularly in source/sink flows, - e.g. in an annulus, fluid cannot flow in radial lines (which is a possible two-dimensional incompressible flow). In fact, it cannot even cross circular cylinders. In practice, it is found that the ϵ term is not negligible near the source/sink, while the ν term comes in near the bottom, and boundary layers are set up.

Non-horizontal boundaries

When z_T, z_B are not constant, geostrophic flows can only exist if there are closed contours of constant depth, and they are therefore much less numerous.

Let $H(x, y) = z_T - z_B$

then $\underline{u} \cdot \nabla H = u H_x + v H_y = \frac{1}{2} [p_x H_y - p_y H_x]$

taking \underline{u} as a geostrophic velocity.

$$\underline{u} \cdot \nabla H = \frac{1}{2} \frac{\partial(p, H)}{\partial(x, y)}$$

Also $\underline{u} \cdot \nabla H = \underline{u} \cdot \nabla (z_T - z_B)$

Now an element of fluid on a boundary can only move along the boundary.

$$w_T = \frac{dz_T}{dt} = \frac{\partial z_T}{\partial t} + \underline{u} \cdot \nabla z_T = \underline{u} \cdot \nabla z_T \quad \text{as boundaries are fixed.}$$

$$\begin{aligned} \text{Thus } \underline{u} \cdot \nabla H &= w_T - w_B = \int_{z_B}^{z_T} \frac{\partial w}{\partial z} dz = - \int_{z_B}^{z_T} (u_x + v_y) dz \\ &= 0 \text{ if } \underline{u} \text{ is geostrophic} \end{aligned}$$

Hence
$$\frac{\partial(P, H)}{\partial(x, y)} = 0 \quad (1.2.6)$$

i.e. P and H have the same contours of constancy. In some cases there can be no geostrophic flows, e.g. a cylinder with a slightly tilted bottom. The solutions exhibit an apparent discontinuity when the bottom is tilted slightly. This seeming paradox is resolved by studying the time-dependent problem: slowly varying flows tend to geostrophic flows as the angle of tilt goes to zero.

Time-dependent Flows:

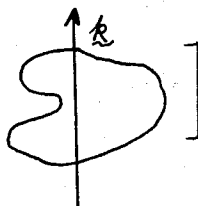
$$\begin{aligned} \underline{u}_t + 2 \underline{k} \times \underline{u} + \nabla P &= 0 \\ \text{(Reminder)} \quad \nabla \cdot \underline{u} &= 0 \\ (\nabla \times \underline{u})_t - 2 \frac{\partial \underline{u}}{\partial z} &= 0 \end{aligned} \quad (1.2.7)$$

Consider a closed three-dimensional region R with $\underline{u} \cdot \underline{n} = 0$ on ∂R (boundary).

Then, if \underline{u} is a solution,

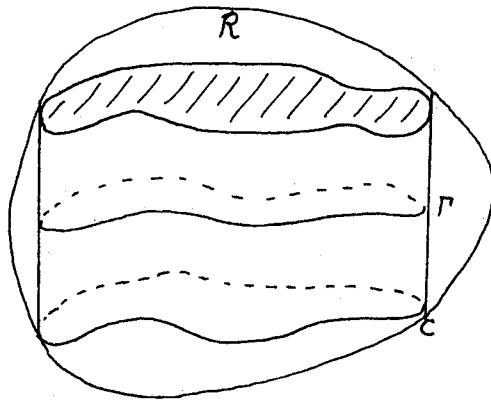
$$\begin{aligned} \underline{u} \cdot \underline{u}_t + \underline{u} \cdot \nabla P &= 0 \\ \frac{\partial}{\partial t} \left(\frac{1}{2} u^2 \right) + \nabla \cdot (P \underline{u}) &= 0 \quad \text{since } \nabla \cdot \underline{u} = 0 \\ \frac{\partial}{\partial t} \int_R \left(\frac{1}{2} u^2 \right) dV &= 0 \quad \text{The Conservation of Energy} \end{aligned} \quad (1.2.8)$$

Suppose now that R has closed contours of constant height everywhere,

[and does not look like ]

Let
$$\int_{z_B}^{z_T} \underline{u} dz = \underline{u} H$$

Consider a particular contour C and the cylinder above it, with vertically translated contours Γ .



The circulation, $\int_{\Gamma} \underline{u} \cdot d\underline{r}$ may depend on Γ , so define a mean circulation

$$Z(c) = \int_{\Gamma} \underline{u} \cdot d\underline{r} = \int_{\Gamma} \underline{\bar{u}} \cdot d\underline{r} \text{ because } d\underline{r} \text{ has the same direction at any station.}$$

Notes submitted by

Philip Hazel.

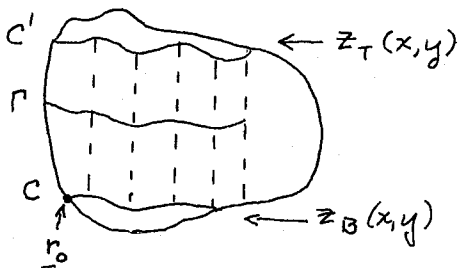
Lecture #2

3. We were examining rapidly rotating (ϵ small) homogeneous flows in a region R with a one-parameter family of closed contours of constant height.

The equations are

$$\underline{u}_t + 2\underline{k} \times \underline{u} + \nabla p = 0, \quad \nabla \cdot \underline{u} = 0, \quad \underline{n} \cdot \underline{u} = 0 \text{ on } \partial R. \quad (1.3.1)$$

We imagine the region R to look like



where $H = z_T(x,y) - z_B(x,y) = \text{constant}$ on a given contour

Then the curve C is a solution of the equation

$$\frac{d\underline{r}}{ds} = \underline{\lambda}(s) : 0 \leq s \leq L \quad (1.3.2)$$

where $\underline{\lambda}(s)$ is the unit tangent to the curve, C is determined by the condition that $\underline{r}(s=0) = \underline{r}_0 = \underline{r}(s=L)$. We want to consider the family of curves Γ which are just vertical translations of C . Thus Γ is a solution of Equation (1.3.2) satisfying the condition that $\underline{r}(s=0) = \underline{r}_1 = \underline{r}(s=L)$ where $\underline{r}_1 = \underline{r}_0 + (0, 0, \underline{z})$ for some \underline{z} . The important fact is that all of these curves Γ have the same tangent direction at a given (x, y) (and the same length L).

For any one of these curves Γ we compute the circulation

$$\oint_{\Gamma} \underline{u} \cdot d\underline{r} = \int_0^L \underline{u} \cdot \underline{\lambda}(s) ds$$

From (1.3.1) we have

$$\oint_{\Gamma} \underline{u}_t \cdot d\underline{r} + 2 \oint_{\Gamma} (\underline{k} \times \underline{u}) \cdot d\underline{r} + \oint_{\Gamma} \nabla p \cdot d\underline{r} = 0$$

Clearly $\oint_{\Gamma} \nabla p \cdot d\underline{r}$ is the net change in pressure as we go around the contour Γ and must vanish. Γ is a fixed curve and so we may take the time derivative outside of the integration:

$$\frac{\partial}{\partial t} \oint_{\Gamma} \underline{u} \cdot d\underline{r} + 2 \oint_{\Gamma} \underline{k} \times \underline{u} \cdot d\underline{r} = 0$$

Averaging this equation over \underline{z} gives

$$\frac{1}{H} \int_{z_B}^{z_T} dz \frac{\partial}{\partial t} \oint_{\Gamma} \underline{u} \cdot d\underline{r} + \frac{2}{H} \int_{z_B}^{z_T} dz \oint_{\Gamma} \underline{k} \times \underline{u} \cdot d\underline{r} = 0$$

which can be written as

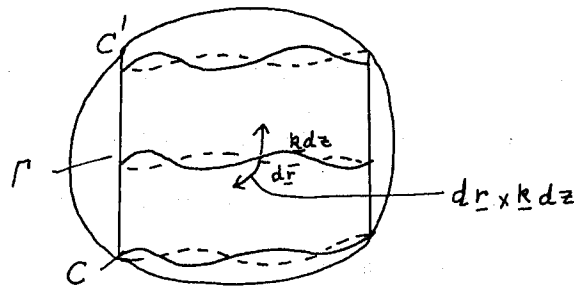
$$\frac{\partial}{\partial t} \frac{1}{H} \int_{z_B}^{z_T} dz \int_0^L ds \underline{\lambda}(s) \cdot \underline{u} + \frac{2}{H} \int_{z_B}^{z_T} dz \int_0^L ds \underline{\lambda}(s) \cdot \underline{k} \times \underline{u} = 0$$

Since $\underline{\lambda}(s)$ is independent of \underline{z} we interchange orders of integration to get

$$\frac{\partial}{\partial t} \int_0^L ds \underline{\lambda}(s) \cdot \left(\frac{1}{H} \int_{z_B}^{z_T} dz \underline{u} \right) + \frac{2}{H} \int_{z_B}^{z_T} dz \int_0^L ds \left[\underline{\lambda}(s) \times \underline{k} dz \right] \cdot \underline{u} = 0.$$

It is clear that the second integral is an integral over the surface formed by all of the vertical translates of the curve C and

$$ds \underline{\lambda}(s) \times \underline{k} dz = d\underline{r} \times \underline{k} dz = \underline{n} d\sigma$$



where \hat{n} is the normal to the surface and $d\sigma$ the element of surface area.

Let the surface generated by the family of curves Γ be Σ . Then

$$\int_{z_B}^{z_T} \int_0^L [ds \underline{\lambda}(s) \times \underline{u} dz] \cdot \underline{u} = \int_{\Sigma} \underline{n} \cdot \underline{u} d\sigma$$

To make Σ into a closed surface we include the caps on the boundary of R which are cut off by the curves C and C' . Since these are portions of the boundary ∂R $\underline{n} \cdot \underline{u}$ vanishes on them and thus

$$\int_{\Sigma} \underline{n} \cdot \underline{u} d\sigma = \int_{\Sigma + \text{caps}} \underline{n} \cdot \underline{u} d\sigma = \int_{\text{enclosed volume } CR} \nabla \cdot \underline{u} dv = 0$$

by the continuity equation. Writing

$$\frac{1}{H} \int_{z_B}^{z_T} \underline{u} dz = \underline{\bar{u}}$$

we have

$$\frac{\partial}{\partial t} \int_0^L ds \underline{\lambda}(s) \cdot \underline{\bar{u}} = \frac{\partial}{\partial t} \int_C d\underline{r} \cdot \underline{\bar{u}} = 0.$$

Thus the mean circulation of any solution to (1.3.1) is constant in time and we have proven the mean circulation theorem. (Greenspan).

Mean Circulation Theorem: Given a solution \underline{u} of $\underline{u}_t + 2\underline{k} \times \underline{u} + \nabla p = 0$, $\nabla \cdot \underline{u} = 0$ in \mathcal{R} satisfying $\underline{n} \cdot \underline{u} = 0$ on the boundary of \mathcal{R} , the mean circulation for any closed contour of constant height is constant in time. We write

$$\oint_c \underline{u} \cdot d\underline{r} = \mathcal{Z}(c) = \mathcal{Z}(H)$$

\mathcal{Z} is constant for a given H .

4. We would like to prove that a steady solution for (1.3.1) is uniquely determined by its mean circulation and the geometry of the region \mathcal{R} . We have seen that $-\frac{1}{2}p$ is a stream function for the horizontal geostrophic flow and the isobars are lines of constant height:

$$\frac{\partial(p, H)}{\partial(x, y)} = 0 \Rightarrow p = p(H).$$

We can write

$$\underline{k} \times \underline{u} = -\frac{1}{2} \nabla p$$

and

$$\underline{k} \times (\underline{k} \times \underline{u}) = \underline{k} (\underline{k} \cdot \underline{u}) - \underline{u} = -\frac{1}{2} \underline{k} \times \nabla p = -\frac{1}{2} p'(H) (\underline{k} \times \nabla H).$$

Now $\underline{k} \cdot \underline{u} = w$ and thus

$$\begin{aligned} \underline{u} &= \underline{k} w + \frac{1}{2} p'(H) (\underline{k} \times \nabla H) \\ &= \underline{k} w + \frac{1}{2} p'(H) (\underline{k} \times [\nabla z_T(x, y) - \nabla z_B(x, y)]) \end{aligned}$$

The vertical component of velocity is easily determined from the boundary condition $\underline{n}_T \cdot \underline{u} = 0$ at the top since $w_z = 0$. For a given H , the top is given by the solution to

$$z - z_T(x, y) = 0$$

and the direction of the normal

$$\underline{n}_T = \nabla(z - z_T(x, y)) = \underline{k} - \nabla z_T(x, y)$$

where $\nabla z_T(x, y)$ is horizontal. Thus

$$\begin{aligned}\underline{n}_T \cdot \underline{u} &= (\underline{k} - \nabla z_T) \cdot \left(\underline{k} w + \frac{1}{2} p'(H) [\underline{k} \times (\nabla z_T - \nabla z_B)] \right) \\ &= w + \frac{1}{2} p'(H) \nabla z_T \cdot (\underline{k} \times \nabla z_B) = 0\end{aligned}$$

so $w = \frac{1}{2} p'(H) \underline{k} \cdot (\nabla z_T \times \nabla z_B)$.

Now both ∇z_T and ∇z_B are horizontal so $\nabla z_T \times \nabla z_B = |\nabla z_T \times \nabla z_B| \underline{k}$

and

$$\begin{aligned}\underline{u} &= \underline{k} \frac{1}{2} p'(H) |\nabla z_T \times \nabla z_B| + \frac{1}{2} p'(H) \underline{k} \times (\nabla z_T - \nabla z_B) \\ &= \frac{1}{2} p'(H) \left\{ \nabla z_T \times \nabla z_B + \underline{k} \times \nabla z_T - \underline{k} \times \nabla z_B \right\} \\ &= \frac{1}{2} p'(H) \left\{ (\underline{k} - \nabla z_T) \times (\underline{k} - \nabla z_B) \right\}.\end{aligned}$$

Now the outward normals to $z = z_T$ and $z = z_B$ are

$$\underline{n}_T = \underline{k} - \nabla z_T \quad \text{and} \quad \underline{n}_B = -(\underline{k} - \nabla z_B)$$

and so

$$\underline{u} = -\frac{1}{2} p'(H) [\underline{n}_T \times \underline{n}_B].$$

We form the mean circulation for this closed contour of constant height H

$$z(H) = -\frac{1}{2} p'(H) \oint (\underline{n}_T \times \underline{n}_B) \cdot d\underline{r}$$

The integral $\oint (\underline{n}_T \times \underline{n}_B) \cdot d\underline{r}$ is independent of the flow and determined by the geometry of the domain R .

Call $\oint d\underline{r} \cdot (\underline{n}_T \times \underline{n}_B) = J(H)$.

Then $z(H) = -\frac{1}{2} p'(H) J(H)$

$$\underline{u}_g = \frac{z(H)}{J(H)} \cdot (\underline{n}_T \times \underline{n}_B).$$

We see that the geostrophic flow \underline{u}_g is determined uniquely by the geometry and its mean circulation $z(H)$.

5. We return to the initial value problem for

$$\underline{u}_t + 2\underline{k} \times \underline{u} + \nabla p = 0, \quad \nabla \cdot \underline{u} = 0 \text{ in } R;$$

$$\underline{n} \cdot \underline{u} = 0 \text{ on } \partial R \text{ and } \underline{u}(t_0) = \underline{u}_0$$

where \underline{u}_0 is a prescribed flow. From the initial condition \underline{u}_0 we can construct the mean circulation $Z(H)$ and from $Z(H)$ a unique geostrophic flow \underline{u}_g associated with \underline{u} . The basic idea is that the general time dependent solution of the initial value problem can be split into a steady or geostrophic flow and a time varying flow with zero mean circulation, and this breakup is unique. We expect, in fact, that the time dependent solutions can be broken up into normal modes with harmonic time dependence. It is easy to see that any solution with a harmonic time dependence has zero mean circulation: $\underline{u}(t) = \underline{u} e^{-i\sigma t}$

and
$$\frac{\partial}{\partial t} \oint_C \underline{u} \cdot d\underline{r} = -i\sigma \oint_C \underline{u} \cdot d\underline{r} = -i\sigma Z(H) = 0.$$

Thus either σ or $Z(H)$ must be zero.

6. There is an alternate route to this breakup of the general solution into a geostrophic component and a time dependent flow. Let \underline{u}_1 and \underline{u}_2 be solutions of the equation (1.3.1) satisfying the boundary condition. Then form

$$\int_R \underline{u}_1 \cdot \underline{u}_2 dV$$

It is easy to show that this is independent of time:

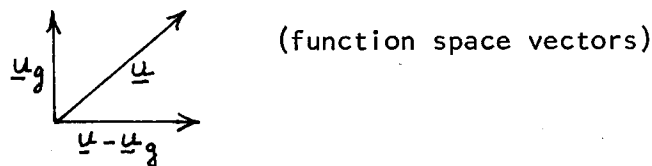
$$\begin{aligned} \frac{\partial}{\partial t} \int_R \underline{u}_1 \cdot \underline{u}_2 dV &= \int_R \left\{ \frac{\partial \underline{u}_1}{\partial t} \cdot \underline{u}_2 + \underline{u}_1 \cdot \frac{\partial \underline{u}_2}{\partial t} \right\} dV \\ &= \int_R \left\{ 2\underline{k} \times \underline{u}_1 \cdot \underline{u}_2 + \nabla p_1 \cdot \underline{u}_2 + 2\underline{k} \times \underline{u}_2 \cdot \underline{u}_1 + \nabla p_2 \cdot \underline{u}_1 \right\} dV \\ &= \int_R \nabla \cdot (p_1 \underline{u}_2 + p_2 \underline{u}_1) dV \\ &= - \int_{\partial R} \underline{n} \cdot (p_1 \underline{u}_2 + p_2 \underline{u}_1) dS = 0 \end{aligned}$$

using the continuity equation and $\underline{n} \cdot \underline{u} = 0$ on ∂R . Using this it is easy to see that two normal modes are orthogonal: if $\underline{u}_1 \sim e^{-i\sigma_1 t}$, $\underline{u}_2 \sim e^{-i\sigma_2 t}$,

$$\frac{\partial}{\partial t} \int_R \underline{u}_1^* \cdot \underline{u}_2 dV = i(\sigma_1 - \sigma_2) \int_R \underline{u}_1^* \cdot \underline{u}_2 dV = 0$$

if $\sigma_1 \neq \sigma_2$, $\int \underline{u}_1^* \cdot \underline{u}_2 dV = 0$ and in particular any harmonically oscillating flow is orthogonal to a geostrophic flow.

We can visualize geometrically the splitting up of a field \underline{u} into a geostrophic part \underline{u}_g and a remainder $\underline{u} - \underline{u}_g$



Clearly \underline{u}_g should be chosen to minimize $\underline{u} - \underline{u}_g$ or rather to minimize the energy of the difference flow, if $\underline{u} - \underline{u}_g$ is to be orthogonal to \underline{u}_g :

$$\frac{1}{2} \int |\underline{u} - \underline{u}_g|^2 dV = I[\underline{u}_g] = \min$$

Since this integral is independent of time we can evaluate it at the initial time so that \underline{u} is the initial value flow. We must vary $\delta \underline{u}_g$ over the manifold of geostrophic flows and determine \underline{u}_g by the condition

$$0 = \delta I[\underline{u}_g] = - \int (\underline{u} - \underline{u}_g) \cdot \delta \underline{u}_g dV$$

The only arbitrariness in $\delta \underline{u}_g$ is the pressure function

$$\delta \underline{u}_g = -\frac{1}{2} \delta P'(H) [\underline{n}_T \times \underline{n}_B]$$

or

$$\delta \underline{u}_g = -\delta f(H) [\underline{n}_T \times \underline{n}_B]$$

where $\delta f(H)$ is an arbitrary function of H .

Then
$$0 = \int (\underline{u} - \underline{u}_g) \cdot [\underline{n}_T \times \underline{n}_B] \delta f(H) dV.$$

Since we have tacitly assumed that the contours of constant height H fill

the projection of R on the (x,y) plane, we can write

$$0 = \int_{z_B}^{z_T} d(H) \delta f(H) ds \int_{z_B}^{z_T} dz (\underline{u} - \underline{u}_g) \cdot [\underline{n}_T \times \underline{n}_B].$$

Choosing $\delta f(H) = \delta(H-H)$ we have

$$0 = \int_{z_B}^{z_T} dz \int ds (\underline{u} - \underline{u}_g) \cdot [\underline{n}_T \times \underline{n}_B].$$

Now $\underline{n}_T \times \underline{n}_B$ is tangent to the curves Γ since the tangent along a curve of constant height is defined by

$$\underline{\lambda}(s) \cdot \nabla H = 0.$$

It is easy to show that $\underline{n}_T \times \underline{n}_B \cdot \nabla H = 0$ since

$$\underline{n}_T = \nabla(z - z_T(x,y)) = \underline{k} - \nabla z_T$$

$$\underline{n}_B = -\underline{k} + \nabla z_B$$

$$\nabla H = \nabla z_T - \nabla z_B$$

$$\underline{n}_T \times \underline{n}_B \cdot \nabla H = [-\underline{k} \times \nabla H - \nabla z_T \times \nabla z_B] \cdot \nabla H = 0.$$

Thus
$$\int_{z_B}^{z_T} dz \int ds \underline{\lambda}(s) \cdot (\underline{u} - \underline{u}_g) = 0$$

and so \underline{u} and \underline{u}_g must have the same mean circulation. This completely determines \underline{u}_g .

Intuitively the harmonic solutions should average to zero and the time averaged flow should be the geostrophic component. Defining the time average by

$$\langle \underline{u} \rangle_a = \lim_{T \rightarrow \infty} \int_0^T dt \underline{u}$$

if the limit exists. Time averaging the equation of motion gives

$$\langle \underline{u}_t \rangle_a + 2\underline{k} \times \langle \underline{u} \rangle_a + \nabla p_a = 0, \quad \nabla \cdot \langle \underline{u} \rangle_a = 0.$$

We can expect $\langle \underline{u}_t \rangle_a = 0$ unless the initial data is pathological and so $\langle \underline{u} \rangle_a$ is a geostrophic flow:

$$2\underline{k} \times \langle \underline{u} \rangle_a + \nabla p_a = 0, \quad \nabla \cdot \langle \underline{u} \rangle_a = 0, \quad \underline{n} \cdot \langle \underline{u} \rangle_a = 0.$$

The mean circulation is independent of time so $(\underline{u})_a$ has the same mean circulation as \underline{u} . Since they have the same mean circulation and $(\underline{u})_a$ is geostrophic, $(\underline{u})_a$ is the geostrophic part of \underline{u} .

7. The natural oscillatory modes are determined by substituting $\underline{u} e^{i\sigma t}$ into the equation of motion:

$$i\sigma \underline{u} + 2\underline{k} \times \underline{u} + \nabla p = 0, \quad \nabla \cdot \underline{u} = 0. \quad (1.7.1)$$

Forming $\underline{k} \cdot (1.7.1)$ and $\underline{k} \times (1.7.1)$:

$$i\sigma w + p_z = 0$$

$$i\sigma (\underline{k} \times \underline{u}) + 2(\omega \underline{k} - \underline{u}) + \underline{k} \times \nabla p = 0 \quad (1.7.2)$$

and

$$i\sigma (\underline{k} \times \underline{u}) - 2\underline{u} + \frac{2}{i\sigma} p_z \underline{k} + \underline{k} \times \nabla p = 0 \quad (1.7.3)$$

We can eliminate $\underline{k} \times \underline{u}$ between (1.7.2) and (1.7.3):

$$(4 - \sigma^2) \underline{u} + i\sigma \nabla p + \frac{4}{i\sigma} \underline{k} p_z - 2\underline{k} \times \nabla p = 0$$

Thus for $\sigma \neq \pm 2$ (dimensional $\sigma_* = \sigma \Omega$ so $\sigma_* \neq \pm 2\Omega$) \underline{u} is determined by the pressure

$$\underline{u} = \left(\frac{1}{4 - \sigma^2} \right) \left(2\underline{k} \times \nabla p - i\sigma \nabla p - \frac{4}{i\sigma} \underline{k} p_z \right). \quad (1.7.4)$$

We can get a single equation for the pressure by taking:

$$\nabla \cdot [\underline{u}_t + 2\underline{k} \times \underline{u} + \nabla p] = (\nabla \cdot \underline{u})_t - 2\underline{k} \cdot (\nabla \times \underline{u}) + \nabla^2 p = 0$$

$$\nabla \times [\underline{u}_t + 2\underline{k} \times \underline{u} + \nabla p] = (\nabla \times \underline{u})_t - 2(\underline{k} \cdot \nabla) \underline{u} = 0$$

Thus

$$\nabla^2 p = 2\underline{k} \cdot (\nabla \times \underline{u})$$

and
$$\nabla^2 p_t = 2 \underline{k} \cdot (\nabla \times \underline{u}_t) = 4 (\underline{k} \cdot \nabla) \underline{u} \cdot \underline{k} = 4 w_z$$

$$\nabla p_{tt} = 4 w_{zt}$$

but

$$w_t + p_z = 0$$

so that

$$\nabla^2 p_{tt} + 4 p_{zz} = 0.$$

This is known as Poincaré's Equation. Putting in the harmonic time dependence we have

$$-\sigma^2 \nabla^2 p + 4 p_{zz} = 0. \tag{1.7.5}$$

We can make the boundary condition $\underline{n} \cdot \underline{u} = 0$ into a homogeneous boundary condition for p using equation (1.7.4). The difficulty is that this boundary condition depends on σ . Another difficulty is that although the equation appears to be an elliptic equation, it is in fact hyperbolic: (if $\sigma^2 < 4$)

$$p_{xx} + p_{yy} + \left(1 - \frac{4}{\sigma^2}\right) p_{zz} = 0 \tag{1.7.6}$$

It can be shown that in a bounded region $0 \leq \sigma^2 < 4$ and in an unbounded region $0 \leq \sigma^2 \leq 4$. Thus the coefficient of the last term is negative and

$$p_{xx} + p_{yy} - \lambda^2 p_{zz} = 0$$

where λ is real. In general a hyperbolic equation subject to elliptic boundary conditions need not have a unique solution. Our problem is essentially finding the values of λ for which a unique solution does exist. It is thought that the set of allowed σ 's is dense in the interval $(-2, 2)$.

As an example of this type of equation, consider

$$u_{xx} - \lambda^2 u_{yy} = 0 \quad 0 \leq x, y \leq \pi$$

subject to

$$u(x, 0) = u(x, \pi) = 0$$

$$u(0, y) = u(\pi, y) = 0$$

Since u vanishes on the edge of a square, we write

$$u = \sum_{nm} A_{nm} \sin nx \sin my.$$

Since the eigenfunctions satisfy the boundary conditions, we can differentiate term by term to get

$$\sum_{nm} [n^2 - \lambda^2 m^2] A_{nm} \sin nx \sin my = 0$$

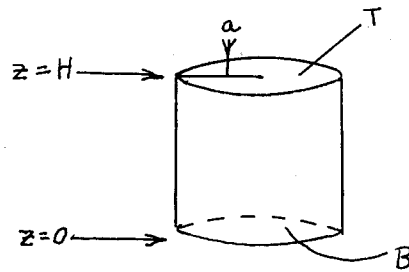
and

$$[n^2 - \lambda^2 m^2] A_{nm} = 0$$

Unless λ is a rational number $A_{nm} = 0$. If $\lambda = n/m$, there are infinitely many eigenfunctions, one for each $A_{kn, km}$ where k is any integer. The spectrum is dense in the real line (but discrete) and the eigenvalue is infinitely degenerate. This situation is forced on us because we insist on looking at normal mode expansions.

When viscosity is introduced the spectrum becomes complex and no longer dense. As the viscosity is taken to zero all of the complex eigenvalues get squeezed onto the real line and become dense in the real line.

As another example we can find the general behavior of the modes in a circular cylinder:



Then the boundary conditions on p at the top and bottom are (by (1.7.4)) $\underline{n} \cdot \underline{u} = 0 \Rightarrow 0 = -\frac{4}{i\sigma} p_z - i\sigma p_z = -i\sigma(1 - \frac{4}{\sigma^2}) p_z$.

Since $0 < \sigma^2 < 4$, $p_z = 0$ at $z = 0, H$.

On the side walls $r = a$, we require

$$\underline{r}_1 \cdot \underline{u} = 0 = \left(\frac{1}{4 - \sigma^2} \right) \left[\underline{r}_1 \cdot (2 \underline{k} \times \nabla p) - i\sigma \underline{r}_1 \cdot \nabla p - \frac{4}{i\sigma} \underline{r}_1 \cdot \underline{k} p_t \right]$$

Now

$$\underline{r}_1 \cdot \nabla p = p_r, \quad \underline{r}_1 \cdot \underline{k} = 0 \quad \text{and} \quad \underline{r}_1 \cdot (2 \underline{k} \times \nabla p) = 2 \underline{k} \cdot (\nabla p \times \underline{r}_1) = -\frac{2}{a} \frac{\partial p}{\partial \theta}$$

So we have, at $r = a$

$$-\frac{2}{a} p_\theta - i\sigma p_r = 0. \quad (1.7.7)$$

Since $p_z = 0$, we use z-eigenfunctions of the form $\cos \frac{n\pi z}{H}$.

Substituting this into Equation (1.7.6) gives

$$\nabla_H^2 p - \left(\frac{4}{\sigma^2} - 1 \right) \left(\frac{n\pi}{H} \right)^2 p_r = 0 \quad \text{or} \quad \nabla_H^2 p_n + \left(\frac{n\pi}{H} \right)^2 \left(\frac{4}{\sigma^2} - 1 \right) p_n = 0.$$

The solutions of this equation are $J_m(kr) e^{-im\theta}$ where m is an integer and $k^2 = \left(\frac{n\pi}{H} \right)^2 \left(\frac{4}{\sigma^2} - 1 \right)$.

Applying the boundary condition (1.7.7):

$$-\frac{2}{a} \left(-im J_m(ka) e^{-im\theta} \right) - i\sigma k J_m'(ka) e^{-im\theta} = 0 \quad \text{for all } \theta.$$

Thus

$$\frac{ka}{\sigma} = \frac{1}{2m} \left(\frac{J_m'(ka)}{J_m(ka)} \right)$$

and solutions of this equation give the spectrum.

There are reasons to suspect that for some regions there is also a continuous spectrum, but the overall picture is not yet clear.

Notes submitted by
James R. Luyten

Lecture #3

8. The Effects of Viscosity

If we include viscosity in the momentum equation, the dimensionless form is

$$\underline{u}_t + \underline{\epsilon} \cdot \nabla \underline{u} + 2 \underline{k} \times \underline{u} + \nabla p = E \nabla^2 \underline{u} \tag{1.8.1}$$

where $E = \frac{\nu}{\Omega L^2}$ is the Ekman number.

Putting $E = 0$ in this equation is no longer a singular perturbation, in that it does not lower the order of the equation. However, it may suppress certain instabilities. It leaves us with a linear equation. Also, E is small when ϵ is small due to fast rotation. Hence we expect a boundary layer type solution.

Simplest Problem:

Consider the boundary conditions:

$$\left\{ \begin{array}{l} z \geq 0 \\ \underline{u} = U_i \text{ for } z \rightarrow \infty \\ \underline{u} = 0 \text{ for } z = 0 \\ \text{No dependence on } x, y, t \end{array} \right.$$

Put $\underline{u} = U_i + \hat{u}(z)$
 $p = -2 U_y + \hat{p}$

i.e. split the flow into the geostrophic part, plus a perturbation which $\rightarrow 0$ at infinity.

Then from the continuity equation, $\frac{dw}{dz} = 0$

$$\implies \omega = 0 \quad \text{everywhere (by bottom condition)}$$

$$\implies \frac{dp}{dz} = 0$$

$$\implies \frac{d\hat{p}}{dz} = 0$$

$$\implies \hat{p} = 0 \quad \text{everywhere (by top condition)}$$

Thus the momentum equation is:

$$2\underline{k} \times \underline{\hat{u}} = E \underline{\hat{u}}_{zz} \quad (1.8.2)$$

Take cross product with \underline{k}

$$-2\underline{\hat{u}} = E \underline{k} \times \underline{\hat{u}}_{zz}$$

Combine these two equations, using $i = \sqrt{-1}$

$$\begin{aligned} E [\underline{\hat{u}} + i(\underline{k} \times \underline{\hat{u}})]_{zz} &= -2i(\underline{\hat{u}} + i(\underline{k} \times \underline{\hat{u}})) \\ &= (1-i)^2 (\underline{\hat{u}} + i(\underline{k} \times \underline{\hat{u}})) \end{aligned}$$

$$\implies \underline{\hat{u}} + i(\underline{k} \times \underline{\hat{u}}) = C \exp[-(1-i)z/E^{1/2}]$$

and $C = -U(i+i\underline{j})$ by boundary conditions at 0

$$\implies \underline{\hat{u}} = -U \operatorname{Re} \left\{ (i+i\underline{j}) \exp(-(1-i)z/E^{1/2}) \right\} \quad (1.8.3)$$

Thus $\underline{\hat{u}}$ is different from zero on a length scale $E^{1/2}$ (in the scaled coordinates). If we return to dimensional variables, we find the scale of the boundary layer is

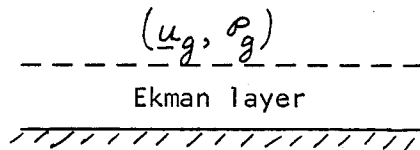
$$z_b = \frac{z_b^*}{L} \sim \left(\frac{\nu}{\Omega}\right)^{1/2} \cdot \frac{1}{L},$$

$$\text{i.e. } z_b^* \sim \left(\frac{\nu}{\Omega}\right)^{1/2} \quad (1.8.4)$$

This is to be expected, as there is no length scale in this infinite half-space problem.

A More General Problem:

Consider a general geostrophic velocity and pressure in an interior region above a rigid boundary:



Write $\underline{u} = \underline{u}_g(x, y) + \hat{\underline{u}}(x, y, z)$

and $P = p_g(x, y) + \hat{p}(x, y, z)$ for this case

the Equation of motion then gives $2\underline{k} \times \hat{\underline{u}} + \nabla \hat{p} = E \nabla^2 \hat{\underline{u}}$ (1.8.5)

Introduce the boundary layer coordinate ζ by the stretching transformation

$$z = E^{1/2} \zeta \quad (1.8.6)$$

$$\implies 2\underline{k} \times \hat{\underline{u}} + \nabla \hat{p} = \frac{\partial^2 \hat{\underline{u}}}{\partial \zeta^2} + \dots \quad \text{small terms} \quad (1.8.7)$$

is the appropriate equation in the boundary layer.

We can now find $\hat{\underline{u}}$ as before, although the boundary condition at infinity has an x,y dependence.

However, the continuity equation is only satisfied to order E. This means that the flow cannot have the form

$$\underline{u} = \underline{u}_g + \hat{\underline{u}}(x, y, \zeta) \quad \text{exactly.}$$

We have really been working with part of an asymptotic expansion:

$$\begin{aligned} \underline{u} = & \underline{u}_{g_0}(x, y) + E^{1/2} \underline{u}_{g_1}(x, y) + \dots \\ & + \hat{\underline{u}}_0(x, y, \zeta) + E^{1/2} \hat{\underline{u}}_1(x, y, \zeta) + \dots \end{aligned} \quad (1.8.8)$$

and similarly for p .

$$\begin{aligned} \text{Thus } \nabla \cdot \underline{u} = & \nabla \cdot \underline{u}_{g_0} + E^{1/2} \nabla \cdot \underline{u}_{g_1} + \dots \\ & + E^{-1/2} \hat{w}_{0\zeta} + (\hat{w}_{1\zeta} + \nabla_H \cdot \hat{\underline{u}}_0) + E^{1/2}(\dots) + \dots \end{aligned} \quad (1.8.9)$$

Hence $2 \underline{k} \times \underline{u} + \nabla p - E \nabla^2 \underline{u} = 2 \underline{k} \times \underline{u}_{g_0} + \nabla p_{g_1} + E^{1/2} (2 \underline{k} \times \underline{u}_{g_1} + \nabla p_{g_1}) + E (2 \underline{k} \times \underline{u}_{g_2} + \nabla p_{g_2} - \nabla^2 \underline{u}_{g_0}) + \dots$

$$E^{-1/2} \frac{\partial \hat{p}_0}{\partial \zeta} \underline{k} \times \left[2 \underline{k} \times \hat{u}_0 + \frac{\partial \hat{p}_1}{\partial \zeta} + \nabla_H \hat{p}_0 - \frac{\partial^2 \hat{u}_0}{\partial \zeta^2} \right] + E^{1/2} [\dots] = 0 \quad (1.8.10)$$

Fix $\zeta \neq 0$ (outside the boundary layer) and let $E \rightarrow 0$

Lowest order terms:
$$\begin{cases} \nabla \cdot \underline{u}_{g_0} = 0 \\ 2 \underline{k} \times \underline{u}_{g_0} + \nabla p_{g_0} = 0 \end{cases} \quad (1.8.11)$$

These give the geostrophic velocities outside the boundary layer.

1st order terms:
$$\begin{cases} \nabla \cdot \underline{u}_{g_1} = 0 \\ 2 \underline{k} \times \underline{u}_{g_1} + \nabla p_{g_1} = 0 \end{cases} \quad (1.8.12)$$

This represents another geostrophic flow (but, of course, multiplied by the factor $E^{1/2}$).

2nd order terms:
$$\begin{cases} \nabla \cdot \underline{u}_{g_2} = 0 \\ 2 \underline{k} \times \underline{u}_{g_2} + \nabla p_{g_2} - \nabla^2 \underline{u}_{g_0} = 0 \end{cases} \quad (1.8.13)$$

This and higher order terms are of similar form.

Now fix $\zeta \neq 0$ and let $E \rightarrow 0$ (i.e. look inside the boundary layer).

-1th order terms
$$\begin{cases} \frac{\partial \hat{w}_0}{\partial \zeta} = 0 \\ \frac{\partial \hat{p}_0}{\partial \zeta} = 0 \end{cases} \quad (1.8.14)$$

Since \hat{w}_0 and \hat{p}_0 vanish as $\zeta \rightarrow \infty$,

$$\hat{p}_0 = \hat{w}_0 = 0$$

Zeroth order terms:
$$\begin{cases} \frac{\partial \hat{w}_1}{\partial \zeta} + \nabla_H \cdot \hat{u}_0 = 0 \\ 2 \underline{k} \times \hat{u}_0 + \frac{\partial \hat{p}_1}{\partial \zeta} \underline{k} + \nabla_H \hat{p}_0 - \frac{\partial^2 \hat{u}_0}{\partial \zeta^2} = 0 \end{cases} \quad (1.8.15)$$

$\hat{p}_0 = 0$ from above, and $\frac{\partial \hat{p}_1}{\partial \zeta} \underline{k}$ in the only term in the third direction.

Hence: $\hat{p}_1 = 0$ as well.

Thus
$$2\underline{k} \times \hat{\underline{u}}_0 - \frac{\partial^2 \hat{\underline{u}}_0}{\partial \zeta^2} = 0.$$

Now the boundary condition on $\hat{\underline{u}}_0$ is that $\hat{\underline{u}}_0 = -\hat{\underline{u}}_{g_0}$ at $\zeta = 0$, to make $\underline{u} = 0$ on the boundary.

Thus

$$\hat{\underline{u}}_0 = -\text{Re} \left\{ \left[\underline{u}_{g_0} + i(\underline{k} \times \underline{u}_{g_0}) \right] \exp[-(1-i)\zeta] \right\} \quad (1.8.16)$$

(by comparison with the solution of (1.8.2))

$$\nabla_H \cdot \hat{\underline{u}}_0 = -\text{Re} \left\{ -i \nabla \times \underline{u}_{g_0} \cdot \underline{k} e^{-(1-i)\zeta} \right\} \quad (1.8.17)$$

Hence, by integrating (1.8.15)

$$\hat{\omega}_1 = -\text{Re} \left\{ \underbrace{(-i \nabla \times \underline{u}_{g_0} \cdot \underline{k})}_{\text{independent of } \zeta} e^{-(1-i)\zeta} \frac{1}{(1-i)} \right\} \quad (1.8.18)$$

This can now be used to get the value of ω_{g_1} at the wall:

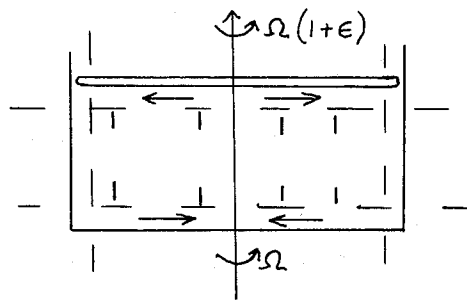
$$\omega_{g_1}(0) = -\text{Re} \left\{ (\nabla \times \underline{u}_{g_0} \cdot \underline{k}) \left(\frac{i}{1-i} \right) \right\} = \frac{1}{2} \left[\nabla \times \underline{u}_{g_0} \cdot \underline{k} \right] \quad (1.8.19)$$

This implies that there is a vertical geostrophic flow of order $E^{1/2}$ if the zeroth order vorticity does not vanish.

Higher order terms in the expansion can be obtained with a certain amount of labour.

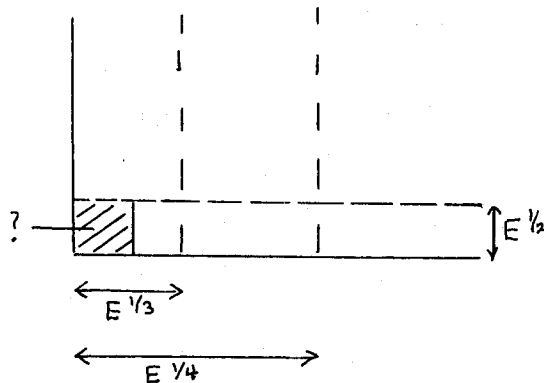
Here endeth the formal treatment. Professor Howard then spent some time in discussing some other problems in a non-rigorous way.

(i) Right circular cylinder with top rotating slightly faster than the bottom and sides.



It is found that the central geostrophic flow rotates with the average angular velocity $\Omega \left(1 + \frac{1}{2}\epsilon\right)$, while at the bottom and top there are Ekman layers of thickness $E^{1/2}$, causing an upward interior flow of order $E^{1/2}$.

The structure of the side wall boundary layers is found to be more complicated, although they only have a local effect.



In the $E^{1/4}$ layer there is no vertical dependence, the horizontal flow is adjusted to the boundary condition, whereas the $E^{1/3}$ layer does have vertical structure. What happens in the corner has not been fully resolved.

(ii) Containers with Sloping Bottoms:

In this case, the expansion becomes more complicated, viz:

$$\begin{aligned} \underline{u} &= \underline{u}'_{g_0}(x, y, z, t) + E^{1/2} \underline{u}'_{g_1} + \dots \\ &+ \hat{\underline{u}}_0(x, y, \zeta, t) + E^{1/2} \hat{\underline{u}} + \dots \\ &+ \underline{u}_{g_0}(x, y, z, \tau) + \dots \\ &+ \hat{\underline{u}}_0(x, y, \zeta, \tau) + \dots \end{aligned}$$

where $\tau = E^{1/2} t$.

In the axisymmetric case, only geostrophic normal modes are excited by small change of rotation rate. The motions are damped on the τ time scale.

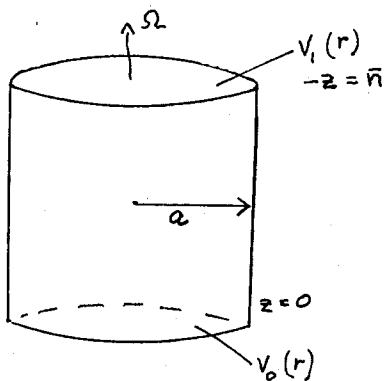
Notes submitted by
Philip Hazel

REFERENCES

- Greenspan, H. P., 1964. J.Fl.Mech. 20: 673
Greenspan, H. P., 1965. J.Fl.Mech. 22(3): 449-462
Greenspan, H. P. and L. N. Howard, 1963. "On a time dependent motion of a rotating fluid". J.Fl.Mech. 17: 385-404

Lecture #4.

9. As an example of a system exhibiting the various boundary layers discussed in the previous lecture, consider a rotating cylinder whose top and bottom are rotating non-rigidly and at different rates. The side wall is rotating with a given tangential velocity. Thus the boundary conditions on the tangential velocity $v(r, \theta, z)$ are:



$$v(r, z=0) = v_0(r)$$

$$v(r, z=\pi) = v_1(r)$$

$$v(r=a, z) = v(z)$$

For the radial and vertical velocities:

$$u, w = 0 \text{ on all of the boundaries.}$$

We assume that the flow is steady and axisymmetric ($\frac{\partial}{\partial \theta} \rightarrow 0$). In cylindrical coordinates the equations of motion and continuity become:

$$-2v + p_r = E (\nabla^2 u - u/r^2)$$

$$2u = E (\nabla^2 v - v/r^2)$$

$$p_z = E \nabla^2 w$$

$$\frac{1}{r} (r u)_r + w_z = 0$$

In the interior region, we expect the motion to be geostrophic and hydrostatic and we have

$$-2v + p_r = 0, \quad u = 0, \quad p_z = 0, \quad w_z = 0.$$

It is clear that in order to match the boundary conditions at top and bottom, we will have an Ekman layer and the interior solution must connect onto the Ekman solution. From the previous lecture we have that solution just above the bottom layer ($z=0$) is proportional to the difference between the vorticity of the interior flow and the flow on the boundary:

$$w_{(0)} = \frac{1}{2} E^{1/2} [\underline{k} \cdot \underline{\omega}^I - \underline{k} \cdot \underline{\omega}^{(0)}] = \frac{1}{2} E^{1/2} \left[\frac{1}{r} (r v)_r - \frac{1}{r} (r v_0(r))_r \right]$$

and just below the top layer ($z=\pi$)

$$w_{(\pi)} = \frac{1}{2} E^{1/2} \left[\frac{1}{r} (r v_1(r))_r - \frac{1}{r} (r v(r))_r \right]$$

Now in the interior $w_z = 0$ so

$$w_{(\pi)} = w_{(0)} \text{ and thus } v(r) = \frac{1}{2} [v_0(r) + v_1(r)]$$

What else could it be? We now have the interior solution

$$v^I(r) = \frac{1}{2} (V_0(r) + V_1(r))$$

$$u^I(r) = 0 \quad O(E)$$

$$w^I(r) = \frac{1}{4} E^{1/2} \left\{ \frac{1}{r} (rV_1(r))_r - \frac{1}{r} (rV_0(r))_r \right\}$$

Since these velocities are independent of z they have no hope of satisfying the boundary conditions at $r=a$. We must have boundary layers at $r=a$.

If the top is turning faster than the bottom, the vertical velocity will be upward in the interior which means that fluid is being transported from bottom to top (driven by the Ekman pumping and suction) - somewhere an equal amount must be going down.

Try a boundary layer near $r=a$ of width $E^{1/4}$:

$$r = a - E^{1/4} \rho$$

The equations of motion become:

$$-2v - E^{-1/4} p_\rho = E^{1/2} u_{\rho\rho}$$

$$2u = E^{1/2} v_{\rho\rho}$$

$$p_z = E^{1/2} w_{\rho\rho}$$

$$-E^{-1/4} u_\rho + w_z = 0$$

If we assume that the solution in this $1/4$ -layer will match onto the interior solution then $v = O(1)$ and $u = O(E^{1/2})$. Then $u_\rho = O(E^{1/2})$ and w_z is $O(E^{1/4})$.

Then p_z is $O(E^{3/4})$. If we take $p_z = 0$, the p_ρ must have a part that is $O(E^{1/4})$ to balance v . Then we have in the $1/4$ -layer:

$$2v - E^{-1/4} p_\rho = 0 \quad 1.9.1 \text{ a}$$

$$-2u = E^{1/2} v_{\rho\rho} \quad 1.9.1 \text{ b}$$

$$p_z = 0 \quad 1.9.1 \text{ c}$$

$$-E^{-1/4} u_\rho + w_z = 0 \quad 1.9.1 \text{ d}$$

From (a), (b) and (c) we have

$$v_z = \frac{E^{-1/4}}{2} \rho \rho_z = 0 \quad \text{and} \quad u_z = \frac{1}{2} E^{1/2} v_{z\rho\rho} = 0$$

and $w_{z\bar{z}} = E^{1/4} u_{z\rho} = 0$. Thus w is a linear function of z in the $1/4$ layer. Since this layer is much thicker than the Ekman ($1/2$) layers we can expect that the w in the $1/4$ layer connects onto the Ekman solutions. If we assume that the vorticity at the wall is $O(1)$ (i.e. $\frac{1}{r} (r v_{\theta,1}(r))_r = O(1)$), we can neglect those terms with respect to $\frac{1}{r} (r v(r))_r$ in the $1/4$ layer.

$$w(0) = \frac{1}{2} E^{1/2} \left[-E^{-1/4} v_\rho + o(1) \right]$$

$$w(\pi) = \frac{1}{2} E^{1/2} \left[E^{-1/4} v_\rho + o(1) \right]$$

Since $w(z)$ is linear in the $1/4$ layer we have,

$$w(z) = E^{1/4} v_\rho \left(\frac{z - \pi/2}{\pi} \right)$$

Substituting this into (1.9.1 d)

$$u_\rho = E^{1/4} w_z = (E^{1/2}/\pi) v_\rho$$

and

$$u = \frac{1}{2} E^{1/2} v_{\rho\rho}$$

so that

$$v_{\rho\rho\rho} - 2/\pi v_\rho = 0.$$

Since this is a boundary layer we pick the decaying exponential and write

$$v(\rho) = K + C e^{-\sqrt{\frac{2}{\pi}} \rho}.$$

Matching this to the interior solution, we have

$$\lim_{\rho \rightarrow \infty} v(\rho) = \lim_{r \rightarrow a} v(r) = \frac{1}{2} (v_0(a) + v_1(a))$$

and

$$v(\rho) = \frac{1}{2} (v_0(a) + v_1(a)) + C e^{-\sqrt{\frac{2}{\pi}} \rho}$$

Then

$$u = \frac{1}{2} E^{1/2} v_{\rho\rho} = \frac{E^{1/2}}{\pi} C e^{-\sqrt{\frac{2}{\pi}} \rho}$$

and

$$w = E^{1/4} \left(\frac{z - \pi/2}{\pi} \right) \left(-\sqrt{\frac{2}{\pi}} C e^{-\sqrt{\frac{2}{\pi}} \rho} \right).$$

Clearly u and w match onto 0 in the interior.

Again we cannot expect to satisfy the boundary condition and set $\lim_{\rho \rightarrow 0} v(\rho) = V(\bar{z})$ since v is independent of \bar{z} . At best we can hope to bring v to the average value of $V(\bar{z})$ over the wall with the constant C . We will have to have another boundary layer narrower than $E^{1/4}$ in which the velocity depends on \bar{z} .

To get a narrower boundary layer, let us try $r = a - E^{1/3} \eta$

$$\begin{aligned} 2v - E^{-1/3} p_\eta &= E^{1/3} u_{\eta\eta} \\ 2u &= E^{1/3} v_{\eta\eta} \\ p_z &= E^{1/3} w_{\eta\eta} \\ -E^{-1/3} u_\eta + w_z &= 0 \end{aligned} \tag{1.9.2}$$

We can expect that $v = O(1)$ in this $1/3$ layer. Then from (1.9.2) we have

$$v = O(1) \Rightarrow u = O(E^{1/3}) \Rightarrow w = O(1) \Rightarrow p_z = O(E^{1/3}).$$

We expect that $p_\eta = O(E^{1/3})$ and balances $2v$. If w is $O(1)$, we seem to be in trouble with the Ekman layers (still assumed to be much thinner than the $1/3$ layer). At the edges of the Ekman layers we have

$$w = \frac{E^{1/2}}{2} [\mp E^{-1/3} v_\eta] = \mp \frac{E^{1/6}}{2} v_\eta$$

This obviously cannot match a w that is $O(1)$ in the interior ($0 < \bar{z} < \pi$) of the $1/3$ layer unless it is zero at top and bottom. The solution must have two terms in the $1/3$ layer - one with a w that is $O(1)$ and goes to zero at $\bar{z} = 0$ and π and one that is $O(E^{1/6})$ and matches the Ekman layer. Presumably one has to expand in powers of $E^{1/12}$ to get the full solution. This is in fact typical when $1/3$ and $1/4$ layers are present.

From (1.9.2) we have

$$\begin{aligned} E^{1/3} w_{\eta\eta\eta} = p_{z\eta} &= -2 E^{1/3} v_z \Rightarrow w_{\eta\eta\eta} = -2 v_z \\ E^{1/3} v_{\eta\eta\eta} = +2 u_\eta &= +2 E^{1/3} w_z \Rightarrow v_{\eta\eta\eta} = 2 w_z \end{aligned}$$

or

$$\left(\frac{\partial^6}{\partial \eta^6} + 4 \frac{\partial^2}{\partial z^2}\right) w = 0 \quad \text{and} \quad v_z = -\frac{1}{2} w_{\eta\eta\eta} \quad (1.9.3)$$

Take w as $O(1)$ and $w(0) = 0 = w(\pi)$. Expanding w in a sine series,

$$w(\eta, z) = \sum_{n=1}^{\infty} w_n(\eta) \sin n z. \quad (1.9.4)$$

Since the eigenfunctions $\sin n z$ satisfy the boundary conditions we can formally differentiate (1.9.4) term by term to get an equation for $w_n(\eta)$,

$$\frac{\partial^6}{\partial \eta^6} w_n(\eta) = 4 n^2 w_n(\eta).$$

We retain the three sixth roots of $4 n^2$ with negative real part:

$$w_n(\eta) = K_n e^{-(2n)^{1/3} \eta} + L_n e^{(2n)^{1/3} \eta} e^{2i\pi/3} + M_n e^{(2n)^{1/3} \eta} e^{-2i\pi/3}$$

Clearly as $\eta \rightarrow \infty$, $w_n(\eta) \rightarrow 0$ and $w(\eta, z) \rightarrow 0$ as they must since there is no w of $O(1)$ in the interior (i.e. $1/4$ layer). From (1.9.3) we obtain

$$v(\eta, z) = \frac{1}{2} W_0(\eta) + \sum_{n=1}^{\infty} \frac{w_n'''(\eta)}{2n} \cos n z$$

where $\frac{1}{2} W_0(\eta)$ is an integration constant which is at most quadratic in η .

Differentiating this gives

$$u(\eta, z) = \frac{E^{1/3}}{2} \left\{ \sum_{n=1}^{\infty} \frac{w_n''(\eta)}{2n} \cos n z + \frac{1}{2} W_0''(\eta) \right\}$$

If $u(\eta, z)$ is to match onto the $\rho \rightarrow 0$ limit of the $1/4$ layer solution

$$\frac{E^{1/3}}{4} W_0(\eta \rightarrow \infty) = \frac{E^{1/2}}{\pi} C \left(1 - \sqrt{\frac{2}{\pi}} \rho\right)_{\rho \rightarrow 0}$$

Since W_0 is at most quadratic W_0'' is a constant and must vanish as there is nothing for it to match up with. Looking at the $\rho \rightarrow 0$ limit of v in the

$1/4$ layer shows that $W_0(\eta)$ must be a constant:

$$\begin{aligned} \lim_{\eta \rightarrow \infty} v(\eta, z) &= \frac{1}{2} W_0(\eta \rightarrow \infty) = \frac{1}{2} [V_0(a) + V_1(a)] + C \left[1 - \sqrt{\frac{2}{\pi}} \rho\right] \\ &= \frac{1}{2} [V_0(a) + V_1(a)] + C - \sqrt{\frac{2}{\pi}} C E^{1/2} \eta. \end{aligned}$$

W_0 is assumed to be $O(1)$ so that it must be a constant. Thus

$$C = \frac{1}{2} W_0 - \frac{1}{2} [V_0(a) + V_1(a)]$$

The tangential velocity at the wall $r = a (\eta \rightarrow 0)$ must be $V(z)$:

$$V(z) = \frac{1}{2} W_0 + \sum_1^{\infty} \frac{1}{2n} W_n'''(0) \cos n z$$

which gives

$$\frac{1}{2} W_0 = \frac{2}{\pi} \int_0^{\pi} dz V(z) \quad (1.9.5)$$

$$W_n'''(0) = \frac{2}{\pi} \int_0^{\pi} dz \cos n z V(z). \quad (1.9.6)$$

Thus we have W_0 and C . Equation (1.9.6) together with the conditions that u and w are zero on the wall give three conditions for each n which are sufficient to determine the constants K_n, L_n and M_n . With the exception of the second ($w \sim E^{1/6}$) part of the solution this completes the boundary layer solutions.

Notes submitted by
James R. Luyten

Lecture #5

II. Rotating Homogeneous Fluids with Free Surfaces

1. Long surface waves in a shallow, rotating, homogeneous fluid:

We suppose that the system we are considering is such that

$\underline{u} \cdot \nabla \underline{u} \ll 2 \underline{\Omega} \times \underline{u}$. Then we have

$$\begin{cases} \underline{u}_t + 2 \underline{\Omega} \times \underline{u} + \nabla p + g \underline{k} = 0 \\ \nabla \cdot \underline{u} = 0 \end{cases} \quad (2.1.1)$$

Consider the third component of the momentum equation:

$$w_t + 2 (\underline{k} \cdot \underline{\Omega} \times \underline{u}) + p_z + g = 0$$

Now w_t and $2 \underline{k} \cdot \underline{\Omega} \times \underline{u}$ are small terms compared with g . Thus we have an approximate hydrostatic balance. If the region containing the fluid is defined by

$$-H(x, y) \leq z \leq \zeta(x, y, t)$$

then, choosing p to be zero at the surface gives

$$p = g(\zeta - z) \quad (2.1.2)$$

The horizontal part of (2.1.1) is then

$$(\underline{u}_t)_H + 2(\underline{\Omega} \times \underline{u})_H + g \nabla_H \zeta = 0 \quad (2.1.3)$$

Now

$$\begin{aligned} (\underline{\Omega} \times \underline{u})_H &= -\underline{k} \times (\underline{k} \times (\underline{\Omega} \times \underline{u})) = -\underline{k} \times (W \underline{\Omega} - \underline{k} \cdot \underline{\Omega} \underline{u}) \\ &= -\underline{k} \times \underline{\Omega} W + (\underline{k} \cdot \underline{\Omega}) \underline{k} \times \underline{u} \end{aligned}$$

Now $W \ll (\underline{u})_H$ for the motions we are interested in. Thus we omit the term $-\underline{k} \times \underline{\Omega} W$. This is tantamount to taking $\underline{\Omega}$ to be vertical, but with magnitude $(\underline{\Omega} \cdot \underline{k})$.

Writing now Ω for the vertical component of $\underline{\Omega}$,

$$\begin{cases} u_t - 2\Omega v + g \zeta_x = 0 \\ v_t + 2\Omega u + g \zeta_y = 0 \end{cases} \quad (2.1.4)$$

The continuity equation is

$$u_x + v_y + w_z = 0$$

Since ζ_x and ζ_y are independent of z , we expect u and v to be independent also. Integrate the continuity equation: (from $-H$ to $+\zeta$)

$$(u_x + v_y)(H + \zeta) + w_T - w_B = 0 \quad (2.1.5)$$

Now the dynamic conditions on the top and the bottom (saying, essentially, that a particle on the surface moves along it) are:

$$\begin{cases} \frac{D}{Dt}(\zeta - \zeta) = 0 = w_T - \zeta_t - u \zeta_x - v \zeta_y \\ \frac{D}{Dt}(\zeta + H) = 0 = w_B + u H_x + v H_y \end{cases} \quad (2.1.6)$$

Substituting into (2.1.5):

$$(u_x + v_y)(H + J) + J_{tt} + u J_x + v J_y + u H_x + v H_y = 0$$

i.e. $J_{tt} + \frac{\partial}{\partial x}(u[H + J]) + \frac{\partial}{\partial y}(v[H + J]) = 0$

We can ignore J with respect to H , giving

$$J_{tt} + \frac{\partial}{\partial x}(uH) + \frac{\partial}{\partial y}(vH) = 0 \quad (2.1.7)$$

Suppose for the moment that the fluid is not rotating. Then substitution of (2.1.4) into (2.1.7), with $\Omega = 0$, gives

$$J_{tt} - g \left\{ (H J_x)_x + (H J_y)_y \right\} = 0$$

The boundary condition is $\frac{\partial J}{\partial n} = 0$ at vertical side walls.

Write $\frac{\partial}{\partial t} = i\sigma$ to get out the normal modes:

$$\implies \frac{\sigma^2}{g} J + (H J_x)_x + (H J_y)_y = 0$$

Multiply by J and integrate over the area of the base:

$$\begin{aligned} \frac{\sigma^2}{g} \int_A J^2 dA &= - \int_A (H J_x)_x J dA - \int_A (H J_y)_y J dA \\ &= - \int_A J \nabla \cdot (H J_x, H J_y) dA \end{aligned}$$

i.e. $\frac{\sigma^2}{g} \int_A J^2 dA = - \int_A \left\{ \nabla \cdot [JH(J_x, J_y)] - \nabla J \cdot (H J_x, H J_y) \right\} dA$

But on the boundary, $(J_x, J_y) \cdot \underline{n}$ is the normal derivative of J , and is therefore zero. Thus, applying the divergence theorem, the first right-hand side integral vanishes.

$$\frac{\sigma^2}{g} = \frac{\int_A H (J_x^2 + J_y^2) dA}{\int_A J^2 dA} \quad (2.1.8)$$

The minimum eigenvalue, σ_0 , can be found from this by minimizing the right-hand side over all functions satisfying $\int_A J dA = 0$.

For the rotating case, looking for normal modes gives

$$\begin{cases} i\sigma u - 2\Omega v = -g J_x \\ 2\Omega u + i\sigma v = -g J_y \end{cases} \quad (2.1.9)$$

from (2.1.4).

Solving for u and v :

$$\begin{cases} (\sigma^2 - 4\Omega^2)u = g(i\sigma J_x + 2\Omega J_y) \\ (\sigma^2 - 4\Omega^2)v = g(-2\Omega J_x + i\sigma J_y) \end{cases} \quad (2.1.10)$$

(N.B. expect peculiarities at $\sigma = \pm 2\Omega$)

Substituting into (2.1.7) gives

$$(\sigma^2 - 4\Omega^2)i\sigma \zeta + \frac{\partial}{\partial x} \left[gH(i\sigma \zeta_x + 2\Omega \zeta_y) \right] + \frac{\partial}{\partial y} \left[gH(-2\Omega \zeta_x + i\sigma \zeta_y) \right] \quad (2.1.11)$$

If we look for a harmonic plane wave,

$\zeta \propto e^{ikx}$ say, we have, in the case $H = \text{constant}$,

$$(\sigma^2 - 4\Omega^2)i\sigma - gHk^2 i\sigma = 0$$

$$\sigma = 0 \quad \text{or} \quad \sigma^2 = gHk^2 + 4\Omega^2 \quad (2.1.12)$$

In the case $\sigma = 0$, we have from (2.1.10)

$$\begin{cases} u = -\frac{g}{2\Omega} \zeta_y \\ v = \frac{g}{2\Omega} \zeta_x \end{cases}$$

So (2.1.7) becomes

$$\frac{\partial}{\partial x} \left(-\frac{gH}{2\Omega} \zeta_y \right) + \frac{\partial}{\partial y} \left(\frac{gH}{2\Omega} \zeta_x \right) = 0$$

This is identically true if $H = \text{constant}$. The geostrophic flows are thus included as normal modes of zero frequency.

If $H \neq \text{const.}$

$$-\frac{\partial H}{\partial x} \zeta_y + \frac{\partial H}{\partial y} \zeta_x = \frac{\partial(H, \zeta)}{\partial(x, y)} = 0$$

This implies that ζ is constant along lines of constant depth.

The Special Case $\sigma = 2\Omega$:

If $\sigma = 2\Omega$, from (2.1.9),

$$\begin{aligned} (u+iv)2\Omega &= ig\zeta_x \\ (u+iv)2\Omega &= -g\zeta_y \end{aligned}$$

$$\Rightarrow \zeta_x = i\zeta_y$$

$\Rightarrow \zeta$ is an analytic function of $(x-iy)$.

(If the flow is unbounded, $\zeta = 0$ is the only solution. This implies motions with inertial period, involving no surface elevation.)

" β -Plane" Solutions:

Return now to the general case, and substitute $H = H_0 + \beta y$ into (2.1.11).

β is taken to be small, so that we may put $H \cong H_0$, but keep $H_y = \beta$. Thus:

$$(\sigma^2 - 4\Omega^2)i\sigma\zeta + gH_0[i\sigma(\zeta_{xx} + \zeta_{yy})] + g\beta(-2\Omega\zeta_x + i\sigma\zeta_y) = 0 \quad (2.1.13)$$

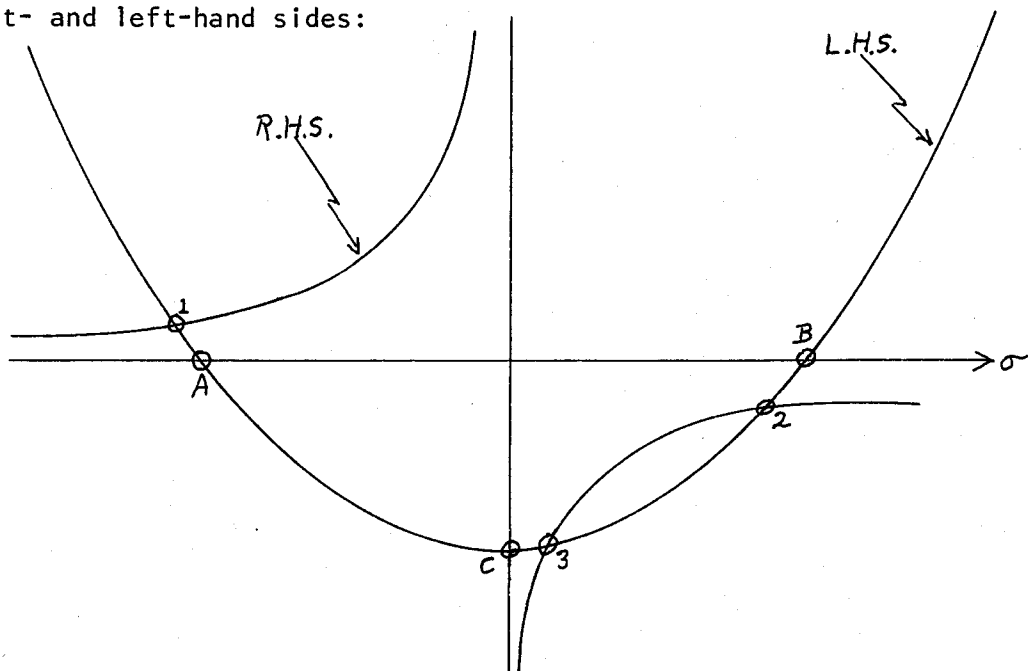
If $\zeta \propto e^{-ikx}$ (plane waves in x direction)

$$(\sigma^2 - 4\Omega^2)i\sigma + gH_0(-k^2i\sigma) + 2\Omega g\beta ik = 0$$

(We note the $\sigma = 0$ is no longer a solution. The geostrophic flows in this system are along lines of constant y , and do not vary with x .) Hence

$$\sigma^2 - 4\Omega^2 - k^2gH_0 = \frac{-2\Omega g\beta k}{\sigma} \quad (2.1.14)$$

The behaviour of the solution to this equation is brought out by plotting graphs of the right- and left-hand sides:

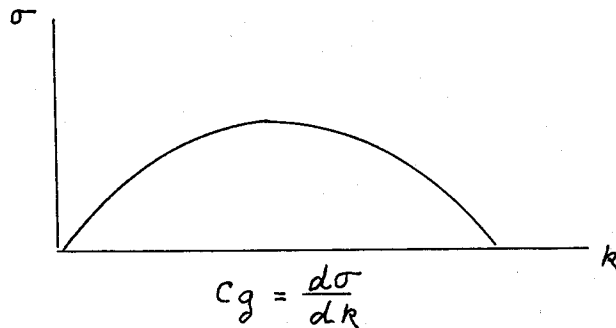


in the previous case where H was constant ($\beta = 0$) the hyperbola degenerates into two straight lines coincident with the axes, and the solutions for σ are given by the points A, B, C. (cf. (2.1.12)). The effect of making β small but non-zero is to shift the solutions slightly off the axes. Solutions 1 and 2 are qualitatively similar to the previous case, but the geostrophic modes represented by solution c have been shifted to oscillatory modes of small frequency (solution 3). Since σ is small, we can solve (2.1.14) approximately to get

$$\sigma_3 \doteq \frac{2\Omega g \beta k}{4\Omega^2 + g H_0 k^2} \quad (2.1.15)$$

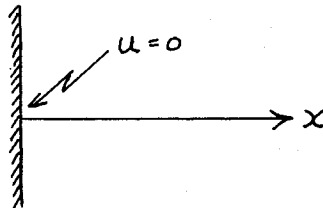
These waves are called Rossby waves. Note that k has the same sign as σ so the waves always have a phase velocity in the same direction (Eastwards if $\beta > 0$).

The group velocity, however, can be in either direction:



The effect of boundaries

Consider a region $x \geq 0$ with $H = H_0$.



Equation (2.1.11) becomes

$$(\sigma^2 - 4\Omega^2)\zeta + gH_0(\zeta_{xx} + \zeta_{yy}) = 0 \quad (2.1.16)$$

The boundary condition, $u = 0$ on $x = 0$, becomes (from (2.1.9)),

$$i\sigma\zeta_x + 2\Omega\zeta_y = 0 \quad \text{on } x = 0$$

provided $\sigma^2 \neq 4\Omega^2$.

Put $\zeta = e^{-iky}\phi(x)$ i.e. Fourier analyse in y .

$$\begin{aligned} \Rightarrow \phi'' + \left[\frac{\sigma^2 - 4\Omega^2}{gH_0} - k^2 \right] \phi = 0 \\ \text{boundary condition: } \phi'(0) = \frac{2\Omega k}{\sigma} \phi(0) \end{aligned} \quad (2.1.17)$$

This is a Sturm-Liouville type system, except that the eigenvalue σ appears in the boundary condition.

$$\text{Solution is } \phi = \exp\left\{-\sqrt{\frac{4\Omega^2 + gH_0k^2 - \sigma^2}{gH_0}} x\right\} \text{ if } \sigma^2 < 4\Omega^2 + gH_0k^2$$

From the boundary condition:

$$-\sqrt{\frac{4\Omega^2 + gH_0k^2 - \sigma^2}{gH_0}} = \frac{2\Omega k}{\sigma}$$

(note this means $\sigma/k < 0$).

$$\text{Thus } 4\Omega^2 + gH_0k^2 - \sigma^2 = \frac{4\Omega^2 k^2}{\sigma^2} gH_0$$

$$\text{i.e. } (\sigma^2 - 4\Omega^2)(\sigma^2 - k^2 gH_0) = 0$$

Ignore the $\sigma = \pm 2\Omega$ root, as we have already discarded this in deriving the boundary condition.

$$\text{Thus } \phi = \exp\left[\frac{-2\Omega}{\sqrt{gH_0}} x\right] \quad (2.1.18)$$

and σ and k have opposite signs. Thus the wave propagates in the negative

y direction, and decays exponentially with x. These waves are called Kelvin waves.

A circular lake with a paraboloidal bottom (brief description).

$$H = H_0 \left(1 - \frac{r^2}{R^2}\right) \quad [\text{cf. Lamb } \S 193]$$

In the non-rotating case we look for modes $\zeta = f(r)e^{in\theta}$

Then, writing $f(r) = g(x), x = r/R$, we get

$$(1-x^2)\left(g'' + \frac{1}{x}g' - \left(\frac{n^2}{x^2}\right)g - 2xg' + \lambda g\right) = 0 \quad (2.1.19)$$

$$\text{where } \lambda = \frac{\sigma^2 R^2}{gH_0}$$

We seek power series solutions for g , and find that the series terminates for particular values of λ .

$$\lambda_{nm} = n(2m+2) + m(m+2)$$

where

$$\begin{cases} n = 0, 1, 2, \dots \\ m = 0, 2, 4, \dots \end{cases}$$

provided n and m are not both zero.

The rotating case:

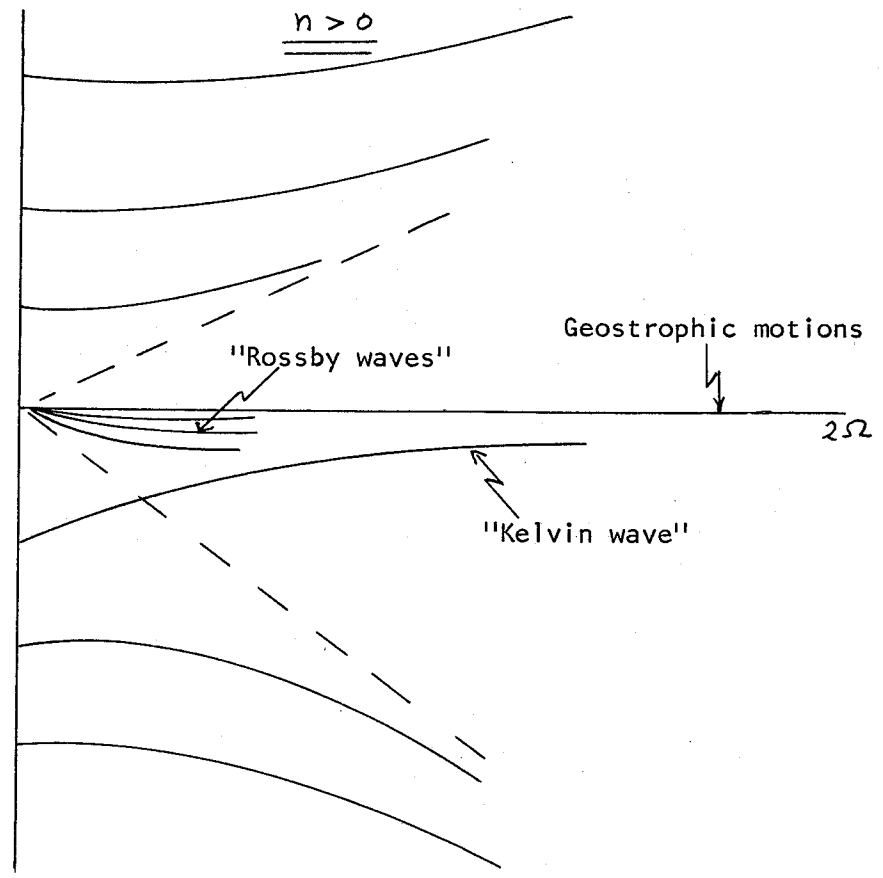
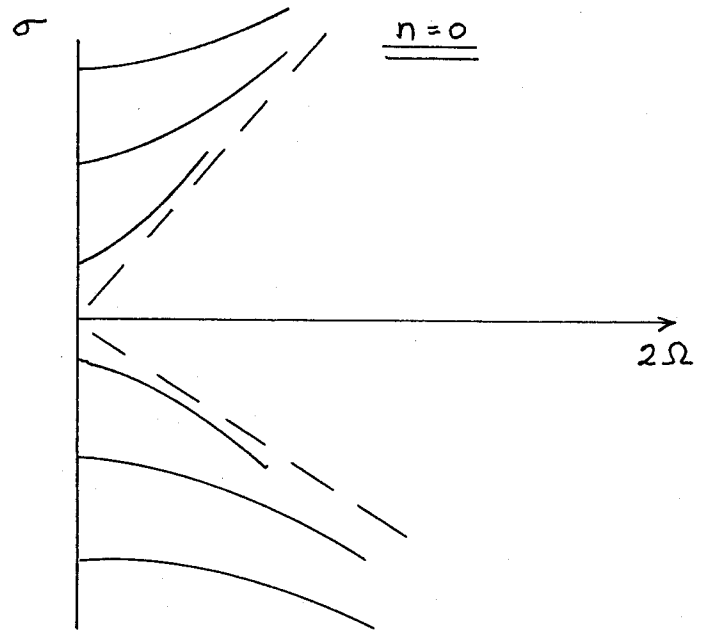
If $n = 0$ (axisymmetric case) we find

$$\sigma^2 = \sigma^{(0)^2} + 4\Omega^2 \quad \text{as we might expect.}$$

If $n > 0$, we find

$$\lambda = (\sigma^2 - 4\Omega^2) \frac{R^2}{gH_0} - \frac{4n\Omega}{\sigma}$$

The following sketches illustrate the behaviour:



Notes submitted by
Philip Hazel

Lecture #6

III. Rotating and Continuously Stratified Fluids - Inviscid Flows

1. Ertel's Theorem

We start by deriving Ertel's Theorem. Consider a non-dissipative, incompressible flow in which the body forces can be derived from a potential function. The governing equations, in an inertial frame of reference, are

$$\nabla \cdot \underline{u} = 0 \quad (3.1.1)$$

$$\underline{u}_t + \underline{u} \cdot \nabla \underline{u} + \frac{1}{\rho} \nabla p + \nabla \phi = 0 \quad (3.1.2)$$

Consider also any function S that satisfied the equation

$$\frac{DS}{Dt} = \frac{\partial S}{\partial t} + \underline{u} \cdot \nabla S = 0 \quad (3.1.3)$$

and the relation

$$\nabla S \cdot (\nabla \rho \times \nabla p) = 0 \quad (3.1.4)$$

By taking the curl of equation (3.1.2) and then the dot product with ∇S we find

$$\nabla S \cdot \frac{D}{Dt} (\nabla \times \underline{u}) - [(\nabla \times \underline{u}) \cdot \nabla \underline{u}] \cdot \nabla S = 0 \quad (3.1.5)$$

If we take the gradient of equation (3.1.3) and then the dot product with $(\nabla \times \underline{u})$ we have

$$(\nabla \times \underline{u}) \cdot \frac{D}{Dt} (\nabla S) + \nabla \times \underline{u} \cdot \nabla \underline{u} \cdot \nabla S = 0 \quad (3.1.6)$$

Adding equations (3.1.5) and (3.1.6) we find

$$\text{ERTEL'S THEOREM} \quad \frac{D}{Dt} (\nabla \times \underline{u} \cdot \nabla S) = 0 \quad (3.1.7)$$

The following are some familiar results that are included in Ertel's theorem.

In a two-dimensional planar flow, independent of the coordinate z , we can choose $S = z$, and (3.1.7) gives the well-known result that

$$\frac{D}{Dt} (\nabla \times \underline{u}) = 0$$

In shallow water theory, consider the function

$$S = \frac{z + H(x, y)}{\zeta(x, y, t) + H(x, y)}$$

where $z = \zeta(x, y, t)$ is the height of the free surface

and $z = -H(x, y)$ is the depth. Note that

$$S = 0 \text{ at } z = -H$$

$$S = 1 \text{ at } z = \zeta$$

and therefore

$$\frac{DS}{Dt} = 0 \text{ at } z = -H \text{ and } z = \zeta \quad (3.1.8)$$

In fact

$$\frac{DS}{Dt} = \frac{1}{(\zeta + H)^2} \left[(\zeta + H) \left(w + \frac{Dw}{Dt} \right) - (z + H) \left(\frac{D\zeta}{Dt} + \frac{DH}{Dt} \right) \right]$$

or

$$\frac{DS}{Dt} = \frac{1}{(\zeta + H)^2} \left[(\zeta + H) (w(\zeta) - w(-H)) - (z + H) (w(\zeta) - w(-H)) \right]$$

In shallow water theory w is a linear function of z and therefore we can write

$$\frac{DS}{Dt} = f_0(x, y) + z f_1(x, y)$$

However, the condition (3.1.8) then implies that, in general,

$$\frac{DS}{Dt} = 0$$

Therefore S is a suitable function for use in Ertel's theorem.

$$\text{With } \nabla \times \underline{u} \cdot \nabla S \simeq (\nabla \times \underline{u}) \cdot \frac{\underline{k}}{H + \zeta}$$

equation (3.1.7) gives

$$\frac{D}{Dt} \left(\frac{\nabla \times \underline{u} \cdot \underline{k}}{H + \zeta} \right) = 0.$$

This result expresses the conservation of potential vorticity.

2. Equations for Flows with Strong Rotation and Stratification

Now we first want to apply Ertel's theorem to a rotating and stratified fluid. The equations (3.1.1) and (3.1.2) are supplemented by the energy equation and the equation of state.

$$\frac{DT}{Dt} = 0 \quad (3.2.1)$$

$$\text{and } \rho = \rho_0 (1 - \alpha T) \quad (3.2.2)$$

If we switch to a frame of reference rotating with angular velocity $\Omega \underline{k}$, then

$$\nabla \times \underline{u} \rightarrow 2 \Omega \underline{k} + \underline{\omega}$$

where $\underline{\omega}$ is the relative vorticity and Ertel's theorem (3.1.7) can be written

$$\frac{D}{Dt} \left[(2 \Omega \underline{k} + \underline{\omega}) \cdot \nabla T \right] = 0 \quad (3.2.3)$$

We further consider a strongly rotating and strongly stratified fluid and linearize about a basic state. That is, we consider

$$|\underline{\omega}| \ll |2 \Omega \underline{k}|$$

and, expressing the temperature as

$$T = T_0(z) + \hat{T},$$

we also consider

$$|\nabla \hat{T}| \ll |T_0'(z)|.$$

Then, including the above linearization and dropping the caret on \hat{T} , equation (3.2.3) becomes

$$\frac{\partial}{\partial t} \left\{ 2 \Omega T_z + T_0'(z) \underline{k} \cdot \underline{\omega} \right\} + 2 \Omega w T_0''(z) = 0 \quad (3.2.4)$$

Now from the linearized form of equation (3.2.1) we have

$$\frac{\partial T}{\partial t} + w T_0'(z) = 0 \quad (3.2.5)$$

Solving for w and substituting in equation (3.2.4), we find

$$\frac{\partial}{\partial t} \left\{ \frac{2\Omega T_z}{T'_0} + \underline{k} \cdot \underline{\omega} \right\} - 2\Omega \frac{T''_0}{(T'_0)^2} \frac{\partial T}{\partial t} = 0$$

Combining terms we obtain

$$\frac{\partial}{\partial t} \left\{ 2\Omega \left(\frac{T}{T'_0} \right)_z + \underline{k} \cdot \underline{\omega} \right\} = 0 \quad (3.2.6)$$

For a closed region another relation comes from taking an area average of equation (3.2.5) in an x, y plane in the region enclosed by the boundaries.

Since
$$\int_A w dx dy = 0$$

equation (3.2.5) gives

$$\frac{\partial \bar{T}}{\partial t} = 0 \quad (3.2.7)$$

where
$$\bar{T} = \int_A T dx dy$$

Now consider the linearized equations, with the Boussinesq approximation,

$$\nabla \cdot \underline{u} = 0 \quad (3.2.8)$$

$$\underline{u}_t + 2\Omega \underline{k} \times \underline{u} + \nabla p - \alpha g T \underline{k} = 0 \quad (3.2.9)$$

$$\frac{\partial T}{\partial t} + w T'_0(z) = 0 \quad (3.2.10)$$

where p is the modified pressure. We nondimensionalize the variables by setting

$$\underline{u} = \frac{\alpha g \Delta T}{\Omega} \underline{u}^*$$

$$T = \Delta T T^*$$

$$t = \Omega^{-1} t^*$$

$$z = L z^*$$

$$p = L \alpha g \Delta T p^*$$

Dropping the stars, the equations in the dimensionless variables become

$$\nabla \cdot \underline{u} = 0 \quad (3.2.11)$$

$$\underline{u}_t + 2 \underline{k} \times \underline{u} + \nabla p - T \underline{k} = 0 \quad (3.2.12)$$

$$\frac{\partial T}{\partial t} + 4S(z)w = 0 \quad (3.2.13)$$

where

$$4S(z) = \frac{\alpha g T'_0(z)}{\Omega^2} = \frac{N^2}{\Omega^2} \quad (3.2.14)$$

We first look at the steady solutions of these equations ("geostrophic flows") in a region \mathcal{R} with the boundary condition

$$\underline{u} \cdot \underline{n} = 0 \text{ on } \partial \mathcal{R} \quad (3.2.15)$$

From equations (3.2.12) and (3.2.13) we find directly

$$\frac{\partial p}{\partial z} = T \quad (3.2.16)$$

$$\text{and } w = 0 \quad (3.2.17)$$

Taking the cross product of \underline{k} with equation (3.2.12) we obtain the horizontal velocity vector

$$\underline{u}_H = \frac{1}{2\Omega} \underline{k} \times \nabla_H p \quad (3.2.18)$$

Therefore, $p = p(x, y, z)$ is a stream function for the horizontal velocities and can be any function, with the restriction, implied by the boundary condition (3.2.15), that p be constant around curves of intersection of $z = \text{constant}$ planes with boundaries in non-horizontal directions. That is

$$p(x, y, z) = \text{constant for } z = \text{constant, } x, y \text{ on } \partial \mathcal{R} \quad (3.2.19)$$

An additional conserved quantity can be found. Taking the dot product of \underline{u} with equation (3.2.12) and using (3.2.13), we have

$$\frac{\partial}{\partial t} \left(\frac{1}{2} \underline{u}^2 \right) + \nabla \cdot (\underline{u} p) + \frac{1}{4S} \frac{\partial}{\partial t} \left(\frac{1}{2} T^2 \right) = 0 \quad (3.2.20)$$

A volume integral of this equation over \mathcal{R} gives the result that

$$\frac{\partial}{\partial t} \frac{1}{2} \int_{\mathcal{R}} \left[(\underline{u}^2) + \frac{T^2}{4S(z)} \right] dz = 0 \quad (3.2.21)$$

Now if we have two solutions, \underline{u}_1, T_1 , and \underline{u}_2, T_2 , and an inner product defined as

$$\langle \underline{u}_1, T_1 | \underline{u}_2, T_2 \rangle = \int_{\mathcal{R}} \left(\underline{u}_1 \cdot \underline{u}_2 + \frac{T_1 T_2}{4S(z)} \right) dV$$

we can show

$$\frac{\partial}{\partial t} \langle \underline{u}_1, T_1 | \underline{u}_2, T_2 \rangle = 0 \quad (3.2.22)$$

To prove this note that, since the equations are linear $\underline{u}_1 - \underline{u}_2, T_1 - T_2$ is also a solution. Therefore, using (3.2.21)

$$\begin{aligned} 0 &= \frac{\partial}{\partial t} \langle | \underline{u}_1 - \underline{u}_2, T_1 - T_2 |^2 \rangle \\ &= \frac{\partial}{\partial t} \left\{ \langle | \underline{u}_1, T_1 |^2 \rangle + \langle | \underline{u}_2, T_2 |^2 \rangle - 2 \langle \underline{u}_1, T_1, \underline{u}_2, T_2 \rangle \right\} \end{aligned}$$

Equation (3.2.22) follows.

Equation (3.2.22) shows that, (with the addition of the complex conjugate in the appropriate place) if there are modes of different frequency, they are orthogonal. That is, if $\underline{u}_1 = \hat{\underline{u}}_1 e^{i\sigma_1 t}$ and $\underline{u}_2 = \hat{\underline{u}}_2 e^{i\sigma_2 t}$ equation (3.2.22) gives

$$i(\sigma_2 - \sigma_1) \langle \hat{\underline{u}}_1, T_1 | \hat{\underline{u}}_2, T_2 \rangle = 0$$

3. The Initial-Boundary-Value Problem - The Geostrophic Component

We now consider the initial value problem governed by equations (3.2.11), (3.2.12) and (3.2.13), boundary conditions (3.2.15), and initial conditions

$$\begin{aligned} \underline{u} &= \underline{u}_{IC}(r) \\ T &= T_{IC}(r) \text{ in } \mathcal{R} \end{aligned}$$

To find the "geostrophic" part of the solution, \underline{u}, T we choose a solution, \underline{v}, θ , of the equations

$$\underline{v} = \frac{1}{2} \underline{k} \times \nabla \varpi \quad (3.3.1)$$

$$\theta = \varpi_z \quad (3.3.2)$$

(where ϖ is the geostrophic pressure function), such that

$$\langle |\underline{u} - \underline{v}, T - \theta|^2 \rangle \text{ is minimized.} \quad (3.3.3)$$

This corresponds to orthogonal projection in the sense of the inner product defined above. Stated in terms of the variation this condition is

$$\delta \langle |\underline{u} - \underline{v}, T - \theta|^2 \rangle = 0 \quad (3.3.4)$$

Further, we do this at $t = 0$, such that $\underline{u} = \underline{u}_{IC}$ and $T = T_{IC}$. Equation (3.3.21) then insures that (3.3.3) is true for all time.

Using equations (3.3.1) and (3.3.2), condition (3.3.4) becomes

$$\int_{\mathcal{R}} \left[(\underline{u} - \underline{v}) \times \underline{k} + \frac{1}{2s} (T - \theta) \underline{k} \right] \cdot \nabla \delta \varpi \, dV = 0. \quad (3.3.5)$$

Integrating equation (3.3.5) by parts to get rid of the derivative of the variation of ϖ , we find

$$\int_{\mathcal{R}} \left\{ \nabla \cdot \left[(\underline{u} - \underline{v}) \times \underline{k} + \frac{1}{2s} (T - \theta) \underline{k} \right] \right\} \delta \varpi \, dV - \int_{\partial \mathcal{R}} \left[(\underline{u} - \underline{v}) \times \underline{k} + \frac{1}{2s} (T - \theta) \underline{k} \right] \cdot \underline{n} \delta \varpi \, dS = 0. \quad (3.3.6)$$

With the particular choice of $\delta \varpi = 0$ on the boundary, equation (3.3.6) yields

$$\nabla \cdot \left[(\underline{u} - \underline{v}) \times \underline{k} + \frac{1}{2s} (T - \theta) \underline{k} \right] = 0 \quad (3.3.7)$$

(Euler's equation in the calculus of variations).

Then equation (3.3.6) becomes

$$\int_{\partial R} \left[(\underline{u} - \underline{v}) \times \underline{k} + \frac{1}{2s} (T - S) \underline{k} \right] \cdot \underline{n} \delta \omega dS = 0 \quad (3.3.8)$$

We can take $\delta \omega$ as an arbitrary function of z on the surface ∂R .

Therefore, it is advantageous to consider the surface specified by

$$r = \rho(\theta, z)$$

so that

$$\underline{n} dS = \frac{\partial \rho}{\partial \theta} \times \frac{\partial \rho}{\partial z} d\theta dz$$

where θ is an angle in the x, y plane. Then equation (3.3.8) becomes

$$\int_{\text{bottom}}^{\text{top}} \delta \omega(z) dz \int_0^{2\pi} \left[(\underline{u} - \underline{v}) \times \underline{k} + \frac{1}{2s} (T - \theta) \underline{k} \right] \cdot \frac{\partial \rho}{\partial \theta} \times \frac{\partial \rho}{\partial z} d\theta = 0. \quad (3.3.9)$$

Using the fact that $\delta \omega$ is an arbitrary function of z , we have

$$\int_0^{2\pi} \left[(\underline{u} - \underline{v}) \times \underline{k} + \frac{1}{2s} (T - \theta) \underline{k} \right] \cdot \frac{\partial \rho}{\partial \theta} \times \frac{\partial \rho}{\partial z} d\theta = 0. \quad (3.3.10)$$

For example, if we consider a circular cylinder

$$\begin{aligned} \rho &= a \underline{r}_1(\theta) + z \underline{k} \\ \frac{\partial \rho}{\partial \theta} &= a \underline{\theta}_1 \\ \frac{\partial \rho}{\partial z} &= \underline{k} \end{aligned}$$

where \underline{r}_1 and $\underline{\theta}_1$ are unit vectors in the r and θ directions of cylindrical polar coordinates, then

$$\frac{\partial \rho}{\partial \theta} \times \frac{\partial \rho}{\partial z} = a \underline{r}_1$$

and (3.3.10) becomes

$$a \int_0^{2\pi} \left[(\underline{u} - \underline{v}) \times \underline{k} \right] \cdot \underline{r}_1 d\theta = 0$$

or, using (3.3.1),

$$\int_0^{2\pi} \underline{u} \cdot \underline{\theta}_1 d\theta = \int_0^{2\pi} \frac{1}{2} \frac{\partial \omega}{\partial r} d\theta \quad (3.3.11)$$

We can see better what equation (3.3.10) means if we, in equation (3.3.8) let $\delta\omega = f(z)$, where f is an arbitrary function of z , and then use the divergence theorem to change the surface integral to a volume integral. The result, using (3.3.7), is

$$\int_{\mathcal{R}} \frac{1}{2S} (T - \theta) f'(z) dV = 0 \quad (3.3.12)$$

This implies

$$\int_A \theta dx dy = \int_A T dx dy \quad (3.3.13)$$

($z = \text{constant}$)

which shows that the horizontal area average of the temperature is carried by the geostrophic flow.

Equation (3.3.7) can be written

$$\underline{k} \cdot \nabla \times \underline{v} + \frac{\partial}{\partial z} \left(\frac{\theta}{2S} \right) = \underline{k} \cdot \nabla \times \underline{u} + \frac{\partial}{\partial z} \left(\frac{T}{2S} \right) \quad (3.3.14)$$

With \underline{v} and θ given by equations (3.3.1) and (3.3.2), equation (3.3.14) gives an equation for ω . The boundary conditions are provided by equations (3.2.19) and (3.3.13) or (3.3.11). In addition, on horizontal parts of the boundary, equation (3.2.13) and boundary condition (3.2.15) give

$$\frac{\partial T}{\partial t} = 0 \quad \text{or} \quad \theta = T (= T_{Ic}).$$

Then, using equation (3.3.2), we have

$$\omega_z = \theta = T \quad \text{on horizontal boundaries.} \quad (3.3.15)$$

We should note that we cannot obtain our previous results, characterizing the steady "geostrophic flows" of a homogeneous fluid, by letting the stratification go to zero in the above expressions. For example, in equation

(3.2.21) S appears in the denominator and it doesn't make sense to formally let $S \rightarrow 0$ in this expression. The present results were obtained from a linearization about a state with strong rotation and strong stratification and, therefore, can not necessarily be expected to reduce smoothly to the case of strong rotation and zero stratification. It might, however, be possible to relate the two cases by including a consideration of the respective unsteady equations and solutions.

Notes submitted by
John S. Allen, Jr.

Lecture #7

In summary, then,

$$\underline{v} = \frac{1}{2} \underline{k} \times \nabla \omega \tag{3.3.16a}$$

$$\theta = \omega_z \tag{3.3.16b}$$

and use of these with (3.3.14) gives

$$\nabla_H^2 \omega + \frac{\partial}{\partial z} \left(\frac{1}{S(z)} \frac{\partial \omega}{\partial z} \right) = 2(\nabla \times \underline{u}) \cdot \underline{k} + \frac{\partial}{\partial z} \left(\frac{T}{S(z)} \right) \tag{3.3.16c}$$

to be solved in R subject to

$$\int_A \theta dx dy = \int_A T dx dy \tag{3.3.17a}$$

where A is an intersection of $z = \text{constant}$ and R .

$$\omega_z = \theta = T \text{ on horizontal parts of } \partial R \tag{3.3.17b}$$

and $\omega = \text{constant}$ on an intersection of ∂R and $z = \text{constant}$.

The right-hand sides of (3.3.16c) and (3.3.17) are independent of time from (3.3.13), (3.3.14) and (3.3.15), so the initial data determine their value.

4. Uniqueness of the steady part of the solution to the initial boundary value problem

Suppose there exist two solutions of (3.3.16) satisfying the same boundary data (3.3.17). Let the difference of those solutions be denoted by ω . Then, (3.3.16c), (3.3.17) are

$$\nabla_H^2 \omega + \frac{\partial}{\partial z} \left(\frac{1}{s(z)} \frac{\partial \omega}{\partial z} \right) = 0 \text{ in } \mathcal{R}, \quad (3.4.1)$$

$$\int_A \omega_z dx dy = 0, \quad (3.4.2)$$

and $\omega_z = 0$ on horizontal parts of $\partial \mathcal{R}$. (3.4.3)

Multiplication of (3.4.1) by ω and integration over \mathcal{R} will give, with an application of the divergence theorem,

$$-\int_{\mathcal{R}} \left[|\nabla_H \omega|^2 + \frac{1}{s} (\omega_z)^2 \right] dV + \int_{\partial \mathcal{R}} \omega \left\{ (\omega_x, \omega_y, \frac{1}{s} \omega_z) \cdot \underline{n} \right\} dS = 0 \quad (3.4.4)$$

The parts of the second integral arising from those horizontal parts of the surface $\partial \mathcal{R}$ are zero by (3.4.3). Hence, only those non-horizontal parts of $\partial \mathcal{R}$, say $\partial \mathcal{R}_V$, contribute to that integral over $\partial \mathcal{R}$. Clearly, $\omega = \omega_B(z)$ on $\partial \mathcal{R}_V$. Using the divergence theorem again,

$$\begin{aligned} & \int_{\partial \mathcal{R}} \omega_B(z) \left\{ (\omega_x, \omega_y, \frac{1}{s} \omega_z) \cdot \underline{n} \right\} dS = \\ & = \int_{\mathcal{R}} \omega_B \nabla \cdot \left\{ (\omega_x, \omega_y, \frac{1}{s} \omega_z) \right\} dV + \int_{\mathcal{R}} \omega_B'(z) \frac{\omega_z}{s} dV = \\ & = \int_{\mathcal{R}} \omega_B'(z) \frac{\omega_z}{s} dV, \text{ by (3.4.1)}. \end{aligned}$$

Putting this into (3.4.4) yields

$$-\int_{\mathcal{R}} \left[|\nabla_H \omega|^2 + \frac{1}{s} \omega_z^2 \right] dV + \int_{\mathcal{R}} \omega_B'(z) \frac{\omega_z}{s} dV = 0$$

Note, however, that because of (3.4.2), the second of these integrals vanishes identically and all that remains of (3.4.4) is

$$\int_{\mathcal{R}} \left(|\nabla_H \omega|^2 + \frac{1}{S} \omega_z^2 \right) dV = 0 \quad (3.4.5)$$

Applying the usual arguments to (3.4.5)

$$\nabla \omega = 0 \quad \text{everywhere in } \mathcal{R} \text{ if } S > 0,$$

which means the solution to (3.4.1) - (3.4.3) is a constant everywhere in \mathcal{R} and hence the solutions to (3.3.16), (3.3.17) are unique to within a constant, i.e. \underline{v} and Θ are unique.

5. The initial-value problem for the cylinder - the steady component

In this section we carry out the above procedure for a right circular cylinder of radius a and height l . Using the original form of the boundary condition for (3.3.16) as derived from the variational principle, (3.3.8) will give, for the cylinder, as previously stated in (3.3.11),

$$\int_0^{2\pi} \omega_r(\vartheta, z) d\vartheta = 2 \int_0^{2\pi} \underline{u} \cdot \underline{\Theta}_1 d\vartheta \quad (3.5.1)$$

Also,

$$\omega_z(r, \vartheta, 0) = T(r, \vartheta, 0)$$

$$\omega_z(r, \vartheta, l) = T(r, \vartheta, l) \text{ by (3.3.17b).}$$

The solution is expected to be of the form

$$\omega = \sum'_{m=-\infty}^{\infty} \sum_{k=1}^{\infty} e^{im\vartheta} J_m(\alpha_k^m r/a) A_{km}(z) + \sum_{k=1}^{\infty} A_k(z) J_0(\alpha_k r/a) + \Gamma(z) \frac{r^2}{2a} \quad (3.5.2)$$

where \sum' means the $m=0$ term is excluded from the sum, and the third term in (3.5.2) is such as to satisfy the boundary value,

$$\frac{1}{2} \int_0^{2\pi} \omega_r(\vartheta, z) d\vartheta = \int_0^{2\pi} \underline{u} \cdot \underline{\Theta}_1 d\vartheta \equiv \pi \Gamma(z) \quad (3.5.3)$$

Since $\omega = \omega(z)$ on $r = a$, one can easily see from (3.5.2) that

$$J_m(\alpha_k^m) = 0 \quad (3.5.4a)$$

and since the last term in (3.5.2) satisfies (3.5.1) identically,

$$J_0'(\alpha_k) = -J_1(\alpha_k) = 0 \quad (3.5.4b)$$

Supposing for the moment that (3.5.2) is a convergent representation of the solution and $\{J_m(\alpha_k^m)\}$ and $\{J_0(\alpha_k)\}$ are complete, one can differentiate term by term and insert (3.5.2) into (3.3.16c). Doing this, one is left with the ordinary differential equation

$$\begin{aligned} \frac{d}{dz} \left(\frac{1}{S(z)} \frac{dA_k}{dz} \right) - \frac{\alpha_k^2}{a^2} A_k = & \left\{ \int_0^a r \left[J_0(\alpha_k r/a) \right]^2 dr \right\}^{-1} \times \\ & \times \int_0^a r J_0(\alpha_k r/a) \left\{ 2(\nabla \times \underline{u}) \cdot \underline{k} + \frac{\partial}{\partial z} \left(\frac{T}{S(z)} \right) - \frac{2\Gamma(z)}{a} \right\} dr \end{aligned} \quad (3.5.5)$$

for the axisymmetric part of the solution, A_k , and another similar doubly-infinite set of equations for the $\{A_{km}\}$, after expanding $\nabla \times \underline{u} \cdot \underline{k} + \frac{\partial}{\partial z} \left(\frac{T}{S(z)} \right)$ in a series of the angular functions $e^{\pm im\vartheta}$.

This is only the steady part of the solution, and in this special case, existence of the solutions of (3.3.16), (3.3.17) has been shown, provided the Fourier-Bessel series is convergent.

6. Oscillations in a Stratified Rotating Fluid

$$\begin{aligned} \text{Putting} \quad \underline{u} &= \hat{\underline{u}}(r) e^{i\sigma t} \\ p &= \hat{p}(r) e^{i\sigma t} \\ T &= \hat{T}(r) e^{i\sigma t} \end{aligned} \quad (3.6.1)$$

into the non-dimensional equations of motion with the Boussinesq approximation, (3.2.11) - (3.2.14), one obtains, dropping the carets,

$$i\sigma \underline{u} + 2\underline{k} \times \underline{u} + \nabla p - T\underline{k} = 0 \quad (3.6.2)$$

$$i\sigma T + 4WS(z) = 0 \quad (3.6.3)$$

$$\nabla \cdot \underline{u} = 0 \quad (3.6.4)$$

The vertical components of (3.6.2), and (3.6.3) are algebraic equations for (T, W) in terms of p_z , and their solution, if $\sigma^2 \neq 4S$, is

$$T = \frac{4S}{\sigma^2 - 4S} \frac{\partial p}{\partial z}, \quad W = \frac{i\sigma}{\sigma^2 - 4S} \frac{\partial p}{\partial z} \quad (3.6.5)$$

Taking the vector product of (3.6.2) with \underline{k} yields the system

$$i\sigma \underline{k} \times \underline{u}_H - 2\underline{u}_H + \underline{k} \times \nabla_H p = 0 \quad (3.6.6)$$

$$2\underline{k} \times \underline{u}_H + i\sigma \underline{u}_H + \nabla_H p = 0$$

which is another algebraic system for $\underline{u}_H (= \underline{u} - \underline{k}w)$ and $\underline{k} \times \underline{u}_H$ in terms of $\nabla_H p$. The solution is easily found to be, provided $\sigma^2 \neq 4$,

$$\underline{u}_H = \frac{1}{\sigma^2 - 4} (i\sigma \nabla_H p - 2\underline{k} \times \nabla_H p) \quad (3.6.7)$$

Insertion of (3.6.5) and (3.6.7) into (3.6.4) then gives an equation for the pressure,

$$\frac{1}{\sigma^2 - 4} \nabla_H^2 p + \frac{\partial}{\partial z} \frac{1}{\sigma^2 - 4S(z)} \frac{\partial p}{\partial z} = 0 \text{ in } \mathcal{R} \quad (3.6.8)$$

and since $\underline{u} \cdot \underline{n} = 0$ there, (3.6.7) will require some combination of directional derivatives to be zero on $\partial \mathcal{R}$. This has been done for the cylinder (cf. Lecture 9).

To determine an upper bound on the values of σ , we multiply (3.6.2) by \underline{u}^* , the complex conjugate of \underline{u} , to give

$$i\sigma \underline{u} \cdot \underline{u}^* + 2 \underline{u}^* \cdot (\underline{k} \times \underline{u}) + \nabla \cdot (p \underline{u}^*) + \frac{4s}{i\sigma} |w|^2 = 0 \quad (3.6.9)$$

using (3.6.3) also. Integrating over \mathcal{R} and $\underline{u}^* \cdot \underline{n} = 0$ on $\partial \mathcal{R}$ (3.6.9)

gives

$$-\int_{\mathcal{R}} (4s|w|^2 - \sigma^2 |\underline{u}|^2) dV + 2i\sigma \int_{\mathcal{R}} \underline{k} \cdot (\underline{u} \times \underline{u}^*) dV = 0 \quad (3.6.10)$$

The second integral can be shown to be purely imaginary, so σ^2 is real.

In fact

$$\left| i \int_{\mathcal{R}} \underline{k} \cdot (\underline{u} \times \underline{u}^*) dV \right| \leq \int_{\mathcal{R}} |\underline{u}|^2 dV$$

so, (3.6.10) is

$$-\sigma^2 \int_{\mathcal{R}} |\underline{u}|^2 dV + \int_{\mathcal{R}} 4s|w|^2 dV \geq -2|\sigma| \int_{\mathcal{R}} |\underline{u}|^2 dV$$

so

$$\begin{aligned} (\sigma^2 - 2|\sigma| + 1) \int_{\mathcal{R}} |\underline{u}|^2 dV &\leq \int_{\mathcal{R}} |\underline{u}|^2 dV + 4 \int_{\mathcal{R}} s|w|^2 dV \\ &\leq \int_{\mathcal{R}} |\underline{u}|^2 dV + 4 \int_{\mathcal{R}} s |\underline{u}|^2 dV \end{aligned}$$

Thus,

$$(|\sigma| - 1)^2 \leq 1 + 4S_{\max},$$

that is

$$|\sigma| \leq 1 + \sqrt{1 + 4S_{\max}}.$$

So, the frequency spectrum is of finite extent, and may also be dense; in any case there must be accumulation points in the interval.

Forced Oscillations

We suppose there is a driving force per unit mass,

$$\underline{u}_t + 2 \underline{k} \times \underline{u} + \nabla p - \underline{k} T = \underline{F}(\underline{r}, t) \quad (3.6.11)$$

as well as a heat source

$$T_t + 4Sw = q(r, t) \quad (3.6.12)$$

$$\nabla \cdot \underline{u} = 0 \quad (3.6.13)$$

and $\underline{u} \cdot \underline{n} = 0$ on ∂R ; \underline{u}, T specified at $t=0$.

In general, of course $\nabla \cdot \underline{F} \neq 0$, so define \underline{V} so that

$$\underline{F} - \nabla \phi = \underline{V} \quad (3.6.14)$$

Now, $\nabla \cdot \underline{F} - \nabla^2 \phi = \nabla \cdot \underline{V}$, and if we suppose $\nabla \cdot \underline{V} = 0$, then with the additional requirement $\underline{V} \cdot \underline{n} = 0$, we have the Poisson Equation to solve.

$$\left. \begin{aligned} \nabla^2 \phi &= \nabla \cdot \underline{F} \text{ in } R \\ \frac{\partial \phi}{\partial n} &= \underline{F} \cdot \underline{n} \text{ on } \partial R. \end{aligned} \right\} \quad (3.6.15)$$

So, one can collapse the $\nabla \phi$ part of \underline{F} into ρ and just consider

$$\left. \begin{aligned} \underline{u}_t + 2\underline{k} \times \underline{u} + \nabla \rho - \underline{k} T &= \underline{v}(r, t) \\ T_t + 4Sw &= q \\ \nabla \cdot \underline{u} &= 0 \end{aligned} \right\} \quad (3.6.16)$$

To solve this, consider

$$\left. \begin{aligned} \underline{u}_{1t} + 2\underline{k} \times \underline{u}_1 + \nabla \rho_1 - \underline{k} T_1 &= 0 \\ T_{1t} + 4Sw_1 &= 0 \\ \nabla \cdot \underline{u}_1 &= 0 \end{aligned} \right\} \quad (3.6.17a)$$

subject to the conditions

$$\left. \begin{aligned} \underline{u}_1(r, t; \tau) &= \underline{v}(r, \tau) \\ T_1(r, t; \tau) &= q(r, \tau) \end{aligned} \right\} \text{ on } t=0 \quad (3.6.17b)$$

Then, the solution of (3.6.16) is

$$\begin{aligned} \underline{u}(\underline{r}, t) &= \int_0^t \underline{u}_1(\underline{r}, t-\tau, \tau) d\tau \\ T(\underline{r}, t) &= \int_0^t T_1(\underline{r}, t-\tau, \tau) d\tau \\ p(\underline{r}, t) &= \int_0^t p_1(\underline{r}, t-\tau, \tau) d\tau \end{aligned} \quad (3.6.18)$$

To prove (3.6.18), note that

$$\underline{u}_t = \underline{u}_1(\underline{r}, 0, t) + \int_0^t \underline{u}_{1,t}(\underline{r}, t-\tau, \tau) d\tau$$

so

$$\begin{aligned} \underline{u}_t + 2\underline{k} \times \underline{u} - \underline{k}T &= \underline{v}(\underline{r}, t) + \int_0^t [\underline{u}_{1,t} + 2\underline{k} \times \underline{u}_1 - \underline{k}T_1] d\tau \\ &= \underline{v}(\underline{r}, t) - \int_0^t \nabla p_1(\underline{r}, t-\tau, \tau) d\tau \end{aligned} \quad (3.6.19)$$

where (3.6.17b) was used first, and then (3.6.17a). Hence, we have (3.6.19)

$$\underline{u}_t + 2\underline{k} \times \underline{u} - \underline{k}T + \nabla p = \underline{v}$$

and similarly

$$T_t + 4wS = Q \quad \text{which are equations (3.6.16)}$$

as are supposed. So, (3.6.18) is the solution of (3.6.16), or the solution of (3.6.11) - (3.6.13) using (3.6.14) to define \underline{v} .

Therefore, by noting (3.6.17b) and using (3.2.6), we get that

$$\underline{k} \cdot \nabla \times \underline{u}_1(\underline{r}, t, \tau) + \left(\frac{T_1(\underline{r}, t, \tau)}{2S} \right)_z = \underline{k} \cdot \nabla \times \underline{F}(\underline{r}, \tau) + \left(\frac{Q}{2S} \right)_z$$

which may then, with (3.6.18), be written as

$$\underline{k} \cdot \nabla \times \underline{u}(\underline{r}, t) + \left(\frac{T(\underline{r}, t)}{2S} \right)_z = \int_0^t \left[\underline{k} \cdot (\nabla \times \underline{F}) + \left(\frac{Q}{2S} \right)_z \right] d\tau \quad (3.6.20)$$

and also

$$T = \int_0^t Q(\underline{r}, \tau) d\tau \quad (3.6.21)$$

Suppose instead that the driving is through the boundary conditions, viz.,

$$(\underline{u} - \underline{V}) \cdot \underline{n} = 0 \quad \text{on } \partial R \quad \text{where } \nabla \cdot \underline{V} = 0.$$

Let $\underline{u} = \underline{V}_t + \underline{v}$ so $\underline{v} \cdot \underline{n} = 0$ on ∂R . Inserting this into (3.2.11) - (3.2.14) gives

$$\begin{aligned} \underline{V}_t + 2\underline{k} \times \underline{v} + \nabla p - \underline{k} T &= -(\underline{V}_t + 2\underline{k} \times \underline{V}) \\ T_t + 4S\omega &= -4S\omega \\ \nabla \cdot \underline{v} &= 0 \end{aligned} \tag{3.6.22}$$

Clearly, the problem with forced boundary conditions is reduced to the previous problem, (3.6.16). For any motion started impulsively, it is known that, at the outset, the motion is irrotational,

$$\nabla \times \underline{V} = 0 \tag{3.6.23}$$

plus $\nabla \cdot \underline{V} = 0$

Using the previous formalism, $\underline{F} = -\underline{V}_t - 2\underline{k} \times \underline{V}$

and $Q = -4S\omega$

Inserting these into (3.6.20) to compute the potential vorticity,

$$\begin{aligned} \nabla \times \underline{F} &= -\nabla \times \underline{V}_t - 2\nabla \times (\underline{k} \times \underline{V}) \\ &= 0 + 2 \frac{\partial \underline{V}}{\partial z} \end{aligned}$$

and $(\nabla \times \underline{F}) \cdot \underline{k} = 2 \frac{\partial \omega}{\partial z}$. However,

so $\underline{k} \cdot \nabla \times \underline{u} + \left(\frac{T}{2S} \right)_z \equiv 0$ for impulsively-started motions, and hence we come to the result that one cannot gain potential vorticity by impulsively-started motions.

Notes submitted by
Michael R. Foster

Lecture #8

IV. Rotating and Stratified Fluids - Viscous Flows

1. Equations

If the effects of viscosity and heat conduction are included, the linearized, non-dimensional, equations (3.2.11) - (3.2.13) become

$$\nabla \cdot \underline{u} = 0 \quad (4.1.1a)$$

$$\underline{u}_t + 2\underline{k} \times \underline{u} + \nabla p - \underline{k} T = E \Delta \underline{u} \quad (4.1.1b)$$

$$T_t + 4Sw = E/\sigma \Delta T \quad (4.1.1c)$$

where $E = \frac{\nu}{L^2 \Omega}$ is the Ekman Number and $\sigma = \frac{\nu}{K}$ is the Prandtl Number.

In this case, the function $S(\underline{z})$ for the basic state should be a linear function of \underline{z} in order to satisfy the right-hand side of equation (4.1.1c).

Writing these equations in cartesian coordinates and considering flows that are independent of y we have

$$u_x + w_z = 0 \quad (4.1.2a)$$

$$u_t - 2v + p_x = E \Delta u \quad (4.1.2b)$$

$$v_t + 2u = E \Delta v \quad (4.1.2c)$$

$$w_t - T + p_z = E \Delta w \quad (4.1.2d)$$

$$T_t + 4Sw = E/\sigma \Delta T \quad (4.1.2e)$$

We can notice the similarity in form between equations (4.1.2b and c) and equations (4.1.2d and e). In fact, in some cases a direct analogy between homogeneous rotating fluids and stratified, non-rotating fluids exists (see

Ref. 1). Without exploring the analogy in full here, we remark that the similarities of the equations, mentioned above, indicate that there should be boundary layers in w and T on vertical boundaries similar to the Ekman layers and the velocity boundary conditions on horizontal boundaries in flows of homogeneous rotating fluids, we can anticipate a similar importance of side-wall boundary conditions and boundary layers in flows of stratified fluids.

2. Spin-up Problems

Let us look just at the simplest spin-up problem, the case of the flow between two infinite parallel plates perpendicular to the axis of rotation, where at $t=0$ the plates are given a small increase in angular velocity. Even though the effect of side walls is important in the flow of stratified fluids, this case, which completely neglects the effects of lateral boundaries, is of interest for comparison with homogeneous flows and with horizontally limited stratified flows.

The equations for axisymmetric flow in cylindrical polar coordinates are

$$\frac{1}{r} (ru)_r + w_z = 0 \quad (4.2.1a)$$

$$u_t - 2v + p_r = E \left(\Delta u - \frac{u}{r^2} \right) \quad (4.2.1b)$$

$$v_t + 2u = E \left(\Delta v - \frac{v}{r^2} \right) \quad (4.2.1c)$$

$$w_t - T + p_z = E \Delta w \quad (4.2.1d)$$

$$T_t + 4ST = E/\sigma \Delta T \quad (4.2.1e)$$

where $\Delta = \left(\frac{\partial^2}{\partial r^2} + \frac{1}{r} \frac{\partial}{\partial r} + \frac{\partial^2}{\partial z^2} \right)$

with boundary conditions

$$u = v = w = T = 0 \quad \text{on } z = \pm 1 \quad (4.2.2)$$

and with initial conditions

$$u = w = T = 0$$

$$v = -r \text{ at } t=0 \quad (4.2.3)$$

Realizing that the solutions for u and v can be represented in the form

$$u = r \mathcal{U}(z, t)$$

$$v = r \mathcal{V}(z, t)$$

and substituting these expressions in equations (4.2.1), we have

$$2\mathcal{U} + w_z = 0 \quad (4.2.3a)$$

$$\mathcal{U}_t - 2\mathcal{V} + \frac{1}{r} P_r = E \mathcal{U}_{zz} \quad (4.2.3b)$$

$$\mathcal{V}_t + 2\mathcal{U} = E \mathcal{V}_{zz} \quad (4.2.3c)$$

$$W_t - T + P_z = E \Delta w \quad (4.2.3d)$$

$$T_t + 4S w = E/\sigma \Delta T \quad (4.2.3e)$$

If we consider the time scale $t \sim O\left(\frac{1}{E^{1/2}}\right)$, similar to the homogeneous case, and anticipate that in the interior

$$V \sim O(1)$$

$$U \sim O(E^{1/2})$$

$$W \sim O(E^{1/2}),$$

the equations for the interior, with $z = t E^{1/2}$, become

$$2\mathcal{U} + w_z = 0 \quad (4.2.4a)$$

$$-2\mathcal{V} + \frac{1}{r} P_r = 0 \quad (4.2.4b)$$

$$E^{1/2} \mathcal{V}_t + 2\mathcal{U} = 0 \quad (4.2.4c)$$

$$-T + P_z = 0 \quad (4.2.4d)$$

$$E^{1/2} T_z + 4SW = E/\sigma \Delta T \quad (4.2.4e)$$

The solutions to these equations, for the velocity components, are

$$V = -e^{-\tau} \quad (4.2.5a)$$

$$u = -\frac{E^{1/2}}{2} e^{-\tau} \quad (4.2.5b)$$

$$w = +E^{1/2} z e^{-\tau} \quad (4.2.5c)$$

where we have used the boundary condition from the Ekman layer theory of $z = \pm 1$.

Therefore W is known and is just a forcing term in equation (4.2.4e).

Representing

$$z = \sum_n b_n \sin n\pi(z+1), \quad b_n = \frac{-2}{n\pi}$$

and

$$T = \sum_n T_n(\tau) \sin n\pi(z+1) \quad (4.2.6)$$

we get the following set of equations for the coefficients $T_n(\tau)$

$$T_n' + b_n e^{-\tau} = -\frac{E^{1/2}}{\sigma} (T_n n^2 \pi^2) \quad (4.2.7)$$

with solutions

$$T_n = \frac{b_n}{\left(\frac{n^2 \pi^2 E^{1/2}}{\sigma} - 1\right)} \left[e^{-n^2 \pi^2 \frac{E^{1/2}}{\sigma} \tau} - e^{-\tau} \right] \quad (4.2.8)$$

We note that, although the time scale for the velocity to adjust is $O\left(\frac{1}{E^{1/2}}\right)$ (the "spin-up time"), the temperature has an additional time scale which is $O\left(\frac{\sigma}{E}\right)$. Since $\frac{\sigma}{E} = \frac{K}{L^2 \Omega}$, we recognize this as the diffusion time.

The solutions (4.2.5) do not satisfy the initial conditions (4.2.3) as $\tau \rightarrow 0$ but rather will match with solutions from equations for variations on the short time scale $t \sim O(1)$ as $t \rightarrow \infty$ (i.e. as $t \rightarrow O(E^{1/2})$). We will talk about the short time scale equations and solutions in lecture 10.

We now look at the solution to the spin-up problem between two parallel infinite plates when the disturbance on the plates is arbitrary and goes to zero at ∞ . The solution we present is included in a paper by G. Walin (Ref. 2) and is similar to that obtained earlier by Holton (Ref. 3).

If we again look on the time scale $O(E^{1/2})$ (i.e. substitute $\tau = t E^{1/2}$) and assume an expansion for the variables in the form

$$\begin{aligned} u &= u_0 + E^{1/2} u_1 + \dots \\ v &= v_0 + E^{1/2} v_1 + \dots \text{ etc.} \end{aligned} \quad (4.2.9)$$

we find that, with the introduction of the function

$$\phi = - \frac{\partial}{\partial \tau} P_0, \quad (4.2.10)$$

the zeroth and first order interior equations, in cartesian coordinates, can be reduced to a single equation for ϕ

$$\frac{\partial^2 \phi}{\partial x^2} + \frac{\partial^2 \phi}{\partial y^2} + \frac{1}{5} \frac{\partial^2 \phi}{\partial z^2} = 0 \quad (4.2.11)$$

For this problem the boundary conditions for the interior flow come from the Ekman layer theory and are

$$w_{INT}(z = \pm 1) = \mp \frac{1}{2} E^{1/2} \left(\frac{\partial v}{\partial x} - \frac{\partial u}{\partial y} \right) \quad (4.2.12)$$

In terms of ϕ this condition becomes

$$\frac{1}{5} \frac{\partial^2 \phi}{\partial \tau \partial z} = \pm \left(\frac{\partial^2 \phi}{\partial x^2} + \frac{\partial^2 \phi}{\partial y^2} \right) \text{ at } z = \pm 1 \quad (4.2.13)$$

A general solution to equation (4.2.12) satisfying the boundary condition (4.2.13) can be written as

$$\phi = \iint_{-\infty}^{+\infty} (A_1(k, \ell) f + A_2(k, \ell) g) e^{i(kx + \ell y)} dk d\ell \quad (4.2.14)$$

where

$$f = e^{-r\tau} \frac{\cosh mz}{\cosh m} \quad (4.2.15a)$$

$$g = e^{-r\tau} \frac{\sinh mz}{\sinh m} \quad (4.2.15b)$$

$$m^2 = S(k^2 + \ell^2) = Sh^2 \quad (4.2.15c)$$

$$h^2 = k^2 + \ell^2 \quad (4.2.15d)$$

$$g = \sqrt{S} h \frac{\cosh m}{\sinh hm} \quad (4.2.15e)$$

$$r = \sqrt{S} h \frac{\sinh m}{\cosh m} \quad (4.2.15f)$$

This solution exhibits different behavior, depending on the value of the parameter $m = \sqrt{S}h$ which involves the amount of stratification and the horizontal scale of the boundary disturbance.

When

$$\sqrt{S}h = m \ll 1$$

we find

$$\begin{aligned} f &= e^{-\tau} (1 + o(m)) \\ g &= o(m) \end{aligned} \quad (4.2.16)$$

and the process is similar to that in a homogeneous fluid, decaying in the ordinary spin-up time. However, for $\sqrt{S}h = m \gg 1$

$$\begin{aligned} f &\approx e^{-m\tau} \left[e^{m(z-1)} + e^{-m(z+1)} \right] \\ g &\approx e^{-m\tau} \left[e^{m(z-1)} - e^{-m(z+1)} \right] \end{aligned}$$

In this case we find that the motion is very different than that in the homogeneous case and is largely confined to layers of thickness $(\sqrt{S} h)^{-1}$ at the boundaries. The time scale of the process can be found from

$$m\tau = \sqrt{S} h E^{1/2} t = E_{\delta}^{1/2} t \quad (4.2.18)$$

and is

$$O\left(\frac{1}{E_{\delta}^{1/2}}\right)$$

where

$$E_{\delta} = \frac{\nu}{\Omega} \left(\frac{\sqrt{S} h}{L}\right)^2 \quad (4.2.19)$$

is essentially the Ekman number based on the boundary layer or penetration thickness

$$\delta = \frac{L}{\sqrt{S} h} \quad (4.2.20)$$

Therefore the time scale can be thought of as the homogeneous spin-up time for a depth based on the penetration thickness δ .

Notes submitted by
John S. Allen, Jr.

REFERENCES

1. Veronis, G. 1967. "Analogous Behavior of Homogeneous, Rotating Fluids and Stratified, Non-rotating Fluids", Tellus 19: 326.
2. Walin, G. 1967. "Some Aspects of Time-dependent Motion of a Stratified Rotating Fluid". (to be published)
3. Holton, J. R., 1965. "The Influence of Viscous Boundary Layers on Transient Motions in a Stratified Rotating Fluid: Part 1". J. Atmos. Sci., 22: 402.

Lecture #9

3. Dissipative Effects on the Normal Modes of a Rotating Stratified Fluid

In general, for $E \neq 0$, viscosity will effect some modification on the interior modes of a rotating stratified fluid. For the initial value problem, the solution may be accomplished by noting the existence of two time scales, Ω^{-1} and $L/(\nu\Omega)^{1/2}$, or the non-dimensional times t and τ of the previous section, as well as singular spatial structure in the flow. To do this, write (Greenspan, 1965)

$$\begin{aligned} \underline{u} = & \underline{u}_o(\underline{r}, \tau) + \sum_k \underline{U}_k e^{s_k t} + E^{1/2} \left\{ \underline{u}_1(\underline{r}, \tau) + \sum_m \underline{u}_{m1}(\underline{r}, \tau) \right\} + \\ & + \underline{\tilde{u}}_o(\zeta, \tau) + \sum_k \underline{U}_k + E^{1/2} \left\{ \underline{\tilde{u}}_1(\zeta, \tau) + \sum_m \underline{\tilde{u}}_{m1}(\zeta, \tau) \right\} + \dots \end{aligned} \quad (4.3.1)$$

where (\sim) denotes a boundary layer solution presumed to be transcendentally small for large ζ , the boundary layer variable; the $\left\{ \underline{U}_k e^{s_k t} \right\}$ are the interior modes of the container. As is the conventional procedure in the two-time method, write

$$s_k = i\sigma_k + E^{1/2} s_{k1} + \dots$$

to remove secularity in time. This is clearly quite a complicated process for a general container; there is the additional complication that there are certain critical latitudes with a singular character (e.g. the equator of a sphere) that are difficult to handle. These are associated, in the homogeneous case, with the disappearance of the Ekman layer and the appearance of more complex shear layers on vertical parts of the boundary.

4. Spin-up in an Arbitrary Container; Time Scales of $O(E^{-1/2})$

Now, for a rotating stratified fluid in a container

$$\begin{aligned} \underline{u} = & \underline{u}_0(r, \tau) + E^{1/2} \underline{u}_1(r, \tau) + \dots + \\ & + \underline{u}_0(\zeta, \tau) + E^{1/2} \underline{u}_1(\zeta, \tau) + \dots \end{aligned} \quad (4.4.1)$$

where there is no attempt at this stage to make the solution uniformly valid in time as in the previous section. Now, if \underline{n} is the outward-drawn normal, then

$$\underline{n} \cdot \nabla = -E^{-1/2} \frac{\partial}{\partial \zeta} + O(1)$$

in the boundary layer.

Putting this sort of expansion for temperature and pressure also into the non-dimensional equations of motion with

$$\frac{\partial}{\partial t} = E^{1/2} \frac{\partial}{\partial \tau}$$

will yield, to $O(1)$ in the interior,

$$\begin{aligned} 2 \underline{k} \times \underline{u}_0 + \nabla p_0 &= \underline{k} T_0 \\ \nabla \cdot \underline{u}_0 &= 0 \\ w_0 &= 0 \end{aligned} \quad (4.4.2)$$

and to $O(E^{1/2})$, also in the interior,

$$\begin{aligned} \frac{\partial \underline{u}_0}{\partial \tau} + 2 \underline{k} \times \underline{u}_1 + \nabla p_1 &= \underline{k} T_1 \\ \frac{\partial T_0}{\partial \tau} + 4 S w_1 &= 0 \\ \nabla \cdot \underline{u}_1 &= 0 \end{aligned} \quad (4.4.3)$$

In the boundary layer, the $O(E^{-1/2})$ equations are

$$\begin{aligned} \frac{\partial p_0^*}{\partial \zeta} &= 0 \\ \frac{\partial}{\partial \zeta} \underline{n} \cdot \underline{\tilde{u}}_0 &= 0 \end{aligned} \quad (4.4.4)$$

Now, to $O(1)$, the boundary layer equations are

$$\begin{aligned} 2 \underline{k} \times \underline{\tilde{u}}_0 - \underline{n} \frac{\partial \tilde{p}_1}{\partial \zeta} - \underline{k} \tilde{T}_0 &= \frac{\partial^2 \underline{\tilde{u}}_0}{\partial \zeta^2} \\ - \frac{\partial \underline{n} \cdot \underline{\tilde{u}}_1}{\partial \zeta} + \underline{n} \cdot \nabla \times (\underline{n} \times \underline{\tilde{u}}_0) &= 0 \\ 4 S \tilde{w}_0 &= \frac{1}{\sigma} \frac{\partial^2 \tilde{T}_0}{\partial \zeta^2} \end{aligned} \quad (4.4.5)$$

Without stratification, (4.4.5) are the usual Ekman layer equations. Some considerable manipulation of (4.4.5) with the boundary condition $\underline{n} \cdot \underline{\tilde{u}}_0 = 0$ on the boundary will give eventually

$$\left. \begin{aligned} \left[\frac{\partial^2}{\partial \zeta^2} - 2i(\underline{n} \cdot \underline{k}) \right] (\underline{n} \times \underline{\tilde{u}}_0 + i \underline{\tilde{u}}_0) &= -\tilde{T}_0 \left[\underline{n} \times \underline{k} - i \underline{n} \times (\underline{n} \times \underline{k}) \right] \\ \frac{1}{\sigma} \frac{\partial^2 \tilde{T}_0}{\partial \zeta^2} &= 4S(\underline{k} \cdot \underline{\tilde{u}}_0) \end{aligned} \right\} \quad (4.4.6)$$

It is clear immediately that when the boundary is horizontal ($\underline{n} \times \underline{k} = 0$), these reduce to the conventional Ekman layer equations, so long as S is $O(1)$. In general, on a sloping boundary like this, the buoyancy layers and Ekman layers are mixed.

In a forced problem, one splits \underline{u} into a part with homogeneous boundary conditions and a part with the inhomogeneous conditions, e.g., Ekman suction. Study of the boundary layers would yield appropriate inhomogeneous boundary conditions for the interior problem.

There is some question of the role of Ekman layers in stratified spin-up problems; (Ref. 2 and 3, Lecture 8; Pedlosky, 1967) they are certainly important on a time scale of $O(E^{-1/2})$. (There was considerable dialogue among Howard, Veronis, Rooth, Welander as to whether this normal mode approach is useful in predicting the character of steady solutions when the fluid is stratified. Howard pointed out that, in a stratified spin-up, not only are time scales of $O(\Omega^{-1})$ and $O(L_1/\sqrt{\Omega \nu})$ important, but also the diffusion time scale L^2/ν .)

5. Time Dependent Modes in a Cylinder - given by W. Siegmann.

In slightly different notation than before, one has, for an unsteady motion in R

$$\begin{aligned} \underline{u}_t + 2\underline{k} \times \underline{u} - 4S\underline{k} + \nabla p &= 0 \\ T_t + \underline{k} \cdot \underline{u} &= 0 \\ \nabla \cdot \underline{u} &= 0 \\ \text{and } \underline{u} \cdot \underline{n} &= 0 \text{ on } \partial R. \end{aligned} \tag{4.5.1}$$

Here, $S \equiv (N/2\Omega)^2$. Again, a little manipulation of the equations with a time dependence $\exp(i\lambda t)$ will give (cf. Lect. #7. Eqs. (3), (6), (8)), if $S = \text{constant}$,

$$\nabla_H^2 p + \frac{4-\lambda^2}{4S-\lambda^2} \frac{\partial^2 p}{\partial z^2} = 0 \tag{4.5.2}$$

For a cylinder,

$$i\lambda p_r + \frac{2}{r} p_\phi = 0 \text{ on } r=A \tag{4.5.3a}$$

$$p_z = 0 \text{ on } z = 0, 1 \tag{4.5.3b}$$

The solution is then, noting (4.5.3b)

$$p = \sum_{m,k} \cos(m\pi z) e^{ik\phi} J_k(\alpha r/A) \tag{4.5.4}$$

Using (4.5.2) and (4.5.4)

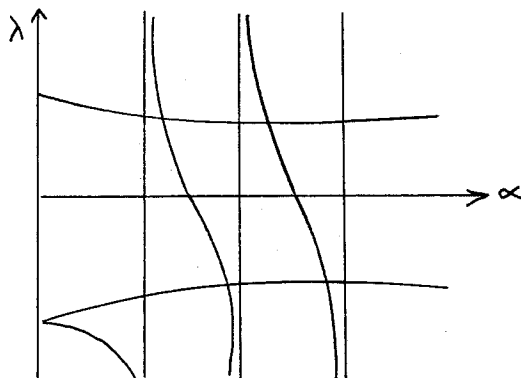
$$\left(\frac{\alpha}{A}\right)^2 = \frac{4-\lambda^2}{4S-\lambda^2} (m\pi)^2 \tag{4.5.5}$$

and from (4.5.3a),

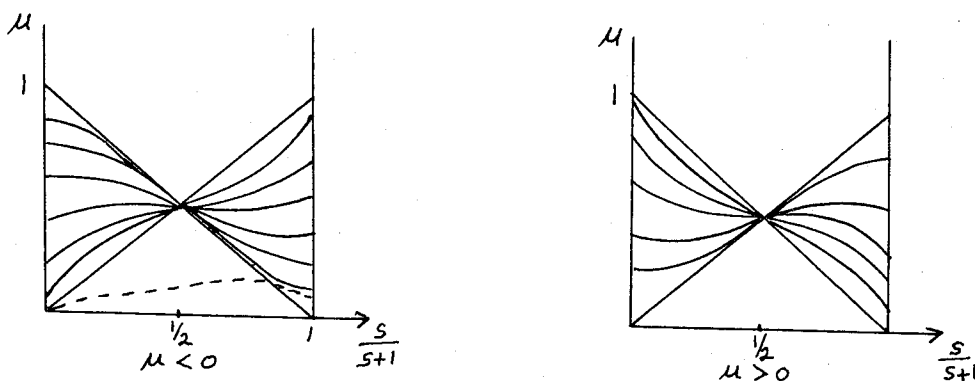
$$\lambda J'_k(\alpha) + 2k J_k(\alpha) = 0 \tag{4.5.6}$$

Equations (4.5.5) and (4.5.6) may be solved graphically by solving each for λ and using α as the abscissa, λ the ordinate; the intersections are the solutions.

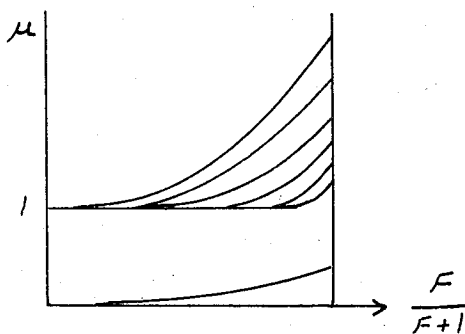
Such a plot is shown below



If $K \equiv 0$, the equations are uncoupled, with $J'_0(\infty) = 0$. If the parameters m and k are held fixed, then the wave spectrum is



where $\mu^2 = (\text{frequency})^2 / [4\Omega^2 + N^2]$. The dotted line represents something like a Kelvin wave in shallow water theory. For comparison, the shallow water spectrum plotted against $F/F+1$, F being a Froude number, at fixed k has a form which is interesting to compare with the above results, viz.,



There is no bound on the frequencies in the shallow water waves, but there is a bound for the modes of the cylinder.

It appears that any solution of the initial value problem for the special case $S = 1$ ($\frac{S}{S+1} = \frac{1}{2}$) is atypical, since there is a focusing of all the waves at that point; one can show that these modes do not decay in a "spin-up" time scale, $E^{-1/2}$, but much more slowly. If $S \neq 1$, then the modes decay on the scale $E^{-1/2}$.

References

Greenspan, H. 1965. "On the general theory of contained rotating fluid motions". J. Fl. Mech., 22: 449-462.
 Pedlosky, J. 1967. J. Fl. Mech., 28: 463-479.

Notes submitted by
 Michael R. Foster

Lecture #10

6. Initial Phase of the Spin-up Problem

We now want to look at the initial phase of the spin-up problem of a stratified fluid in a cylindrical container. That is, we look at the behavior on the short time scale where the dimensionless time $t \sim O(1)$ (and the dimensional time is $O(\frac{1}{\Omega})$).

The governing equations in cylindrical polar coordinates are those that were written in Lecture 8 as equations (4.2.1 a - e). The boundary conditions are

$$u = v = \omega = T = 0 \quad \text{on the boundary} \quad \begin{matrix} z = \pm 1 \\ r = a \end{matrix} \quad (4.6.1)$$

The initial conditions, at $t = 0$, are

$$\begin{aligned} u = \omega = T &= 0 \\ v &= +r \quad (\text{spin-down problem}) \end{aligned} \quad (4.6.2)$$

Taking the Laplace Transform of equations (4.2.1) and using the notation

$$\bar{u} = \int_0^{\infty} e^{-\Delta t} u dt, \text{ etc.}$$

we have

$$\frac{1}{r} (r\bar{u})_r + \bar{\omega}_z = 0 \quad (4.6.3a)$$

$$\Delta \bar{u} - 2\bar{v} + \bar{p}_r = E \left(\Delta - \frac{1}{r^2} \right) \bar{u} \quad (4.6.3b)$$

$$\Delta \bar{v} + 2\bar{u} = E \left(\Delta - \frac{1}{r^2} \right) \bar{v} + r \quad (4.6.3c)$$

$$\Delta \bar{\omega} + p_z = E \Delta \bar{\omega} + \bar{T} \quad (4.6.3d)$$

$$\Delta \bar{T} + 4S \bar{\omega} = E/\sigma \Delta T \quad (4.6.3e)$$

To solve these equations we again make use of the fact that $E \ll 1$ and solve for the appropriate boundary layers. Defining the coordinate ζ by

$$z = -1 + E^{1/2} \zeta,$$

the equations for the layer on the lower boundary become

$$E^{-1/2} \bar{\omega}_\zeta = 0 \quad (4.6.4a)$$

$$\Delta \bar{u} - 2\bar{v} + \bar{p}_r = \bar{u}_{\zeta\zeta} \quad (4.6.4b)$$

$$\Delta \bar{v} + 2\bar{u} = \bar{v}_{\zeta\zeta} + r \quad (4.6.4c)$$

$$\bar{p}_\zeta = 0 \quad (4.6.4d)$$

$$\Delta \bar{T} + 4S \bar{\omega} = \frac{1}{\sigma} \bar{T}_{\zeta\zeta} \quad (4.6.4e)$$

Note that equations (4.6.4a-d) do not include any terms resulting from the effects of stratification.

Multiplying (4.6.4c) by $i = \sqrt{-1}$ and adding to (4.6.4b) we have

$$\frac{\partial^2}{\partial \zeta^2} (\bar{u} + i\bar{v}) - (\Delta + 2i)(\bar{u} + i\bar{v}) = \bar{p}_r - ir \quad (4.6.5)$$

with the solution

$$\bar{u} + i\bar{v} = \frac{\bar{p}_r - ir}{\Delta + 2i} + C e^{-(\Delta + 2i)^{1/2} \zeta} \quad (4.6.6)$$

With the knowledge that in the interior

$$\bar{u} \sim o(E)$$

$$\bar{v} \sim o(1)$$

(Note: the symmetry of the cylinder is necessary for this conclusion) we match the solution (4.6.6) to the interior solution by requiring

$$\bar{u} \rightarrow 0 \text{ as } \zeta \rightarrow \infty$$

or

$$\operatorname{Re} \left(\frac{\bar{p}_r - ir}{\Delta + 2i} \right) = 0 \quad \text{for real } \Delta.$$

Using this condition, which can be written

$$\operatorname{Re} \left[(\bar{p}_r - ir)(\Delta - 2i) \right] = \bar{p}_r \Delta - 2r = 0,$$

and the condition that $\bar{u} = \bar{v} = 0$ at $\zeta = 0$, we have

$$\bar{u} + i\bar{v} = \frac{ir}{\Delta} \left(1 - e^{-(\Delta + 2i)^{1/2} \zeta} \right) \quad (4.6.7)$$

The final solution can be found by taking the inverse transform. The above development shows that the Ekman layer is set up on this $o(1)$ time scale.

Now with the expansion

$$\bar{w} = \bar{w}_0 + E^{1/2} \bar{w}_1 + \dots$$

(where $\bar{w}_0 = 0$ from (4.6.4a) and the boundary conditions) the first order continuity equation in the boundary layer is

$$\bar{w}_{1\zeta} + \frac{1}{r} (r \bar{u}_0)_r = 0 \quad (4.6.8)$$

With

$$\bar{\omega}_1(\zeta \rightarrow \infty) = \int_0^{\infty} \bar{\omega}_{1\zeta} d\zeta = - \int_0^{\infty} \frac{1}{r} (r \bar{u}_0)_r d\zeta$$

we have, using (4.6.7),

$$\bar{\omega}_1(\zeta \rightarrow \infty) = - \int_0^{\infty} \text{Re} \left[\frac{2i}{\Delta} \left(1 - e^{-(\Delta+2i)^{1/2} \zeta} \right) \right] d\zeta = \text{Re} \left[\frac{2i}{\Delta} \frac{1}{(\Delta+2i)^{1/2}} \right] \quad (4.6.9)$$

Multiplying (4.6.9) by Δ and letting $\Delta \rightarrow 0$ to find the behavior as $t \rightarrow \infty$, we obtain

$$\bar{\omega}_1(\zeta \rightarrow \infty, t \rightarrow \infty) \rightarrow 1 \quad (4.6.10)$$

Now with

$$\bar{T} = \bar{T}_0 + E^{1/2} \bar{T}_1 + \dots$$

equation (4.6.4e) and the boundary conditions give $\bar{T}_0 = 0$.

However, with $\bar{\omega}_1 \neq 0$ we will find some $\bar{T}_1 \neq 0$.

Note that the above analysis has been for the case

$$S \sim O(1)$$

If we considered, more generally,

$$S \sim O(E^n)$$

then as n decreased from zero the effects of stratification in the boundary layer would enter at a lower order when n reached $-1/2$ and would enter in the lowest order solution when $n = -1$.

The full solution to the equations on the $t \sim O(1)$ time scale, as $t \rightarrow \infty$, will provide the initial conditions for the equations on the $t \sim O(E^{-1/2})$ or spin-up time scale.

Notes submitted by
John S. Allen, Jr.



OBSERVATIONS OF TIME DEPENDENT OCEAN CURRENTS

T. Ferris Webster

July 1, 1968

A discussion of the major characteristics of long-period flows ($T > 10$ hours) observed by Woods Hole Oceanographic Institution from moored arrays of recording current meters was presented. (Much of this material will be found in two papers by Webster which are in press and which are cited in the References.) Major emphasis was devoted to the analysis of records made at a site (Site "D"; $39^{\circ}20'N$, $70^{\circ}W$) south of Woods Hole, Massachusetts. This site is located on the continental rise where the water depth is about 2.6 km; it is about 50 km south of the continental shelf and 175 km north of the mean Gulf Stream axis. Nearly continuous observations have been made at about 6 levels over a period of 2.5 years by replacing arrays every 2 months. Typically, records 20-to-60 days in length were acquired. The basic sampling procedure used was that of forming a two-minute average every 15 minutes from a "burst" of 24 samples obtained at 5-second intervals. (The objective of this sampling procedure is the suppression of high frequency noise due to mooring or other spurious motions, while yielding a Nyquist sampling frequency of 2 cph.) Five "primary" levels were always sampled: 10, 100, 500, 1000, and 2000 meters; two "secondary" levels were occasionally sampled: 50 and 200 meters. The depth of the permanent pycnocline was generally between 100 and 500 meters. The material presented below is a digest of the discussion.

Progressive vector diagrams (PVD's)*, see Figs. 1 and 2 as examples, were used to convey several notions about the gross features of the flow:

*A PVD is simply a graphical addition of successive velocity vectors measured at a "fixed point"; it is not, in general, to be interpreted as the trajectory of water parcels. Since PVD's are essentially "low-passed" plots, they are useful for characterization of the principal long-period motions.

- a) the flow was highly variable (see Figs. 1 and 2) at all levels; the daily mean speed varied from 0.1 to 70 cm/sec over the entire measurement set and by as much as a factor of 200 at a single sensor; this result is consistent with the order of magnitude of the variable flows indicated by neutrally buoyant floats and by Swallow (see Crease, 1965) in deep water near Bermuda.
- b) there was generally low qualitative coherence between records at various levels, i.e., the motion was not strictly barotropic.
- c) inertial motions (with a period $T_2 \approx 19$ hours) occurred intermittently, i.e., bursts several cycles in duration were prevalent; they were predominant at some levels, especially near the surface, while not visually apparent at others; all inertial motions rotated clockwise, i.e., according to theoretical expectations (see Fig. 1 where an epoch of low mean flow and of 12 days duration is expanded, showing inertial eddies).
- d) there was a general trend indicating a decrease in the mean daily speed with increase in depth.
- e) the mean flow in all seasons and at all depths, with a single exception, was from east to west; perhaps the flow was part of an inshore counter-current associated with the Gulf Stream.

Two observational sets were given special attention. The first set involved measurements made in the autumn at two sites (including site "D") separated horizontally by 3.2 km. At one site, the overall pattern of the records at 7 and 88 meters were very similar, though the sensors were separated by the seasonal

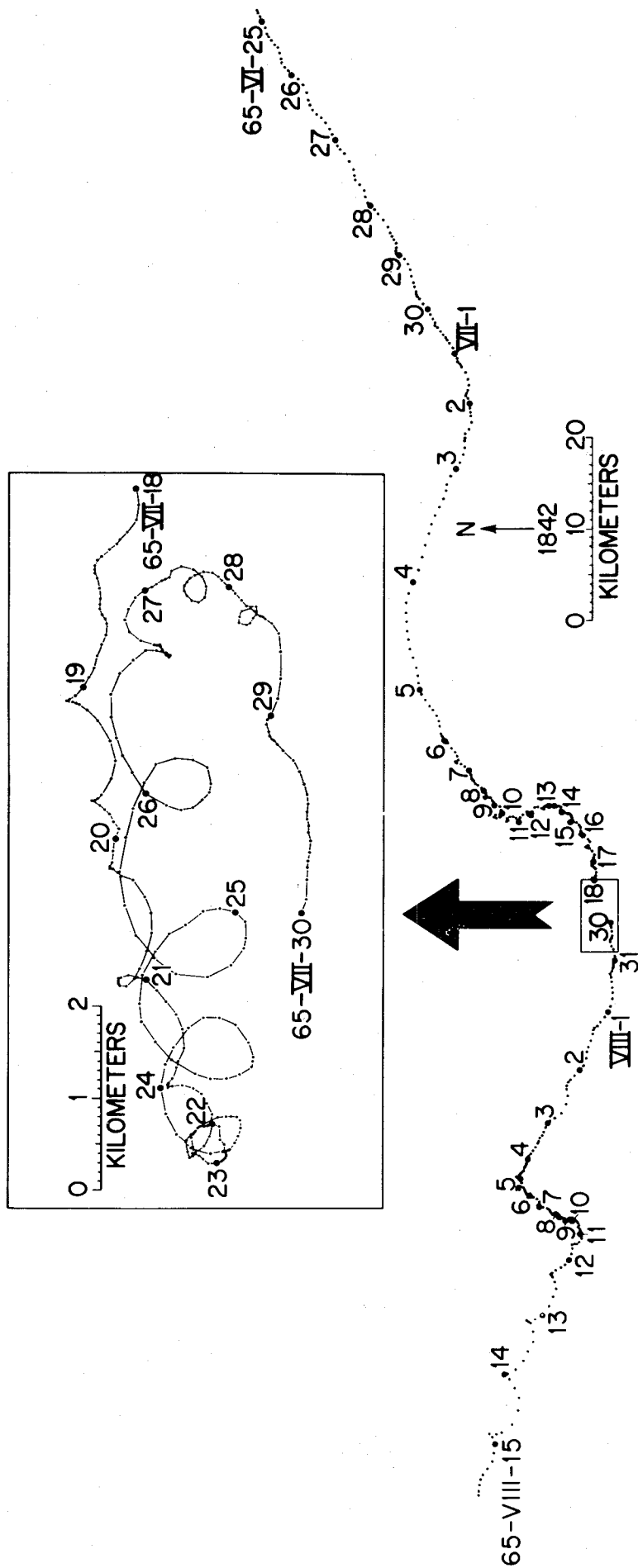


Fig. 1. Progressive vector diagram, site "D", at a depth of 522 m. The period from July 18th to July 30th is shown expanded at a 10X scale in the upper inset. The rotary motions in the inset have the inertial period of 19 hours.

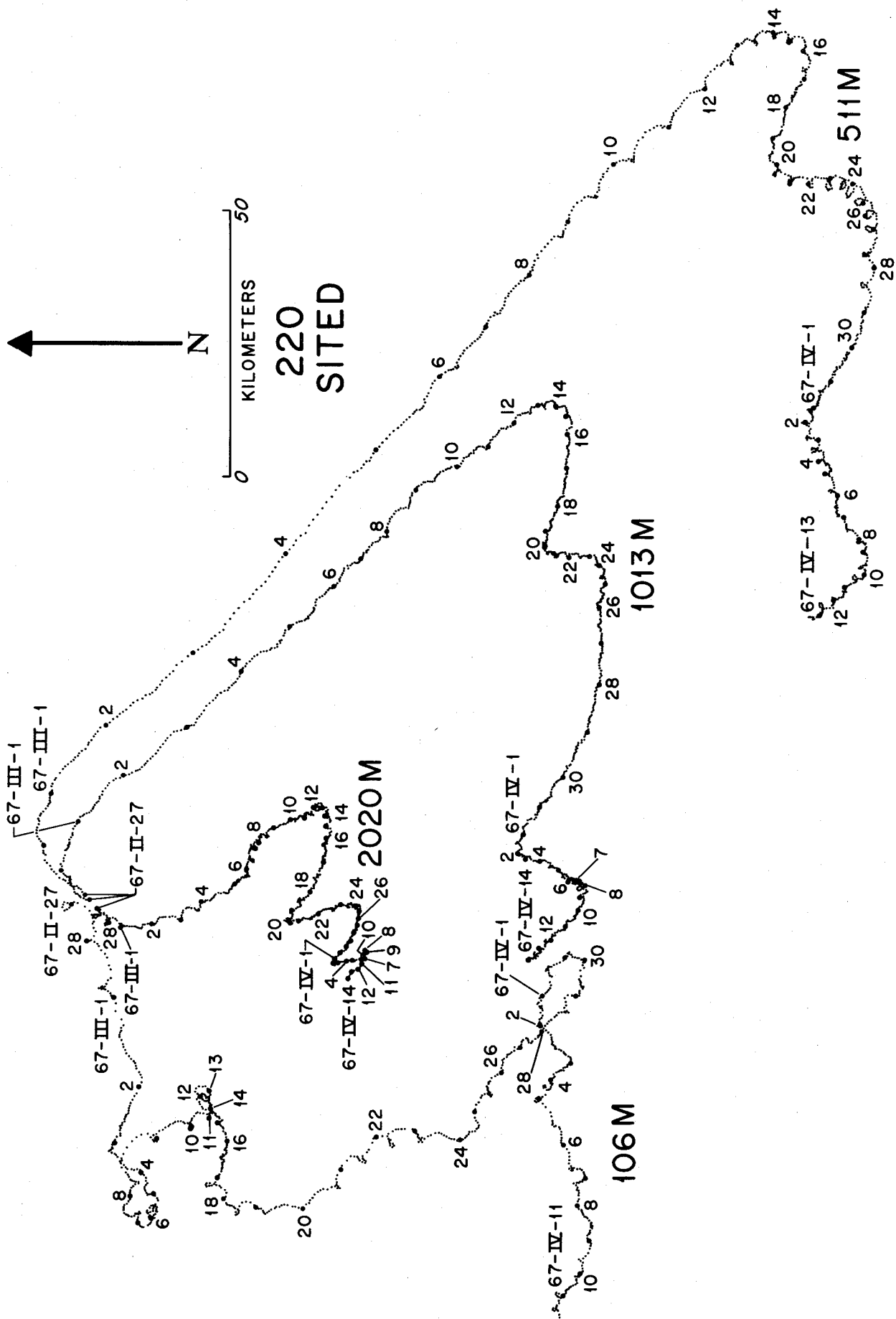


Fig. 2. Progressive vector diagrams, site "D", at different depths. These PVD's aid in distinguishing barotropic and baroclinic aspects of the flow.

thermocline, which was at about 50 meters depth. The records at 88 and 98 meters (separated by 3.2 km) were very similar; they both were without large inertial oscillations. At the second site, the measurements at 98 and 1000 meters were not similar in kind; further, representative speed values at 98 meters were about 5 times those at 1000 meters. The second measurement set emphasized was acquired in February-to-April at site "D" and at depths of 106, 511, 1013, and 2020 meters (see Figure 2). At 106 and 511 meters, the inertial motion was apparent. The record at 106 meters was poorly correlated (in the qualitative sense) with those at the other depths, while the latter were well correlated with one another: particularly striking was the simultaneous occurrence of large, low frequency oscillations of nearly the same amplitude at all three sensors from 14-to-26 March, i.e., they were barotropic in character.

A few spectral calculations were shown (see Figure 3). Since the sum of Cartesian velocity component spectra is invariant under orthogonal coordinate transformation, the total horizontal kinetic energy per unit mass spectra, i.e.,

$$KE_{TOT}(\sigma) = [E_{uu}(\sigma) + E_{vv}(\sigma)]/2,$$

were chosen for display. There were five frequencies, σ , chosen for emphasis in the analysis; the corresponding periods were

T_1 : semi-diurnal

T_2 : inertial (~ 19 hours)

T_3 : diurnal

T_4 : $T_1 T_3 / (T_1 - T_3)$

T_5 : 60 hours (similar to theoretical expectations for the lowest mode planetary wave)

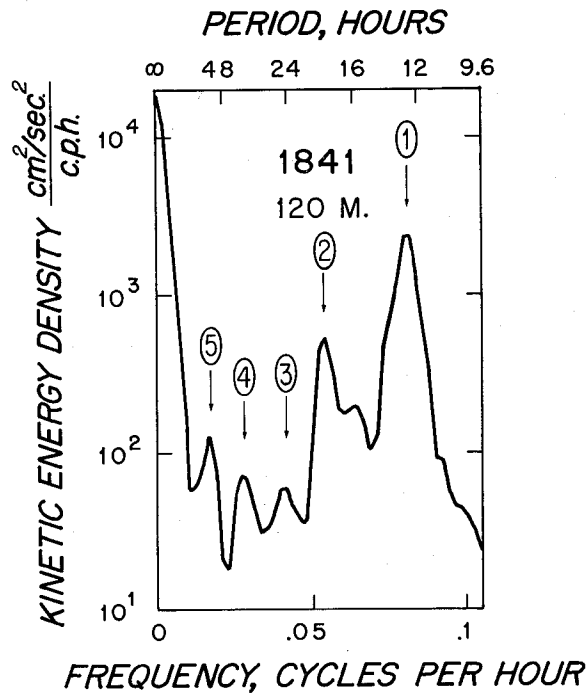


Fig. 3. Spectrum for data from site "D" at 120 m. The ordinate is the logarithm of kinetic energy density per unit frequency and per unit mass. The identified peaks are: (1) semi-diurnal tide 12.42 hrs., (2) inertial motions, 18.9 hrs., (3) diurnal, 24 hrs., (4) interference between inertial and semi-diurnal, 36.4 hrs., (5) of unknown causes, 60 hrs. (degrees of freedom, 3).

(There are about 9 degrees of freedom in Figure 3, giving a 90% confidence band of about 0.4 to 1.9 of the computed spectral value.) Motions with periods T_1 and T_2 appeared to be "preferred" motions but their amplitudes seemed to be quite variable, perhaps as if they were amplitude modulated by a random variable. One general pattern which emerged was that of a tendency for the amplitude of the motion at T_1 to increase with depth, while those of the motions at lower frequencies decreased. The data analysis technique of complex demodulation, which is basically a numerical heterodyning procedure, was used to study the amplitude, $A_i(t)$, and phase, $\theta_i(t)$, of the motion near a given frequency, $\sigma_i(t)$, as a function of time, where

$$v_i(t) = A_i(t) \cos(\sigma_i(t) + \theta_i(t))$$

is a Fourier component of a time series. One of the difficulties with this type of analysis is that its accuracy is limited by the finite length of data records and by the fact that the amplitudes of inertial motions, in particular, are observed

to vary by an order of magnitude in only 3-to-4 inertial periods. The results for the cross spectral calculation of the coherence, $\gamma(\sigma)$, based on the autumn experiment mentioned above, are given in Table 1 for the inertial frequency:

TABLE 1
Inertial Frequency Coherence between Pairs of Sensors
($\sigma_2 \equiv 2\pi/T_2$)

<u>Sensor Pair</u>	<u>$\gamma(\sigma_2)$</u>
7 vs. 88 meters	0.3
88 vs. 98 meters (3.2 km between stations)	0.7
98 vs. 99 meters	0.9
1000 vs. 2000 meters	0.3

(Note: There were 16 degrees of freedom used in these analyses, giving a 90% confidence level of $\gamma = 0.7$.)

The low vertical coherence observed suggests the predominance of large vertical wavenumbers at the inertial period. A study of local winds, from a wind recorder mounted on a surface float, indicated poor correlation with the currents and, in fact, far too little energy in the wind-induced Ekman currents to account for the variable currents; thus, it appears that inertial motions in particular must arrive via wave packets because they can't be attributed to local generation.

The only two-week set of simultaneous measurements made on either side of the Gulf Stream axis, at sites "D" and "J", revealed an interesting feature at a depth of 8-to-10 meters: in a low-passed plot of the downstream velocity component, a motion with an amplitude of about 40 cm/sec and a "period" of

about 2 weeks occurred; the motion was essentially in-phase at the two sites, which suggests that both sites were influenced by the Gulf Stream.

Current measurements were related to stratification and depth by plotting the log of the total time-averaged kinetic energy, $K\bar{E}(z)$, versus log depth. This plot was said to be approximately linear; the plot of log Väisälä-Brunt frequency, $N(z)$, versus log depth was also linear, having a slope equal to that of $K\bar{E}(z)$. The conclusion was that $K\bar{E}(z)$ is proportional to $N(z)$, which will be supported theoretically in the following lecture by Dr. Fofonoff.

In summary, it is safe to say that significant progress has been made in the technology and science of acquiring meaningful observations from moored recording current meter observations and of analyzing them statistically. It is also only fair to add that considerable more work is necessary to be able to carry out Stommel's (1954) outline of hypothesis testing on circulation theories by the use of such observational tools. The observations to date indicate the time and space scales, and their order of magnitude significance, which must be accounted for in the study of deep ocean motions.

References

- Crease, J. (1962). Velocity Measurements in the Deep Water of the Western North Atlantic, J. Geophys. Res., 67(8): 3173-3176.
- Stommel, Henry (1964). Why do Our Ideas About the Ocean Circulation have Such a Peculiarly Dream-Like Quality? WHOI unpublished informal manuscript.
- Swallow, M. (1961). Deep Currents in the Open Ocean, Oceanus 7(3): 2-8.
- Webster, T.F. On the Representativeness of Direct Deep-Sea Current Measurements, (in press) to appear in Progress in Oceanography, Vol.V, Pergamon Press.
- Webster, T.F. Observations on Inertial-Period Motions in the Deep Sea, (in press) to appear in Reviews of Geophysics, 6(4).

Notes submitted by

Christopher N. K. Mooers and

Gunnar E. B. Kullenberg

MEASUREMENTS OF INTERNAL WAVES FROM MOORED BUOYS

Nicholas P. Fofonoff

July 2, 1968

A physical interpretation of observed ocean current energy spectra was made on the basis of two theoretical models (see Phillips (1966) for an extensive discussion of these topics). Attention was focused on the high frequency portion of the energy spectrum, viz. for $\sigma > 0.1$ cph. The first theoretical model discussed was based on an isotropic turbulence model of limited validity and was developed to the point where order of magnitude calculations suggested that it was rather unlikely that the observed spectra could have been formed by a predominantly turbulent field of motion. The second theoretical model discussed was based on a linear internal gravity wave model which was demonstrated to be more plausible than the previous model. The energy spectra discussed were primarily based on the set of recording current meter measurements made in moored arrays by the Woods Hole Oceanographic Institution between Woods Hole and Bermuda (some of these measurements were described in the previous lecture by Dr. T. F. Webster); the other spectra were based on the few wind, temperature, and vertical displacement spectra available. The analyses investigated several properties related to the kinetic energy density per unit frequency per unit mass, $KE(\sigma, z)$, where

$$KE(\sigma, z) \equiv \frac{1}{2}(u^2 + v^2 + w^2)$$

σ is angular frequency,

z is depth,

u and v are horizontal velocity components,

w is the vertical velocity, which is considered negligible for $\sigma \lesssim N$. The kinetic energy density, $E(\sigma, z)$, is investigated,

where $E = \frac{\partial KE}{\partial \sigma}$, with units $\text{cm}^2/\text{sec}^2//\text{cycle}/\text{hour}$. The principal properties of the energy spectra displayed (see Fig. 1 for example) can be summarized:

- a) The inertial period has a significant peak in most current spectra, the semi-diurnal peak is also generally dominant, and the second harmonic of the inertial period occurs occasionally.
- b) Though the low frequency end of the spectra varies with geographic position, season, depth, etc., the spectra generally agree within a factor of 10 through the frequency range of 0.1 to 10 cph; at higher frequencies, the spectra are masked by noise.
- c) The spectra have a slope of about $-5/3$, or about -2 if that is preferred, in the frequency range of 0.1 to 10 cph.
- d) A comparison of wind and current spectra, based on observations at the Woods Hole Oceanographic Institution site "D", shows that they have similar slopes in the frequency band of 0.01-to-0.1 cph.

The existence of a spectral slope approximating the $-5/3$ law of Kolmogoroff's theory of isotropic turbulence suggested the exploration of the possibility that the high frequency portion of the current energy spectra could be attributed to isotropic turbulence. Knowing full well that $W \ll u$ or V , so that the condition of three-dimensional isotropy was not satisfied, the analysis proceeded with the assumption that this limitation would not restrict the validity of the order of magnitude calculations. According to Kolmogoroff's hypothesis, in the inertial subrange of the equilibrium range of isotropic turbulence

$$E(k) = A \epsilon^{2/3} k^{-5/3}, \text{ where}$$

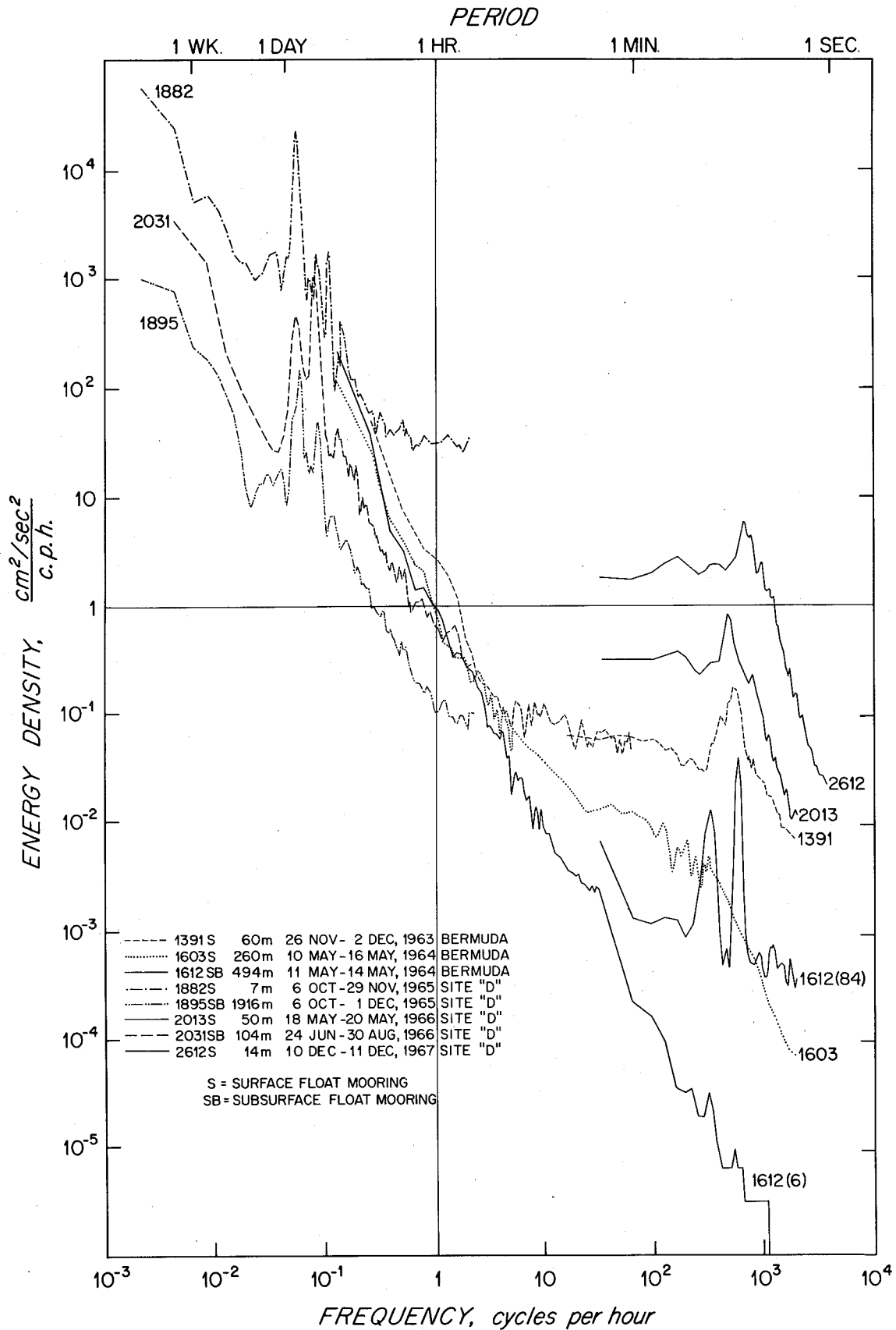


Fig. 1. Energy Spectra for data from various locations and times in the Western North Atlantic; they show qualitative and quantitative similarity.

A is a universal constant,

ϵ is the energy dissipation rate, and

k is the wave number.

Taylor's hypothesis is used to convert the above relationship to the frequency domain, viz., $\sigma = k\bar{u}$, where \bar{u} is a characteristic speed value, the selection of which is not unequivocal in the oceanographic case. The conversion yields

$$E(\sigma) = A(\epsilon\bar{u})^{2/3} \sigma^{-5/3}, \quad \text{or} \quad \epsilon\bar{u} = \frac{1}{(3A)^{3/2}} (3E(\sigma)\sigma)^{3/2}$$

a form convenient for use in the sequel. Since the variance of \vec{u} equals $\int_0^{\infty} E(\sigma) d\sigma$ identically, then for the "turbulent" velocity, \vec{v} , and the "turbulent" portion of the spectrum,

$$\sigma > \sigma_0 = \frac{2\pi}{T_0} = \frac{2\pi}{\bar{u}L_0},$$

where L_0 is a characteristic spatial scale,

$$\begin{aligned} \frac{1}{2} V_{RMS}^2 &= \int_{\sigma_0}^{\infty} A(\epsilon\bar{u})^{2/3} \sigma^{-5/3} d\sigma \\ &= \frac{3}{2} E(\sigma_0)\sigma_0, \end{aligned}$$

so

$$\begin{aligned} \epsilon &= \frac{1}{(3A)^{3/2}} \frac{V_{RMS}^3}{\bar{u}} \frac{2\pi}{T_0} \\ &= \left(\frac{2\pi}{(3A)^{3/2}} \right) \frac{V_{RMS}^3}{L_0}. \end{aligned}$$

Because $\left[\frac{2\pi}{(3A)^{3/2}} \right] \approx 0.7 \sim 1$, $\epsilon \sim \frac{V_{RMS}^3}{L_0}$. (In practice, the upper limit of the integral can be replaced by $\sigma = 10\sigma_0$, since the value of the consequent integral is more than 3/4 of the value of the original integral with an upper limit of $\sigma = \infty$.) Using a value of $T_0 = 10$ hours, Table I was compiled based on observed spectra at Site "D":

TABLE I

DEPTH (m)	$\frac{E(\sigma_0)}{(\text{cm}^2/\text{sec}^2//\text{cph})}$	$\frac{V_{RMS}}{(\text{cm}/\text{sec})}$	$\frac{\bar{u}}{(\text{cm}/\text{sec})}$	$\frac{L_0}{(\text{km})}$	$\frac{\mathcal{E}}{(\text{ergs}/\text{gm-sec})}$
10	200	7.8	12	4.3	100×10^{-5}
100	30	3.0	7	2.5	1×10^{-5}
1000	10	1.7	4	1.4	3×10^{-5}
2000	7	1.4	2	0.7	4×10^{-5}

When compared with Munk's estimated value of 2×10^{-5} ergs/gm-sec for the oceanic tidal dissipation rate, the tabulated values for \mathcal{E} appear too high to be attributed to turbulence without identification of an available energy source.

(Note: The rate at which work is done by the mean wind and the mean current gives an estimated energy dissipation rate which is also only about 2×10^{-5} ergs/gm-sec). The time, τ , to dissipate the total turbulent energy can also be estimated:

$$\tau \equiv \frac{\frac{1}{2} V_{RMS}^2}{\mathcal{E}} \sim \frac{1.4 \frac{\text{ergs}}{\text{gm}}}{3 \times 10^{-5} \text{ ergs}/\text{gm-sec}} \approx 5 \times 10^4 \text{ sec} \sim \frac{1}{2} \text{ day},$$

which is a very short dissipation time. The estimates for \mathcal{E} and τ , together with the neglect of buoyancy effects, i.e., the effects of density stratification which contravene the isotropy hypothesis, make this turbulence model unlikely.

(See Phillips (1966) for a discussion of theoretical models which attempt to account for effects of stratification on turbulence. In brief, a buoyancy subrange is thought to occur at frequencies less than those of the inertial subrange; it is thought to have a spectrum obeying either a $-11/5$ or -3 power law, the extent of the buoyancy subrange is limited by $\ell^{-1} \leq k \leq k_b$, where ℓ is a characteristic depth scale, $k_b = C^{3/4} N^{3/2} \mathcal{E}^{-1/2}$, and C is a positive constant.)

The second model discussed was a linearized internal gravity wave model. The Boussinesq approximation, no (mean) flow and hydrostatic balance in the zero

order state, incompressibility, and the inconsequence of the horizontal component of the Coriolis force were assumed. The first order perturbation equations are then:

Equations of Motion (EOM's)

$$\begin{aligned} \rho_0 (u_t - f v) &= -P_x \\ \rho_0 (v_t + f u) &= -P_y, \text{ and} \\ \rho_0 w_t &= -P_z - \rho g \end{aligned}$$

Equation of Continuity (EOC)

$$u_x + v_y + w_z = 0$$

Conservation of Mass (COM)

$$\rho_t + w(\rho_0)_z = 0$$

where, in particular, $\rho = \rho_0(z) + \rho'(x, y, z, t)$ is the density field which consists of a zero order term, ρ_0 , and a first order term $\rho' \ll \rho_0$.

Let

$$N^2 \equiv -\frac{g}{\rho_0} \frac{d\rho_0}{dz}, \quad N \text{ is the Brunt-Väisälä frequency,}$$

$$\zeta_t = w, \quad \zeta \text{ is the vertical displacement, and}$$

$$P \equiv P_0(z) + \rho_0(z) \pi(x, y, z, t),$$

then $\rho g = \rho_0 [g + N^2 \zeta],$

so $-P_z - \rho g = -\rho_0 [\pi_z + N^2 \zeta],$ since $(P_0)_z = +\rho_0 g$ and

neglecting the product $(\rho_0)_z \pi.$

Further, the EOM's take a simpler form:

$$u_t - f v = -\pi_x,$$

$$v_t + f u = -\pi_y, \text{ and}$$

$$\zeta_{tt} + N^2 \zeta = -\pi_z;$$

then, assuming simple harmonic motion in time (i.e., $\sim e^{i\sigma t}$),

$$u = \frac{i\sigma \pi_x + f \pi_y}{\sigma^2 - f^2},$$

$$v = \frac{i\sigma \pi_x - f \pi_y}{\sigma^2 - f^2}, \text{ and}$$

$$\zeta = \frac{-\pi_z}{N^2 - \sigma^2}.$$

Substitution in the EOC yields:

$$\frac{\nabla_H^2 \pi}{\sigma^2 - f^2} - \left[\frac{\pi_z}{N^2 - \sigma^2} \right]_z = 0$$

or, alternatively,

$$(N^2 - \sigma^2) \nabla_H^2 W - (\sigma^2 - f^2) W_{zz} = 0. \quad (1)$$

If plane wave propagation is assumed in the horizontal dependence, i.e.,

$\sim e^{-i(k_x x + l_y y)}$, and if N^2 is allowed to be a slowly varying function of z ,

then

$$W_{zz} + m^2(z) W = 0,$$

where

$$m^2(z) \equiv \frac{(N^2(z) - \sigma^2)}{(\sigma^2 - f^2)} (k^2 + l^2)$$

is the dispersion relation (see Figure 2 for a general depiction of dispersion relations for various classes of wave motions in the ocean and in order to see where the class of internal waves appears in the general scheme of permissible wave motions). The ratio

$$\frac{m^2}{k^2 + l^2} = \frac{N^2 - \sigma^2}{\sigma^2 - f^2} = \tan^2 \theta$$

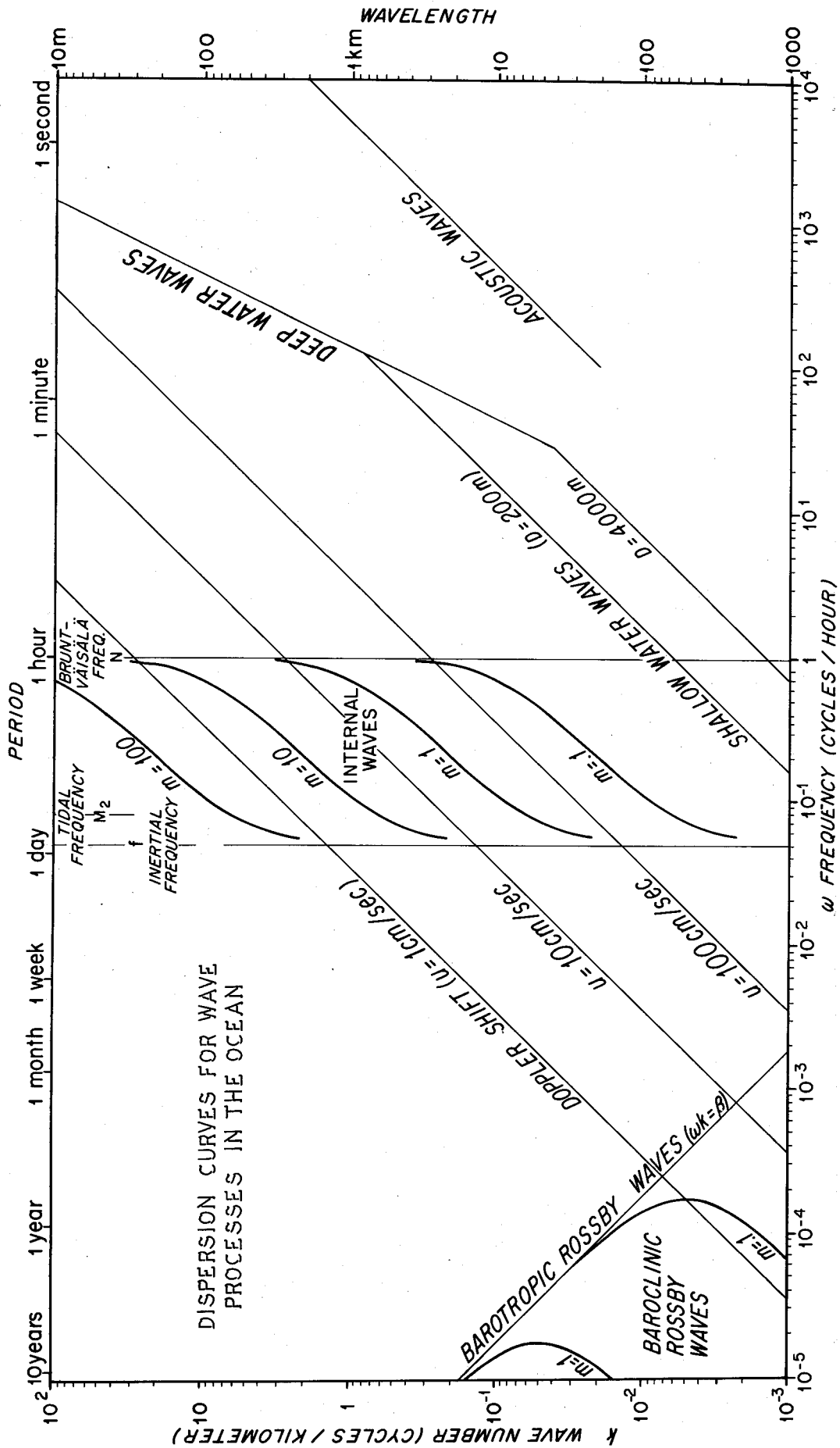


Fig. 2. Dispersion diagram for wave processes in the ocean.

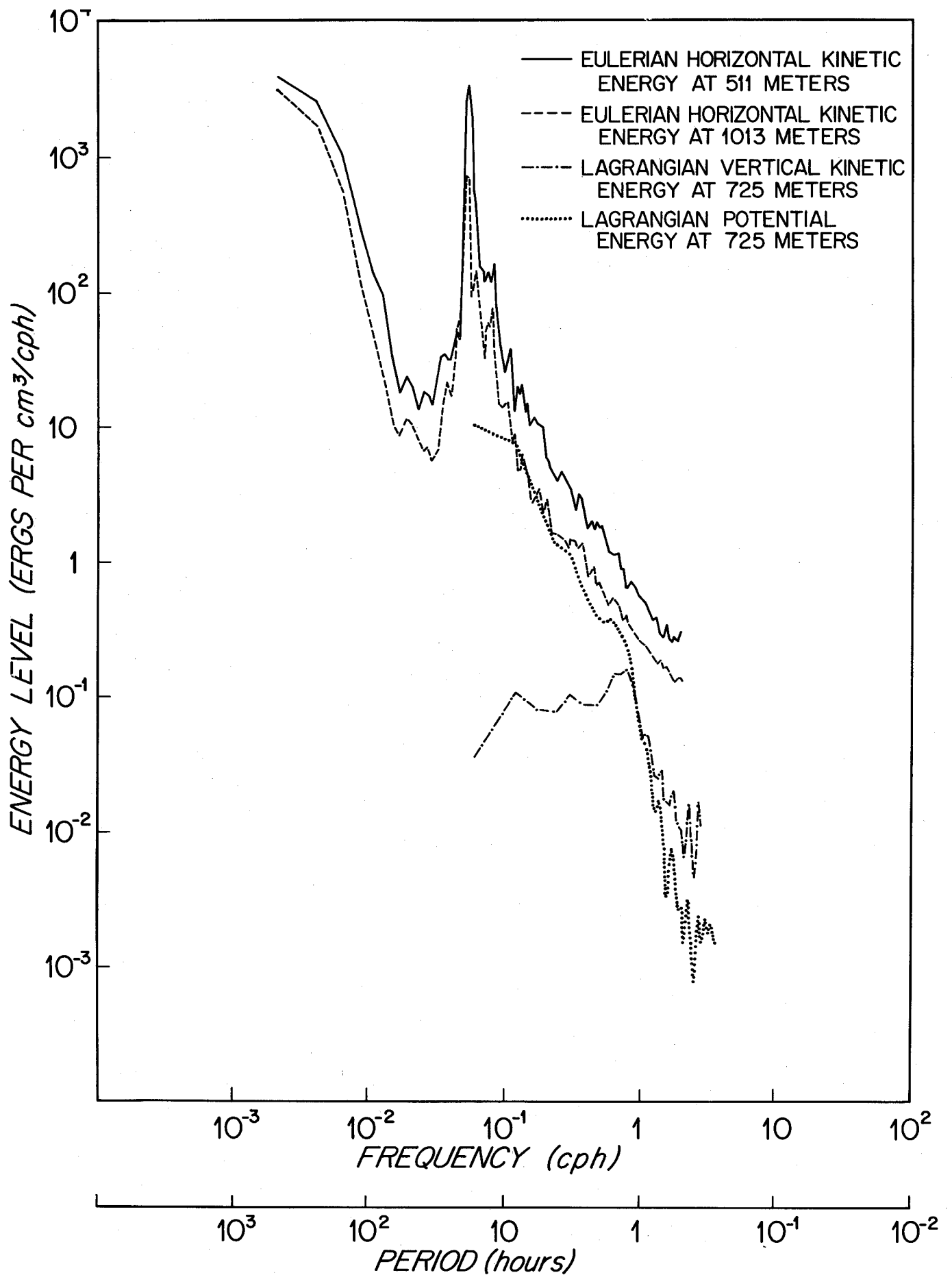


Fig. 3. Energy Spectra computed from various kinds of observations of horizontal and vertical motions; the objective is the testing of the internal gravity wave hypothesis mentioned in the lecture.

gives the angle θ at which these waves propagate with respect to the horizontal. (Note: Stability oscillations ($\sigma = N$) propagate (direction of phase velocity) horizontally and inertial oscillations ($\sigma = f$) propagate vertically, while the water parcels oscillate (direction of group velocity) in the vertical and horizontal, respectively.) The W-K-B approximation gives $W(\rightarrow, z) \propto m^{-1/2} e^{i \int m dz}$ as a solution. In the mid-range of permissible frequencies $f^2 \ll \sigma^2 \ll N^2$, assuming $f^2 < N^2$ so that N is the high-frequency limit and f the low-frequency limit for the domain of hyperbolicity of the governing equation (1), $m \approx \frac{N}{\sigma} k_H$, where $k_H^2 = k^2 + l^2$, so $W \sim N^{-1/2}$, assuming the horizontal phase speed, $\frac{k_H}{\sigma}$, is approximately constant. Now, if all functions are considered proportional to $e^{-i \int m dz}$, which is consistent with the WKB approximation, then

$$\pi = \left[-i \frac{(N^2 - \sigma^2)}{m} \right] \zeta,$$

$$u = \left[\frac{\sigma k - i f l}{\sigma^2 - f^2} \right] \pi = - \left(\frac{N^2 - \sigma^2}{\sigma^2 - f^2} \right) \left(\frac{f l + i \sigma k}{m} \right) \zeta$$

$$\approx -i \left(\frac{N^2}{\sigma} \right) \left(\frac{k}{m} \right) \zeta, \text{ and}$$

$$v = \left[\frac{\sigma l + i k f}{\sigma^2 - f^2} \right] \pi$$

$$= \left(\frac{N^2 - \sigma^2}{\sigma^2 - f^2} \right) \left[\frac{k f - i \sigma l}{m} \right] \zeta \approx -i \left(\frac{N^2}{\sigma} \right) \left(\frac{l}{m} \right) \zeta.$$

Consequently,

$$E(\sigma) = (u^2 + v^2) / 2 \approx \frac{N^4 k_H^2}{2 \sigma^2 m^2} \zeta^2 \approx \frac{N^2 \zeta^2}{2},$$

and, the potential energy, PE , equals

$$PE = N^2 \zeta \frac{d\zeta}{dt} = \frac{N^2 \zeta^2}{2},$$

so $PE \approx KE$, as expected, and $\zeta_{RMS} \approx \frac{\zeta_{RMS}}{N}$. Estimates of ζ_{RMS} were

made for observations at Site "D"; the results are entered in Table II, where

$T_N = \frac{2\pi}{N}$ is the Brunt-Väisälä period:

TABLE II

Depth (m)	v_{RMS} (cm/sec)	T_N (hours)	ζ_{RMS} (m)	L_z (m)
100	3	0.3	5.5	17
1000	1.7	1.0	10.0	31
2000	1.4	1.5	12.0	38

In order to develop some idea of the limits to the vertical scale of the internal gravity wave motion, Richardson's criterion for dynamic instability was invoked, viz.

$$R_i \equiv \frac{N^2}{(v_z)^2} \text{ and for}$$

$$R_i \begin{cases} < 1/4, \text{ wave unstable} \\ > 1/4, \text{ wave stable} \end{cases}$$

From above, $v_z = (v_{RMS})_z \approx Nm\zeta$, so $R_i \approx \frac{1}{m^2 \zeta^2}$. Let $L_z \equiv \frac{2\pi}{m}$, then

$$L_z \begin{cases} < \pi \zeta, \text{ wave unstable} \\ > \pi \zeta, \text{ wave stable.} \end{cases}$$

Several computed values of L_z are entered in Table II. They can be viewed as estimates of the scale of the microstructure in the thermocline; it is striking how similar these values are to the size of the "steps" observed in the thermocline by STD-type instrumentation. An analogous stability criterion can be derived for the steepness of the wave slopes:

$$\text{Since } \zeta_x \sim k_H \zeta = \left(\frac{k_H}{m}\right)m\zeta \approx \left(\frac{\sigma}{N}\right)m\zeta,$$

and since for stability $m \zeta^{(must)} < 2$,

$$\text{then } \zeta_x^{(must)} < 2 \frac{k_H}{m} \text{ or, } \zeta_x^{(must)} < 2 \frac{\sigma}{N}.$$

The relationship $v_{RMS} \sim N \zeta_{RMS}$ is subject to experimental verification by the analysis of direct or indirect observations of vertical displacements (see Figure 3). One indirect method is the analysis of temperature spectra. With $\theta \approx T_z \zeta$ denoting a temperature fluctuation and T_z the mean temperature gradient, θ 's variance is given by

$$\begin{aligned} \overline{\theta^2} &= (T_z)^2 \overline{\zeta^2} = 2 \frac{(T_z)^2}{N^2} \overline{\left(\frac{1}{2} \zeta^2 N^2\right)} \\ &= C \left(\frac{1}{2} v_{RMS}^2\right), \end{aligned}$$

where $C \equiv 2 \left(\frac{T_z}{N}\right)^2$; then, $E_{\theta\theta}(\sigma) \stackrel{(should)}{=} C E(\sigma)$, where again E is the kinetic energy spectrum and $E_{\theta\theta}$ is the temperature spectrum. Order-of-magnitude agreement was achieved for non-simultaneous, in either space or time, measurements at Bermuda; agreement within a factor of two was achieved at Site "D" for one temperature record at 1000 meters. A direct test was made at Site "D" using a neutrally buoyant float equipped to efficiently measure vertical displacements. The ζ_{RMS} observed was 20 meters and ζ_{RMS} computed was 10 meters. The spectra agreed in the band $0.2 < \left(\frac{\sigma}{2\pi}\right) < 1 \text{ cph}$. The following relationship was also verified: with $\overline{w^2} = \sigma^2 \overline{\zeta^2} \approx \frac{\sigma^2}{N^2} v_{RMS}^2$, and $E_H(\sigma) \sim \sigma^{-5/3}$ then $E_V(\sigma) \sim \sigma^{1/3}$; also $E_V \ll E_H \sim PE, \sigma < N$, and $E_H \ll E_V \sim PE, \sigma > N$. (Note: A sharp fall-off generally occurs in the spectrum of E_H for $\sigma > N$.)

In conclusion, the observational evidence supports the validity of the internal gravity wave model in the specified frequency band. (Note: The internal gravity wave model presented must be augmented by the hypothesis of the existence of a continuum of internal gravity waves in some sort of statistical equilibrium and by a mechanism for determining the spectral shape in order to

explain more completely the observed spectra. If the above stability criterion is used to specify the saturation level of energy as a function of frequency:

$$\zeta < \frac{2}{m} \approx \frac{2}{N} \frac{\sigma}{k_H},$$

$$\text{then } E(\sigma) \sim \left(\frac{\sigma}{k_H}\right)^2,$$

and, using the depth-dependent dispersion law to estimate the dependence of k_H on σ ,

$$E(\sigma) \sim \begin{cases} \sigma^{-1}, & \sigma \ll \sigma_c \\ \sigma^{-3}, & \sigma \gg \sigma_c \end{cases}$$

where $\sigma_c \approx c/d$, c is horizontal phase speed, and d is the water depth.

Reasonable order of magnitude estimates are: $c \sim 4\text{m/sec}$ for the first mode and $d \sim 2.5\text{ km}$, so $\sigma_c \sim 1.6 \times 10^{-3}\text{ rad/sec}$, i.e. $\sigma_c \approx \sigma_0$; thus, it is not unreasonable to expect $E(\sigma) \sim \sigma^{-2}$ within the range $\sigma_0/10 < \sigma < 10\sigma_c$, or $1\text{ hour} < T < 100\text{ hours}$.

Note: (This minus three power low frequency band is not necessarily related to the buoyancy sub-range mentioned earlier, and which has the same power law.)

Notes submitted by

Christopher N. K. Mooers and

Gunnar Kullenberg

Reference

Phillips, O. M. (1966). The Dynamics of the Upper Ocean, Cambridge Press, 261 pp.

A DISCUSSION OF THE SOURCES AND CIRCULATION OF NORTH ATLANTIC DEEP WATER

L. Valentine Worthington

July 3, 1968

A comprehensive discussion of the North Atlantic deep water was presented. Both classical descriptive water mass distributions and modern direct current measurements were analyzed.

First, a review of the climatic history of the North Atlantic was made, linking sea level to principal events in the history of glacial ice cover over the past few thousand years. One feature of note is that there was a minimum of ice cover about 1000 B.C., so sea level stood about 1.6 meters higher than today. The subsequent withdrawal of water during the little ice age of 0-1800 A.D. may have caused the observed fact that the North Atlantic has a greater salinity today than the other oceans; the amount of water withdrawn could account for an increase in salinity of 0.2 ‰ in North Atlantic deep water. Another noteworthy feature is that it is possible to estimate ancient θ -S relations (θ : potential temperature; S: salinity) for deep water; it was reported that no "fossil" water has been found nor is it likely to be found. The apparent age of oceans has been estimated by C^{14} dating; though the reliability of these estimates is still in doubt, they lead to the following values:

	ATLANTIC	PACIFIC
Deep Water	800 yrs.	1500-1800 yrs.
Surface Water	500 yrs.	1000 yrs.

In each layer, the Atlantic appears youngest in the north, while the Pacific appears youngest in the south.

Second, the θ -S relationships were investigated en toto for the North Atlantic, then those of the deep water were subjected to special scrutiny. In several respects, this work is an extension of studies by Montgomery (1958),

Cochrane (1958), and Pollak (1958). The data used in the present work is based on samples taken from 1954-to-1962, i.e., centered on the 1958 IGY. Deep water is considered to consist of all water contiguous with the bottom and with $\theta \leq 4^{\circ}\text{C}$; it represents 90% of the ocean's volume.

The dominant mode of deep water, containing 75% of the water, has a salinity of 34.90 - 35.00 ‰ in the Atlantic and of 34.60 - 34.70 ‰ in the Pacific, demonstrating the greater salinity of the Atlantic deep water with respect to that of the Pacific. Charts showing the distribution of salinity, and thus of identifiable water sources, were shown on successive surfaces of constant θ for the North Atlantic. A synopsis of features on several θ surfaces is given below:

$\theta \leq 1.0^{\circ}\text{C}$. The overflow from the Denmark Strait (DSO), with $S = 34.9$ ‰, and the Antarctic Bottom Water (ABW), flowing across the Equator with $S = 34.8$ ‰, appear.

$\theta \leq 1.4^{\circ}\text{C}$. The DSO penetrates south to 53°N and part of it turns north along the east Labrador Basin. The ABW penetrates north to the Puerto Rican trench. The depth of this surface varies between 500 and 3500 meters in the north and 4000 to 6000 meters in the south.

$\theta = 1.8^{\circ}\text{C}$. This is the "last" (i.e., shallowest) surface on which the DSO and ABW remain distinct, and there is evidence for mixing, so salinities can't be accurately traced to sources, e.g., the DSO has $S = 34.92$ ‰ and ABW has $S = 34.89$ ‰, which can't be traced to the Antarctic. They both continue to penetrate along the western side of the basin. The DSO is a very thin layer, while the ABW is a thick layer; they reach a depth of about 4500 ± 500 meters.

$\theta = 2.4^{\circ}\text{C}$. The third source, the Iceland-Faroes overflow (IFO), appears; its salinity, $S = 34.99$ ‰, can't be found in the Norwegian Sea, so it must be

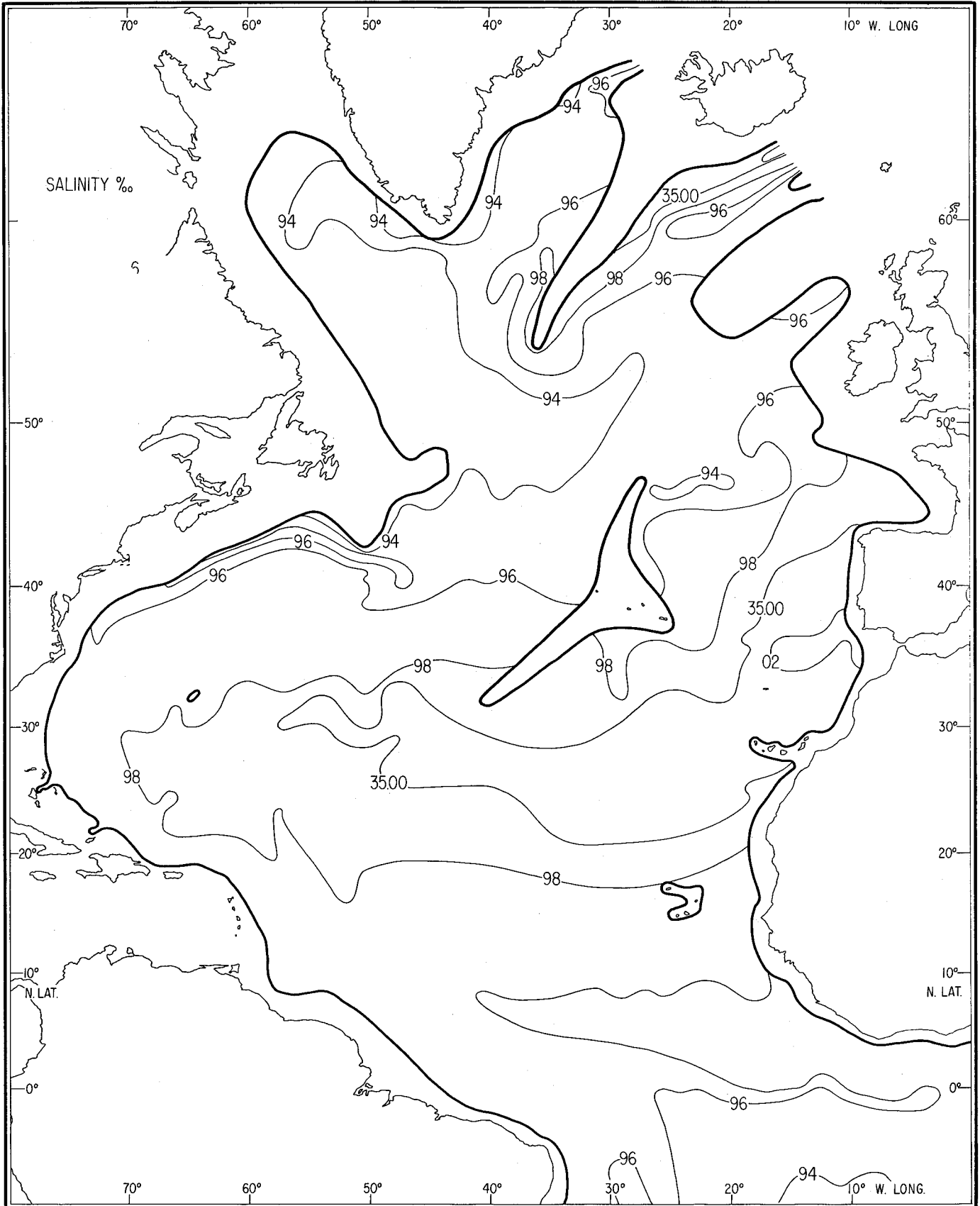


Fig. 1. Salinity at the 3.2°C potential temperature surface in the North Atlantic.

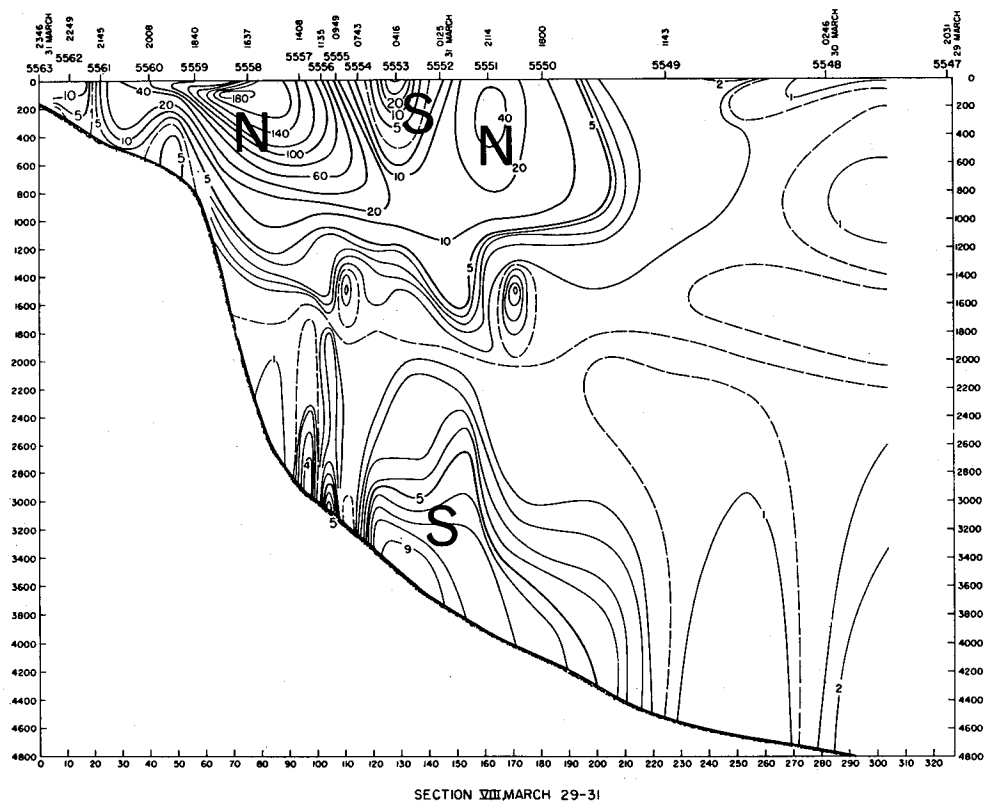
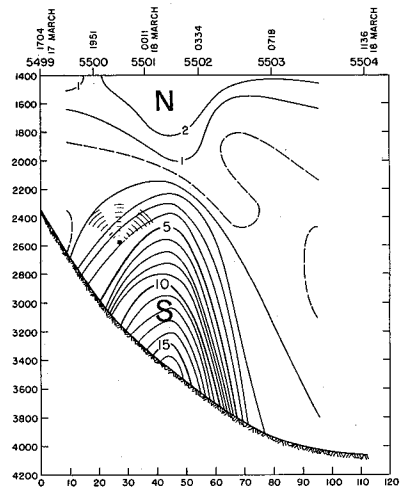
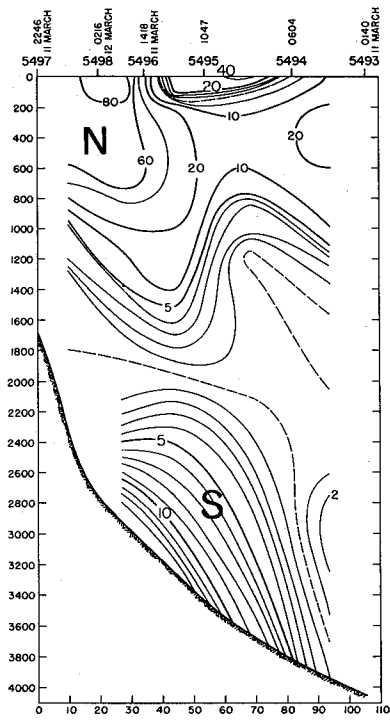


Fig. 2. Sample hydrographic sections with direct current measurements used to calibrate velocity field, from Swallow et al. (1961).

water which has mixed with northward flowing North Atlantic water, with $S = 35.10$ ‰, before sinking.

$\theta = 3.2^{\circ}\text{C}$. The fourth source, Mediterranean outflow (MW), appears and gradually sinks west of Gibraltar. The IFO penetrates a gap in the mid-Atlantic Ridge at 53°N and develops a northerly flow on the western side of the ridge. (Figure 1).

$\theta = 4^{\circ}\text{C}$. The fifth and final source, Labrador Sea Water (LSW), appears. The MW extends across the Atlantic, separating the waters of northern and southern origin. This surface varies in depth from the sea surface at Labrador to 1000 meters at the western boundary, and to 2000 meters at Gibraltar.

Third, the direct measurements of deep flows ($\theta \leq 4^{\circ}\text{C}$) were discussed; the bulk of this data has been acquired in the past ten years and in conjunction with hydrographic sections. The direct measurements were made primarily by Lagrangian means, viz., with neutrally buoyant floats (NBF's) developed by Swallow, but some were made by Eulerian means, viz., with moored arrays of recording current meters developed by WHOI. Various hydrographic sections were shown to give evidence for the existence of deep density gradients and thus pressure gradients and, finally, geostrophic currents. It was remarked that the most interpretable results come from making hydrographic stations between NBF "stations" where two or more NBF's are set on a common vertical. The NBF mean currents are then used to calibrate the geostrophic calculations by aiding in the selection of a level-of-no-motion, or "null flasher". In turn, the geostrophic calculations make the NBF measurements more meaningful by giving a vertical section of isotachs which can be used to make transport calculations in addition to point-wise velocity determinations. Three hydrographic sections are shown in Figure 2 which have had their reference level determined with aid of NBF's.

A summary of deep current transport calculations in the North Atlantic is presented in Figure 3 for eight sections or regions; the units are sverdrup's. At Section I (Steele et al., 1962) near Iceland, NBF's gave westward currents with mean speeds of 23 and 8 cm/sec at depths of 1300 and 1800 meters, respectively. The calculated southward transport was 5.4 sv (a sv is a sverdrup, $1 \text{ sv} = 10^6 \text{ m}^3/\text{sec}$). At Section II, again near Iceland, 2 NBF's and moored meters were used (Worthington and Volkmann, 1965). Transports of 4.6 sv flowing through a gap (53°N , 36°W) in the Mid-Atlantic ridge and of 0.7 sv going south along the ridge were calculated. In Section III, the Denmark Straits, an ambitious installation of moored temperature recorders and current meters was made in late winter. Only three temperature recorders and current meters of the seven recovered gave useful results. The records ran a little more than a month. Southwestward currents about 100 meters above the bottom in at least 815 meters of water occurred in 8 "bursts" at about 4-day intervals, each with a duration of about 2 days. The maximum speed was 143 cm/sec. Correlated with the current bursts were temperature bursts; the onset occurred first at 815 meters, then at 760 meters, and finally at 655 meters; each burst cessation occurred simultaneously at the three sensors. There is a possibility that the lower 200-to-300 meters of the channel was filled intermittently with cold water "sloshing-over" the sill. It is also possible, since these current measurements were made in mid-channel, that the cold water flowed continuously along the northern side of the channel and only occasionally "sloshed-over" to mid-channel. Transport calculations produced an estimate of 10 sv. From Swallow et al. (in preparation) at Section IV, the Labrador Straits, there is a northward flow on the Greenland side and a southward flow on the Labrador side, with transports of 10 sv. South of Woods Hole, Volkmann (1962) reported a westward flow with a transport of 50 sv. from the surface to the bottom. This was probably the western boundary undercurrent, though subsequent measurements

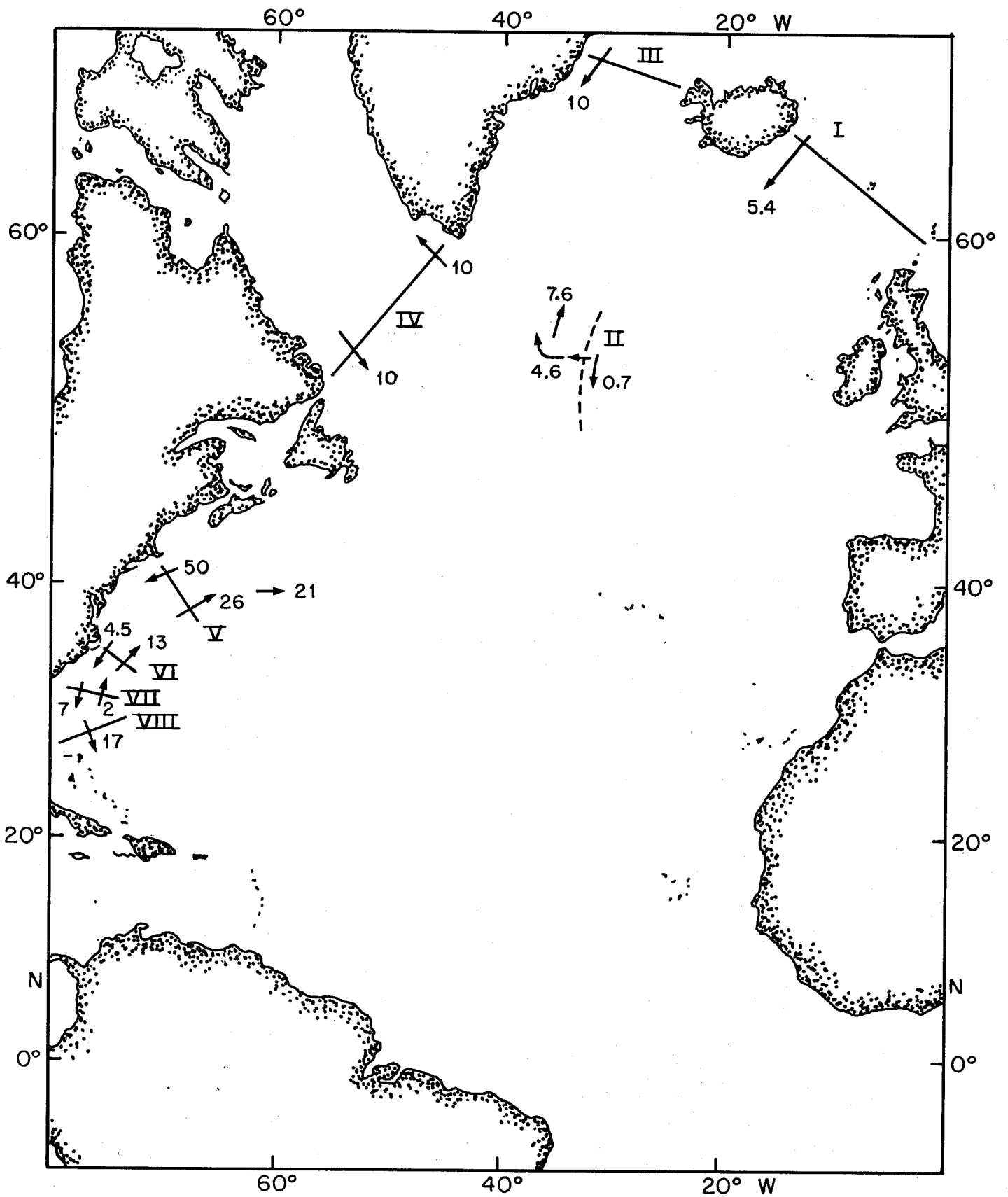


Fig. 3. Sections referred to in the text where direct measurements of deep water transports have been made. Quantities are transport values in sverdrups.

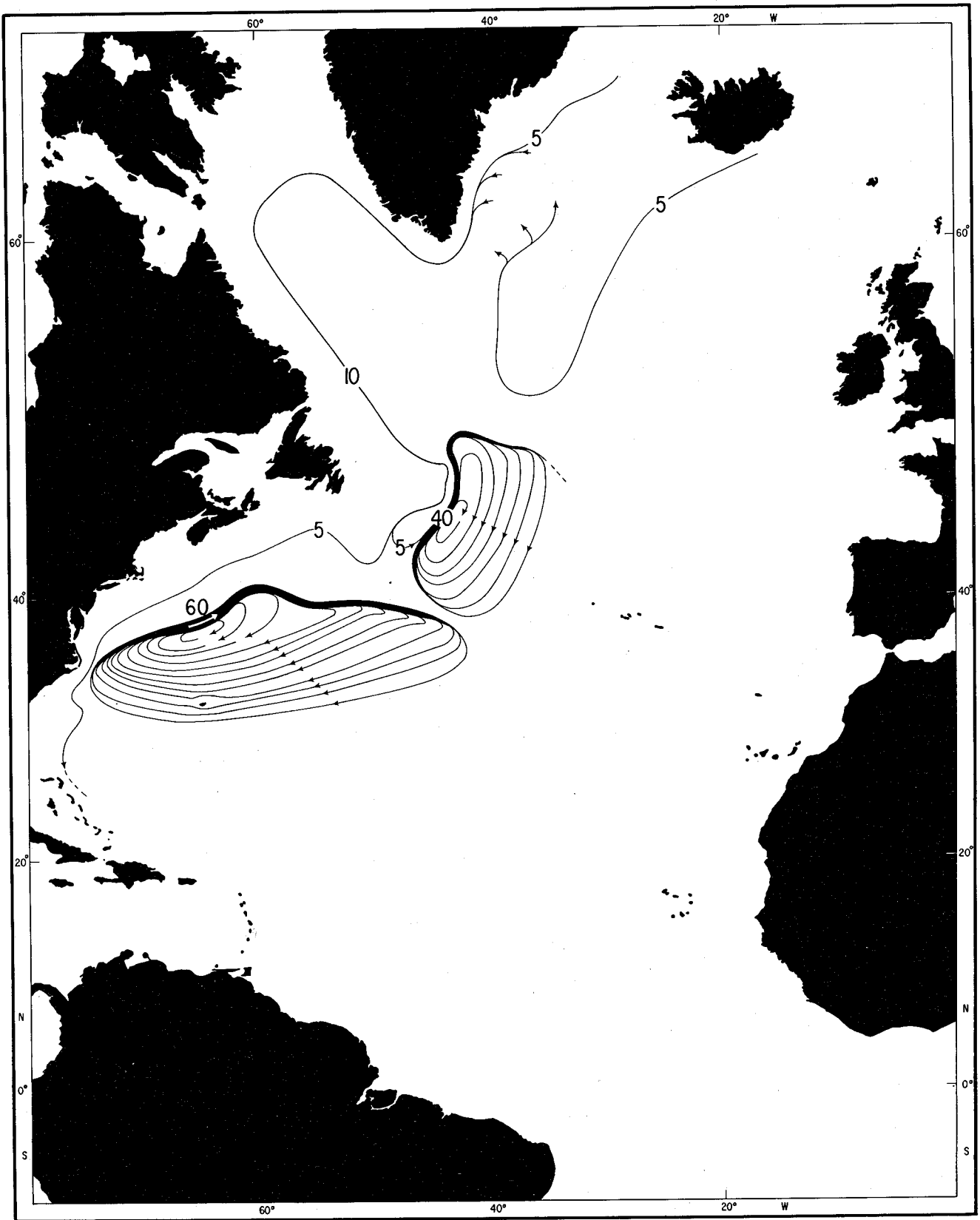


Fig. 4. Proposed deep water circulation system, based on observations. Quantities are transport values in sverdrups.

have never again detected such a high transport value. Water budget considerations suggest that this value is too high. In a section across the Gulf Stream south from Woods Hole, Section V, an eastnortheastward flow of deep water was found by Warren and Volkmann (1968); it was about 300 kilometers wide and had a transport of 26 sv. The maximum flow was found at 64°W and was 60 sv. This flow decreased eastward. North of this latitude, 36°N , there is an apparent east-west "barrier" between the northward and southward flows of deep water. The "barrier" corresponds to a "trough" filled with Mediterranean water.

At Cape Hatteras, Section VI, Swallow and Worthington (1961) found the undercurrent; its core was at a depth of about 2400 meters, and its transport was about 4.5 sv. Further east, there was also a transport of 13 sv northward. At sections from the Bahamas to Bermuda and Cape Romain to Bermuda, Sections VII and VIII respectively (Swallow and Worthington, 1961), the southward transport was about 17 and 7 sv through the former and latter, respectively. There was also a transport of about 2 sv northward on the latter section.

Finally, the high transport values calculated cannot be balanced geostrophically everywhere. Two anticyclonic gyres near the western boundary are hypothesized in order to close the deep circulation. This leads to the proposed water budget for the deep North Atlantic shown in Figure 4.

Notes submitted by
Gunnar Kullenberg and
Christopher N. K. Mooers.

References

1. Cochrane, J. D. (1958). The Frequency Distribution of Water Characteristics in the Pacific Ocean. Deep-Sea Research, 5: 111-127.
2. Montgomery, R. B. (1958). Water Characteristics of the Atlantic Ocean and of the World Ocean. Deep-Sea Research, 5: 134-148.

3. Pollak, M. E. (1958). Frequency Distribution of Potential Temperature and Salinities in the Indian Ocean. Deep-Sea Research, 5: 128-133.
4. Steele, J. H., J. R. Barret and L. V. Worthington (1962). Deep Currents South of Iceland, Deep-Sea Research 9: 465-474.
5. Swallow, J. C. and L. V. Worthington (1961): An Observation of a Deep Counter-current in the Western North Atlantic. Deep-Sea Research 8: 1-19.
6. Swallow, J. C. and L. V. Worthington (in preparation): Tentative Title: Notes on the Erika Dan Current Measurements (concerning deep currents in the Labrador Sea).
7. Volkmann, G. H. (1962). Deep Current Observations in the Western North Atlantic. Deep-Sea Research, 9: 493-500.
8. Warren, B. A. and G. H. Volkmann (1968). Measurement of Volume Transport of the Gulf Stream South of New England. J. Marine Res. 110-126.
9. Worthington, L. V. and G. H. Volkmann (1965). The Volume Transport of the Norwegian Sea Water in the North Atlantic. Deep-Sea Research 12: 667-676.

GULF STREAM RINGS

Frederick C. Fuglister

July 5, 1968

A bi-decennial progress report was presented on the patterns of irregularities in the Gulf Stream downstream of Cape Hatteras and west of the Grand Banks. (The original objective of this work had been the tracing of the Gulf Stream downstream to the Grand Banks; this objective has never been achieved, but, rather, an increasingly detailed documentation of Gulf Stream meanders and rings has been obtained.) A Gulf Stream ring is defined to be a member of a special class of eddy; this class consists of closed segments of the Gulf Stream which have become detached from the Gulf Stream per se. Rings found to the south of the Gulf Stream rotate cyclonically and contain cold water (slope water) from north of the Stream in their centers, while those found to the north of the Gulf Stream rotate anti-cyclonically and contain warm water (Sargasso Sea water) from south of the Stream in their centers.

A summary of the principal observational considerations and techniques is given below:

a) The region studied is a 2100 km segment of the Gulf Stream, running from about 35°N , 75°W to about 40°N , 50°W .

b) The principal indicator of the position of the Gulf Stream is the topography of the main thermocline, a consistent index of which is the depth of the 10°C isotherm; the depth of the 10°C isotherm is about 200-to-300 meters north of the Stream and 800-to-900 meters south of the Stream; a core of warm water near the surface is usually located over the shallow edge of the Gulf Stream frontal layer (i.e., where the main thermocline is strongly inclined with respect to the horizontal).

c) When the Gulf Stream is traversed, and when warm cores and thermoclines are intersected more than once, ambiguities in interpretation frequently arise, especially if an ordinary BT with a depth range of only 250 meters is used; among the ambiguities are the possibilities that such a multiple intersect may represent meanders, rings, or several filaments of a diffuse stream; to remove the ambiguities, new techniques have been employed, e.g., multiple ship surveys, isotherm followers (V-fin's) which can track the fiducial 15°C (which is more convenient for this purpose than the 10°C isotherm) at 200 meters depth, deeper (and expendable) BT's, plank-on-edge floats which can "tag" selected rings for months, neutrally buoyant floats, airborne radiometers, etc.

d) The anticyclonic rings north of the Stream have been less thoroughly studied than the cyclonic rings to the south for two reasons: generally more inclement weather prevails to the north than to the south and the anticyclonic rings are inherently more difficult to detect because they have intrinsically

weaker horizontal gradients. Both types of rings are cyclostrophic flows, but because the Coriolis and centrifugal forces act in the same direction (as in an atmospheric low), the opposing radial pressure gradient and thus the temperature gradient in a cyclonic ring must be more intense than in an anticyclonic ring. A further complication in detection of anticyclonic rings is that, while cyclonic rings are formed "from above", giving rise to a readily identifiable upright cone structure to the thermocline, the anticyclonic rings are formed "from below" giving rise to an inverted cone structure which is often too deep to be properly identified when using ordinary BT's.

While the dynamics of the formation, migration, and decay processes in the rings' life cycle are not yet clearly understood (see Warren (1967) for some ideas about these questions), observations have progressed to the point where a number of qualitative and quantitative statements can be made about the rings:

- a) The rings appear to form at or to the east of the New England seamount range, i.e., east of 70°W and north of 37°N ; the eastern limit of their formation zone is unknown, see Figure 1 for examples.
- b) Rings appear to be formed when the "bight" of a large meander is cut off at the "neck", the two "bitter ends" then joining.
- c) Rings have been observed between 37° and 38°N and 60° and 66°W ; they tend to drift to the west and south in an irregular fashion at speeds of the order of 10 cm/sec; long term studies of a few rings have shown that, while they rotate cyclonically with a period of about two days in their fast, shallow sections, they revolve anticyclonically in a large orbit with a period of about two months, thus water parcel trajectories can vary widely as a function of depth; there is some speculation that they may occasionally collide and merge with the Gulf Stream but no observations unequivocally confirm this.

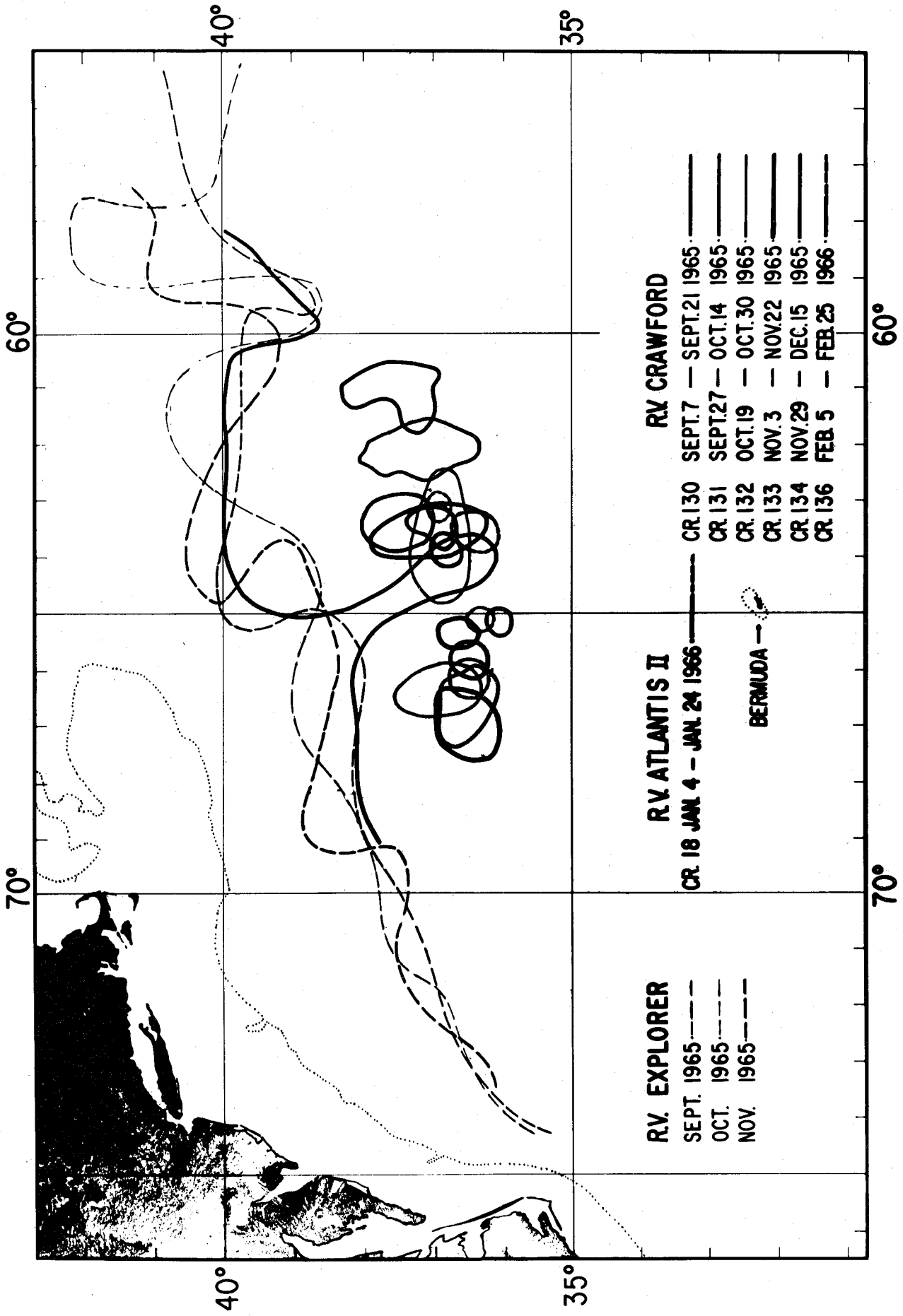
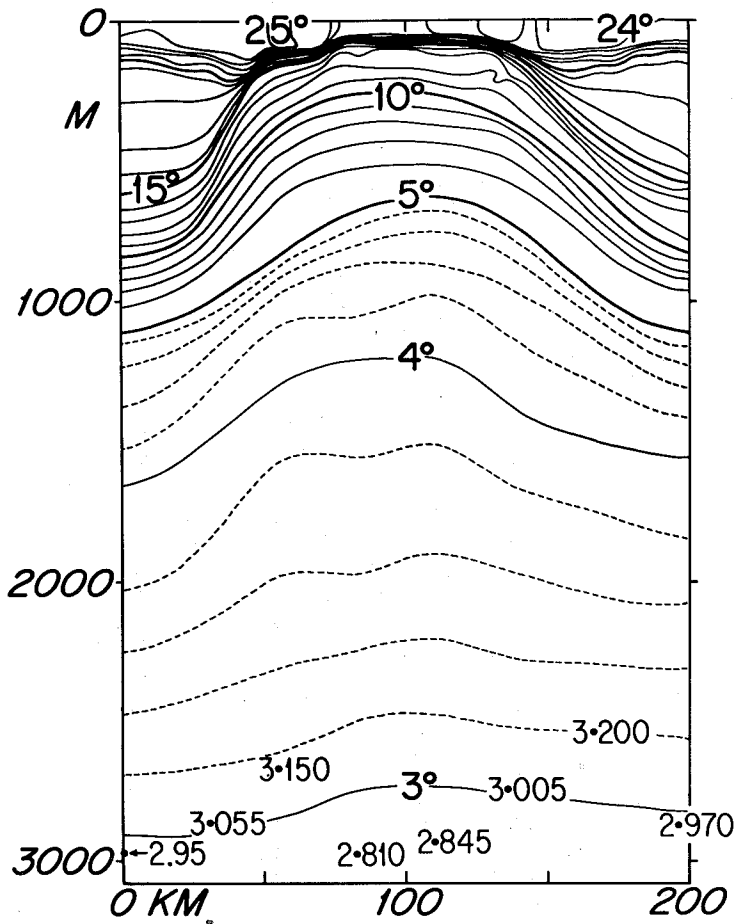


Fig. 1. Recent observations of the Gulf Stream path in a six-month period.



THE WESTERN EDDY
 October 1965 (left) and
 January 1966 (right)

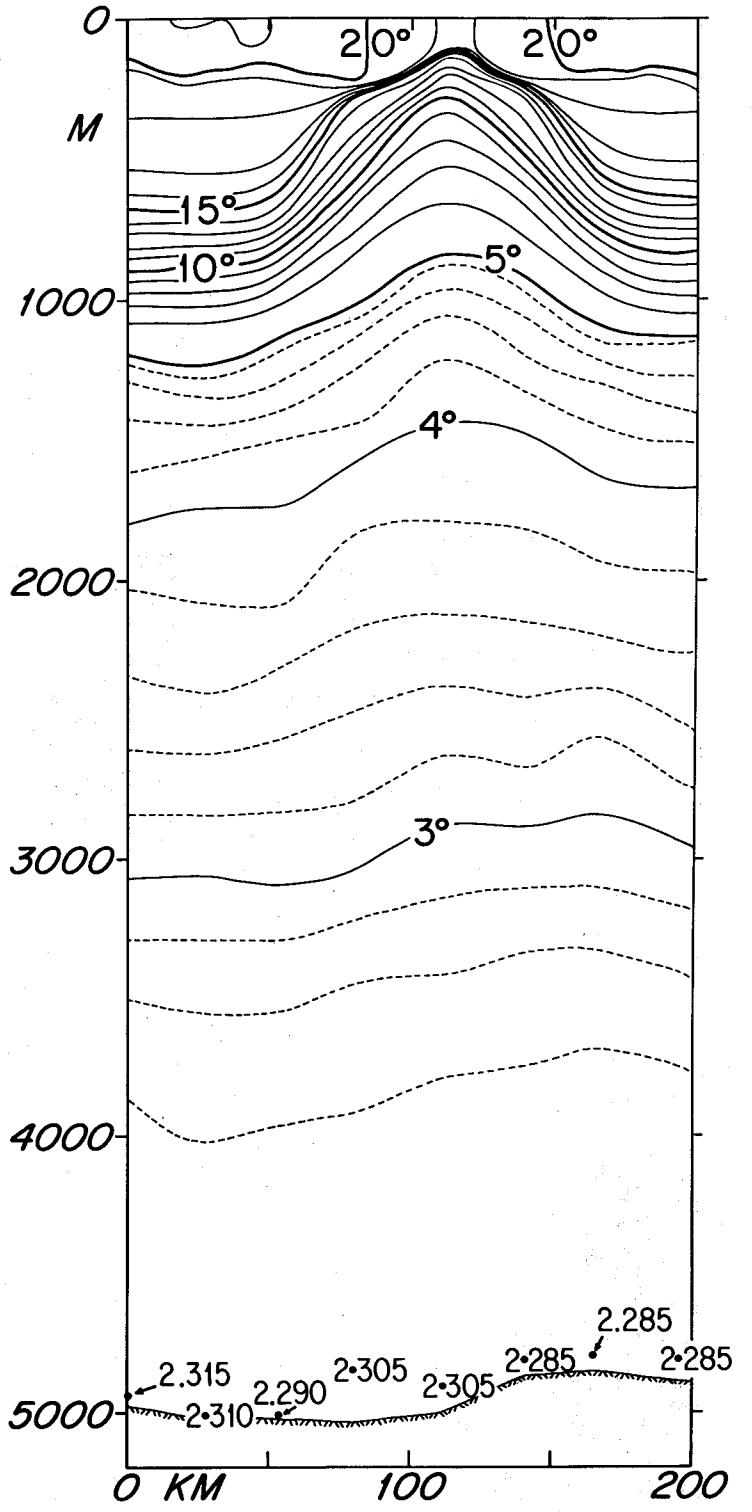


Fig. 2. The vertical hydrographic structure of a Gulf Stream ring.

d) Figure 2 shows a temperature section through a typical cyclonic ring; note the "upwelled" dome in the center; as time progresses, it will "sink" and become narrower in lateral extent; the lateral and vertical extents of a ring are typically 100 and 2-to-3 kilometers, respectively; rings are often circular in shape but are sometimes elongated, with arbitrary orientation; the rotating currents of a cyclonic ring are typically of the order of 50-to-150 cm/sec, with the maximum value at the surface (when only a single traverse of a ring is made, and when ship's drift records are available, it is practical to use this information to decide which side of a ring has been traversed and, thus, something of its size and of the location of its center can be inferred).

e) On one occasion, a pair of rings, referred to as the eastern and western rings, were tracked for 5 months; Figure 3 gives a record of their joint history; observe the near coalescence of the two during the 27-29 October survey.

f) Two independent estimates of the number of rings formed per year were made; one estimate was based on the difference in the average annual inflow and outflow (+25 cm/sec) over the 2100 km segment of the Gulf Stream under discussion and gave a value of 15 rings; the other estimate was based on the monthly net departure of the Gulf Stream from its mean position over the same segment and gave a value of 14 rings; presumably, an equal number of cyclonic and anti-cyclonic rings would occur, say 7 per year; to date, the formation of only 4 rings has been observed.

g) It takes about 6 months to erode the upper 200 meters of a ring and perhaps 18 months for the complete decay of a ring.

In closing, it is appropriate to point out a simple fact in the distinction between rings and ordinary eddies: rings rotate in the "wrong" sense with

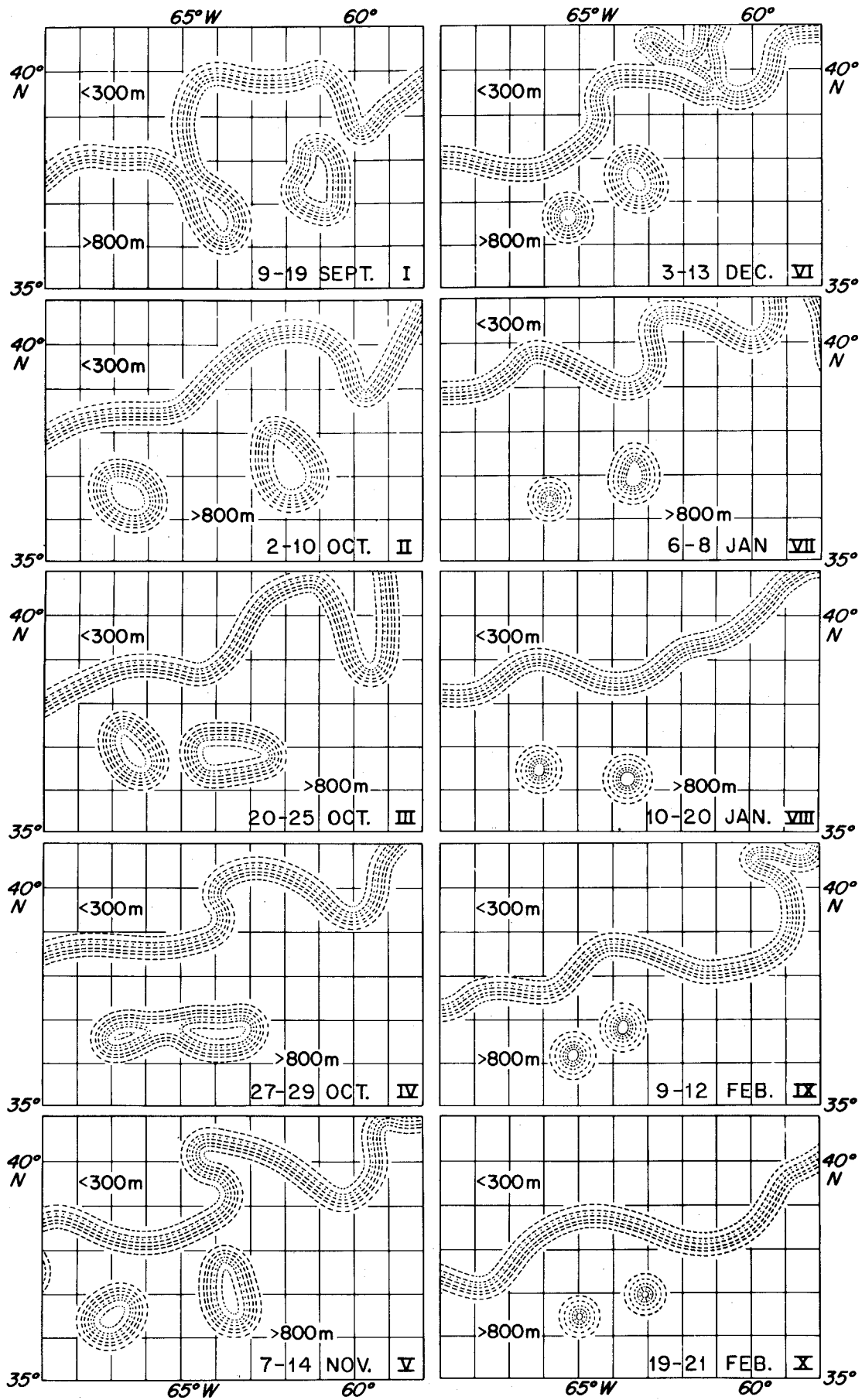


Fig. 3. A sequence in the life cycle of a current ring. Ring formation is shown in upper left. Figures 300 and 800 m indicate the depth of the main thermocline.

respect to ordinary eddies from the Gulf Stream. Since the Gulf Stream has anticyclonic shear (or vorticity) on its warm side, ordinary eddies south of the Gulf Stream would be expected to have anticyclonic rotation while the rings have cyclonic rotation. A similar, but opposite, relationship holds for anticyclonic rings and cyclonic ordinary eddies north of the Stream.

It is also necessary to mention that the present discussion of meanders and rings does not contradict earlier discussions which emphasized the multiple stream nature of the Gulf Stream System, especially downstream or the New England seamount range.

Notes submitted by
Gunnar Kullenberg and
Christopher N. K. Mooers

References

- Fuglister, F. C. (1955). Alternative Analyses of Current Surveys, Deep-Sea Research, 2: 213-229.
- Fuglister, F. C. (1963). Gulf Stream '60. In: Progress in Oceanography, 1: 265-373.
- Fuglister, F. C. and L. V. Worthington (1951). Some Results of a Multiple Ship Survey of the Gulf Stream, Tellus, 3: 1-14.
- Warren, B. A. (1967). Notes on Translatory Movement of Rings or Current with Application to Gulf Stream Eddies. Deep-Sea Research, 14(5): 505-524.

ABSTRACTS



SUMMARY OF DISCUSSIONS ON CHEMICAL TRACERS IN THE OCEANS

Wallace S. Broecker, Harmon Craig, Göte Ostlund,
Kilho Park and Karl K. Turekian

Chemical properties of ocean water that do not show simple linear relationships to salinity are potentially useful in the study of physical oceanographic problems such as the construction of large scale circulation models; the determination of rates and mechanisms of transport in the mixed layer, thermocline, deep water and bottom water; and the study of air-sea interactions. The chemical properties that may be useful can be divided into several groups:

Natural radioactivity: Several radioactive isotopes naturally produced by cosmic rays or as members of the uranium decay series have been proposed as useful in large scale circulation models and transport mechanism studies.

These are:

Carbon-14,	5700 year half-life
Silicon-32,	800 year half-life
Radium-226,	1600 year half-life
Radium-228,	7 year half-life
Radon-222,	4 days half-life.

Of these Carbon-14 has been the most useful. To a first approximation the concentration of Carbon-14 per liter of sea water is the same in all major parts of the ocean. This is maintained by large scale circulation and addition of Carbon-14 to depth via organic carbon (80%) and inorganic calcium carbonate (20%).

Radium-226 distribution in the ocean is controlled not only by large scale circulation but also biological transport from surface to depth. Most of

the radium in the ocean appears to be supplied from the sediments. An indicator of the biologically controlled radium distribution may be the distribution of barium in ocean water profiles.

Silicon-32 may be useful, but the difficulty of collecting large enough samples (requiring the processing of up to one million liters of sea water) has made the accumulation of data a slow process.

Radon-222, in excess of that to be expected in equilibrium with the measured concentration of its parent, Ra-226, has been used to study mixing rates near the ocean bottom and in the surface. It is supplied from the ocean bottom at a more rapid rate than Ra-226 and is lost to the atmosphere at the ocean surface. At the surface it can also be used as a test of models of gas exchange between the atmosphere and the ocean.

Radium-228 is just now being explored for use in oceanographic problems. It is supplied from the sediments as the result of Th-232 decay. It will give further information in mixing rates at the ocean bottom.

Man-made radioactivity: Bomb-produced Cs-137, Sr-90 and H-3 (tritium) have been used in oceanic problems especially those in the top 500 meters of the column.

Cs-137 and Sr-90 measurements indicate that mixing in the thermocline is as low as would be predicted from the natural C-14 data. Huge amounts of Sr-90 and Cs-137 are clearly not transported below 500 meters by biological means, a result compatible with the lack of great variation in the stable cesium and strontium concentrations in the oceans.

The properties of the mixed layer and thermocline are further elucidated by the distribution of Cs-137 and H-3 which indicate that "sheets" of water may retain their identity for great distances in the upper layers of the ocean and that vertical diffusion proceeds at a relatively slow rate.

Tritium has also been employed in studies of air-sea interactions especially as applied to the generation and nourishment of hurricanes.

Gases: The use of O_2 and $\sum CO_2$ (most of the CO_2 is as the bicarbonate ion but is included under gases for convenience here) as ocean mixing indicators was suggested. If two water masses with typical O_2 and $\sum CO_2$ concentrations are mixed in different proportions and also modified by the conversion of organic carbon to $\sum CO_2$ by the utilization of dissolved O_2 , the complex patterns of O_2 plotted against $\sum CO_2$ can be explained.

The rare gases (He, Ne, Ar, Kr, Xe) can be used in ocean mixing models if the temperature of the source water is roughly known and mixing of the water masses takes place out of contact with the atmosphere. The differences to be measured are small but initial results indicate the utility of such an approach especially in understanding the origin of the intermediate waters.

Hydrogen and oxygen isotopes: These two isotopes respond essentially identically during the processes of evaporation, precipitation, freezing and melting so that information on one or the other is often sufficient in tracing water masses. Work on oxygen isotopes (O^{16}/O^{18} ratios) indicates that North Atlantic Deep Water and Atlantic Surface Water form a continuum on an oxygen isotope salinity plot, hence show a close kinship. This is not true of Pacific Deep Water when compared to Pacific Surface Water. Antarctic Bottom Water

produced in the Weddell Sea shows a characteristic isotope composition. Pacific Deep Water is not a linear combination of Antarctic Bottom Water and North Atlantic Deep Water indicating the addition of a third component.

Phosphate and alkalinity: Deep Pacific Water has a constant "pre-formed" phosphate content from about 50°S northward indicating that most of the oxidation of biological material and phosphate release from organic material derived from the Antarctic takes place rapidly.

The injection of water from the north is clearly seen as both an oxygen and a phosphate increase.

Alkalinity plots with depth in the ocean indicate that in the Atlantic (where the alkalinity is lowest of the ocean deep waters) there is an alkalinity increase near the bottom (about 4000 meters) whereas in all the other oceans there is rarely an increase at the bottom and some indications of maxima in the water column at depths between 3000 and 4000 meters. These may be relatable to ocean mixing processes.

ABYSSAL RADIOCARBON - Σ CO₂ - OXYGEN

Harmon Craig

Several recent studies have used radiocarbon data in diffusion-advection equations of the type:

$$\kappa C'' = \omega C' + \lambda C \quad (1)$$

where λ is the radioactive decay constant, C is concentration, and the successive derivatives are taken with respect to z or x in vertical or horizontal transport studies. Radiocarbon data used for relative concentrations were taken from the

Δ values tabulated by radiocarbon laboratories; these Δ values represent specific activities (C^{14}/C^{12} ratios) in carbonate extracted from sea water, rather than absolute C^{14} concentrations which must be used in the diffusion equation. Absolute radiocarbon concentrations can be obtained by multiplying the specific activities by the corresponding total dissolved carbonate (ΣCO_2) concentrations; the corrections thus introduced are large and variable, ranging up to 40% in $C^{14}\Delta$ values (300 years in "advective" time).

Moreover, equation (1) neglects the continuous production of CO_2 by oxidation of particulate organic matter, and by solution of associated particulate organic matter, and by solution of associated particulate $CaCO_3$. Thus if the steady-state oxygen equation is written

$$k(O_2)'' = \omega(O_2)' + \nu \quad (2)$$

with ν the oxygen consumption rate (cc/kg yr), the stable carbon equation can be written

$$kC'' = \omega C' - \nu - J \quad (3)$$

where $C = \Sigma CO_2$ (cc/kg), J is CO_2 production by solution of carbonate, and the small imbalance between ν and CO_2 production by oxidation has here been neglected. The complete radiocarbon one-dimensional equation is then:

$$k(C^*)'' = \omega(C^*)' + \lambda C^* - \nu R_\nu - J R_J \quad (4)$$

in which C^* is absolute C^{14} concentration, R is the isotope ratio C^{14}/C^{12} , and the subscripts denote the ratio for CO_2 produced by the two sources.

Profiles of ΣCO_2 and O_2 were measured by Weiss and Craig along a N-S track in the central Pacific on SIO Expedition NOVA during 1967. Using the ΣCO_2 data, approximate corrections were applied to the Bien-Rakestraw-Suess

Pacific radiocarbon specific activities to give absolute C^{14} concentrations (C^*). The ΣCO_2 data were measured at sea, using shipboard gas chromatography with electrolytically generated H_2 as a carrier and thermistor detectors. Precision of the data is about 0.3 percent so that measurement errors are not significant compared to the ± 1 percent errors assigned to the C^{14} data.

In contrast to the specific activity profiles, which show a marked C^{14} minimum at about 2.5 km depth, the corrected absolute activities decrease by about 40-50‰ from one km down to 2 km, and are then essentially constant to the bottom. They definitely do not fit the curves plotted by Munk (1966) using equation (1) with specific activities and finite ω/λ ratios; the best fits are given by $\omega = \text{infinite}$, or even by a small negative value for λ .

Values of ν/ω can be obtained by fitting O_2 data to equation (2); values of J/ω can be obtained most precisely by fitting data on $(\Sigma CO_2 + O_2)$ to an equation which is the sum of (2) and (3), and individual values of ν and J can be roughly estimated from O_2 consumption and geochemical data. If we normalize terms in equation (4) by multiplication with C/C^* , then neglecting insignificant differences between R , R_ν , and R_J , the last three terms on the RHS are approximately:

$$\nu \approx + 0.005 \text{ cc/kg yr}$$

$$J \approx + 0.001 \text{ cc/kg yr}$$

$$\lambda C \approx \frac{50 \text{ cc/kg}}{8033 \text{ yrs}} \approx 0.006$$

so that $(\nu + J) \approx \lambda C$ and the last three terms on the RHS of equation (4) approximately cancel. The advective term (normalized) is $(\omega C/C^*) (dC^*/dZ)$, which varies from about 0.03 to zero (for ω perhaps 8 m/year). Therefore C^{14} essentially obeys the simple equation for a conservative substance:

$$\kappa C'' = \omega C' \tag{5}$$

with considerable scatter in the profiles reflecting slight variations in the various production rates. For this reason no information on absolute values for K and ω can be obtained from C^{14} profiles, and the numbers derived by Munk (1966) should be discarded.

The C^{14} specific activity minima at depths between 1-4 km are due to the fact that ΣCO_2 shows a broad maximum in these depths because of the particulate input $\nu + J$. This input produces C^{14} at a rate closely equal to the radioactive decay rate; thus the absolute activity is essentially constant, resulting in a minimum in specific activity or C^{14}/C^{12} ratio. Using the specific activity curves, Munk calculated a diffusive flux of C^{14} upward from the horizontally advecting bottom water layer, resulting in a continuous loss of C^{14} at a rate much greater than the radioactive decay rate within the bottom layer. He thus concluded that the Bien-Rakestraw-Suess horizontal flow velocity for this layer was a lower limit, and must actually be 15 times greater than their mean figure of 0.07 cm/sec. However, the absolute activity curves show that there is actually almost no vertical diffusion gradient at this depth, but that, if anything, the net C^{14} flux is downward. The B-R-S flow velocities will therefore be upper limits, but will not be strongly affected by diffusion. On the other hand, some of their "bottom water" data actually are samples from about 3000 m, in the specific activity minimum, and therefore their assigned relative ages for bottom water are too large in some cases, especially in the North Pacific.

AIR-SEA EXCHANGE OF WATER IN HURRICANES

H. Göte Ostlund

Seawater, tropospheric vapor, and stratospheric vapor, are characterized by different tritium concentrations. The sea surface is at the lower end of the scale, the tropospheric humidity is intermediate, and the stratospheric vapor highest. When the "undisturbed" air around the hurricane, "ambient air", is entrained into the envelope of the storm, the air-sea exchange will lower the tritium concentration of the water vapor. This effect, the molecular exchange, occurs primarily at the surface of spray droplets of seawater formed in the high winds, and the lowering of the tritium concentration in the vapor is a quantitative measure of the magnitude of air-sea exchange of water. From data on tritium versus radial distance, conclusions can be drawn on possible distribution of mass inflow and influence of wind speed on rate of air/sea exchange of water.

Of more pragmatic interest is the relative importance of local evaporation. If the (radial) water vapor inflow at some large radius is $V \text{ g sec}^{-1}$, the total evaporation inside that radius is $E \text{ g sec}^{-1}$, and the loss of water to the outflow layer is neglected, $R = E/(E + V)$, is the interesting ratio. The tritium data can supply information on this ratio, and our measurements are good enough for the purpose, but three more parameters are essential. Absolute humidity at cloud base and at the very sea surface, can be reasonably well measured. We also need the radial distribution of the vapor inflow. This information is presently not available with any degree of reliability, due to the inability of the airborne Doppler-wind instruments to resolve the very small radial component of the wind.

In the future we hope to perform tracer experiments in hurricanes. Let us assume that we at one point release one tracer for air and one for water vapor

(e.g. HT gas and HTO vapor). The concentration ratio between the two tags in air samples downwind, will have a direct bearing on our R, without need of information on radial wind component. In addition, the rate of inflow might possibly be derived from the time and position of samples containing the tags.

A NONLINEAR MODEL OF AN OCEAN DRIVEN BY WIND AND DIFFERENTIAL HEATING

Kirk Bryan

A numerical experiment is carried out to investigate the circulation of an ocean, driven by a prescribed density gradient and wind stress at the surface. The mathematical formulation includes in one model most of the physical effects considered in previous theoretical studies. Starting out from conditions of uniform stratification and complete rest, an extensive numerical integration is carried out with respect to time. Care is taken in the final stages of the calculation to use a finite difference net which resolves the very narrow boundary layers which form along the side walls of the basin.

A detailed description is made of the three-dimensional velocity and temperature patterns obtained from the final stage of the run. Since inertial effects play an important role in the western boundary current, it is possible to verify with a baroclinic model two results obtained previously with barotropic models, i.e. (a) a concentrated outflow from the western boundary takes place along the upper boundary of the subtropical wind gyre, (b) inertial recirculation may increase the total transport of the boundary current to a value well above that given by linear theory. In addition to the western boundary current, a strong eastward flowing current is found along the equator. Taking into account

a difference in Rossby number between model and prototype, the intensity of the computed currents agree very closely to observation in the Gulf Stream and the Equatorial Current.

BOUNDARY LAYERS AND LARGE SCALE NUMERICAL MODELS

Henry Charnock

The boundary layers of the atmosphere and ocean are among the regions where small-scale motions--smaller than the grid size of foreseeable numerical models--are dynamically important. They can perhaps be incorporated by empirical methods of the kind here discussed: the treatment is based on a paper by H. Charnock and T. H. Ellison presented at the GARP Planning Conference, Stockholm, 1967.

For this purpose we take the atmospheric boundary layer to be the region near the surface where turbulence on a scale not much greater than the height transfers significant quantities of heat matter and momentum. It is to be distinguished from the Ekman layer, where the wind differs from its (complete) frictionless value. The Ekman layer may fill the boundary layer but will often occupy only a portion of it. Another subdivision of the boundary layer is the surface layer, where the fluxes are approximately constant with height and where the Monin-Obukhov scaling is appropriate.

The interfacial layer has a thickness of the same order as the surface roughness: its dynamics and thermodynamics are complex, especially over the sea.

The climatology of the boundary layer is not well known. Plots of Taylor diagrams (characteristic diagrams of specific humidity against potential temperature) indicate that its top is well defined for more than half the time, at heights

below 850 mb. On these occasions it consists of a stable layer overlying an unstable or neutrally stratified one.

This situation can perhaps be modelled using sea temperature, temperature, humidity and wind at the top of the boundary layer, the wind, $\partial v/\partial t$, $\partial v/\partial x$ etc., and the density gradient in the stable layer. All but the surface temperature could be obtained from a large-scale numerical model.

The present treatments are empirical and messy but they are worth trying since they can, once their usefulness is established, be progressively improved as our knowledge of boundary layer processes increases.

It is assumed that the heating of the layer, through a surface flux, controls the depth of the layer. The heat flux does not affect the free atmosphere directly since the turbulent transfer is taken to vanish outside the boundary layer.

The height of the boundary layer is controlled by a combination of mean vertical velocity and by entrainment of "free" air into the turbulent boundary layer. The mean vertical velocity is made up of the frictionless component and a larger contribution due to the frictional convergence in the Ekman layer.

The treatment should be applicable to the oceanic boundary layer, though the effect of waves and of the different radiation input complicates it. Perhaps the boundary layer can be identified with the seasonal thermocline but winter conditions, away from the equator, may represent vertical convection over greater depths. These will have to be modelled in a different way.

THERMAL MICROSTRUCTURE IN THE SEA

Charles S. Cox

It is possible to measure the structure of temperature in the sea to a sufficiently fine scale (and with sufficient sensitivity) to resolve structure down to the smallest existing scales. Measurements have been made from a freely falling body which has an attached thermister probe. The falling velocity of the instrument is controlled by attached propellor-type blades which revolve in the manner of unpowered helicopter blades. It is possible to adjust the falling speed V over a range < 3 to > 10 cm/sec by altering the pitch of the blades.

Changing signals from the thermister are interpreted as changes of temperature with depth. Hence the vertical component of temperature gradient is measured. The "rise time" τ of the thermisters to a sudden change of temperature is 40 milliseconds. Hence the minimum resolvable scale of temperature fluctuation is a few millimeters. The noise level in the thermister and amplifier is equivalent to temperature fluctuations of less than 10^{-4} °C.

Measurements have been made in two locations: 1) Near San Diego where the ocean is 1 km deep and bottom very rough. Measurements were made while the instrument dropped between 600 and 700 m. 2) 1500 km offshore where the ocean is 5 km deep and the bottom smooth. Measurements were made between 600 and 1300 m.

In the near-shore water it was found that temperature decreases downwards in a series of nearly isothermal steps separated by zones of steep gradient. The steps are widely variable in thickness but average several meters thick. The gradient zones are occasionally as thin as one centimeter but usually consist of a close packed series of sharp gradients extending over a meter or less.

The measurements offshore occasionally show a stair-step structure but more usually the distinction between "isothermal" and sharp gradient zones is less clear.

The horizontal extent of structures has been studied by dropping a series of instruments behind a fast moving ship. At both locations similarity of larger temperature structures could be traced over horizontal distances of 200 m but not over 500 m.

Within the "isothermal" layers there are residual temperature fluctuations which vary in amplitude greatly from one layer to another. The spectrum of fluctuations within some layers is not inconsistent with that proposed by Batchelor for weak temperature variations carried by homogeneous isotropic turbulence. For example, in one measurement one can estimate the viscous cutoff at a wavenumber of 0.3 cm^{-1} while the conductive cutoff is at 3 cm^{-1} . The ratio of the two is appropriate for the Prandtl number of water.

If the temperature fluctuations are indeed isotropic in this layer, the mean square temperature gradient $\overline{\nabla\theta^2}$ will be three times the mean square vertical component. The eddy coefficient of thermal diffusivity can be estimated from the mean square gradient according to

$$K = \kappa \overline{\nabla\theta^2} / (\overline{d\theta/dz})^2$$

where κ is the molecular thermal diffusivity and $\overline{d\theta/dz}$ the mean temperature gradient. Two values of K estimated from two different layers at the off-shore station are $K = 270 \text{ cm}^2/\text{sec}$ and $9 \text{ cm}^2/\text{sec}$. The widely varying values suggests that turbulence is intermittent and localized in the ocean.

OBSERVATIONAL EVALUATION OF TOPOGRAPHIC EFFECTS ON THE GULF STREAM

Donald V. Hansen

The meandering path of the Gulf Stream as defined by the position of the 15°C isotherm at 200 meters depth between Cape Hatteras and the Grand Banks was delineated during 14 consecutive monthly cruises of the U.S. Coast and Geodetic Survey ship EXPLORER. The indicator isotherm could generally be crossed at least every six to ten kilometers to show the course of the Stream at comparatively high resolution between 74°W and about 58°W by means of a towed thermister system. The sequence of pathlines observed during the first nine months were all of a regular wavelike nature but with continuing variation. These observations are interpreted as a wavelike disturbance of mean wavelength 320 km which is advected eastward with a net phase speed of 8 cm/sec. The eastward increase of amplitude corresponds to an e -folding time on the order of 100 days. In subsequent months the pathlines' variations and their interpretation became more complicated in both space and time. Although the time-dependent behavior of the meander pattern is an obvious departure from their interpretation as a quasi-stationary topographic-beta wave, the propagation speed and growth rate are both much less than predicted by instability theories. Comparison of the position and curvature data for the observed Stream paths with the observed variations of depth and latitude along the Stream paths indicate that for reasonable Gulf Stream transport, momentum flux, and near-bottom current speed, the mean position of the Stream is consistent with the topographic-beta control hypothesis, but that depth variations are generally too small to force the observed curvature of meanders on the Stream, except intermittently in the region over the continental slope just east of Cape Hatteras. Comparison of the progressive wave interpretation of the meander patterns with buoyed current meter measurements and movement of detached cyclonic eddies near the Stream suggest

a relationship between the meanders and the meridional motion outside the Stream. The statistics of this meridional motion are similar to those of the well-known float measurements near Bermuda.

THE NUMERICAL SOLUTION OF VIBRATION PROBLEMS

Myrl C. Hendershott

The properties of a finite difference approximation to the Helmholtz problem specifying the harmonic motion of a rigid plate with fixed or free edges are examined regarding the convergence of the difference solution to the analytic one as the mesh spacing is decreased and regarding efficient solution of the difference equations. Uniform convergence is deferred to increasingly finer meshes as the analytic problem approaches resonance and the replacement of smooth boundaries by step-like ones having reentrant corners may result either in no convergence or in convergence to a limit different from the analytic solution. The method of sequential over-relaxation is a convergent iteration only when the plate is being driven at a frequency lower than the frequency of its grave free mode. Because the matrix of coefficients of the difference equations is sparse and has a very regular distribution of non-zero elements, an explicit inverse operator may be obtained by writing this matrix as a product of a lower triangular matrix and an upper triangular matrix. The availability of the inverse operator makes possible solution of certain very large problems by partitioning them into smaller sub-problems which are repeatedly solved in an iterative sequence (Parker, personal communication). Systems of difference equations which have similar eigenvalue spectra may be solved by the repeated application of the inverse of only one of the systems, thus avoiding recomputation of the inverse for every new system. Very high order difference formulae may be used in one direction without materially increasing the computational effort.

A NUMERICAL SOLUTION OF LAPLACE'S TIDAL EQUATIONS

Myrl C. Hendershott

Laplace's Tidal Equations are the linearized, inviscid, shallow-water approximation to the Navier-Stokes Equations for a homogeneous fluid envelope on a rotating sphere. Energy loss may be via bottom friction in shallow seas or via conversion to internal waves. At the boundaries, we may (i) require agreement of the computed field with observations, (ii) require flow parallel to the coast or (iii) define a complex impedance which parameterizes the mechanisms of energy dissipation at the coasts. In regions where the energy flow is nearly parallel to the coast, as it is in Kelvin waves, (i) may result in a good extrapolation to the deep water but will be of limited utility in regions where tidal energy is concentrated by a shoaling bottom and then diverted into small scale turbulence. If one is dealing directly with the tidal elevation, (ii) is numerically difficult. If (ii) is imposed, one must moreover include regions of energy dissipation within the computation and then use a computational grid of sufficient fineness to resolve details of the flow in these regions. (iii) is numerically just as difficult as (ii) but allows formulation of a meaningful problem in which bottom friction is present only in the boundary conditions.

A solution of Laplace's Tidal Equations for the M2 tide in the world ocean has been obtained using coastal observations as boundary conditions. The quality of the prediction is variable, being excellent in the Atlantic and Western Pacific but quite poor in the Indian Ocean and the Central Pacific. Further exploration of the manner in which individual boundary values influence the numerical solution is needed.

ON THE DISTRIBUTION OF SOME TRACERS IN THE OCEAN

William R. Holland

The distributions of certain conservative and non-conservative tracers such as temperature, salinity, oxygen, and radiocarbon have been used extensively to understand the patterns of motion in the sea. In this study we turn the problem around and ask what the distributions of some tracers would be if the velocity field and the coefficients of vertical and horizontal eddy diffusion are known. We shall take as our known velocity field that found by Bryan and Cox in a numerical study including both wind and thermal driving forces.

Two tracers have been treated so far, oxygen and radiocarbon. With various combinations of parameters and various assumptions about the decay, seven cases for the oxygen distribution and five for radiocarbon have been calculated. The results suggest the range of parameters of interest in the real ocean and show some promise of leading to good comparison with observations, at least in their gross features.

The experiments run so far should be regarded as a preliminary study to test the numerical technique and to determine its behavior for a variety of coefficients. The method of solution will be used further in future experiments to look into the salinity and temperature distributions as well as to explore further the cases of dissolved oxygen and radiocarbon.

SOME EFFECTS OF STRATIFICATION ON ROTATING FLUIDS

Ants Leetmaa

In the framework of a linear theory of rotating stratified fluids, some aspects of the effects of stratification on rotating fluids were investigated. In homogeneous Ekman layer theory, the stress on the surface of a fluid is balanced by a net transport to the right of the stress. Horizontal variations in the stress can thus cause convergencies or divergencies in this transport. These are of major importance in driving motions in homogeneous fluids. The introduction of stratification allows horizontal pressure gradients to be set up within the Ekman layers and these allow part of the stress to be directly transmitted to the body of the fluid. In the limit of strong stratification or small horizontal scales of variation in the stress, all the stress is transmitted to the body of the fluid, and the Ekman transport in the boundary layer disappears with the consequence that there are no convergencies or divergencies. Throughout the body of the fluid, the motion is Couette flow in which the geostrophic shear is balanced by a thermal wind. The results converge to homogeneous theory for weak stratification.

It is thought that these ideas might have some application to a theory of coastal upwelling. There, it is postulated, the horizontal density gradients in the upwelling zone are of primary importance in modifying the dynamics of Ekman layers near the coasts. As a model of a uniform wind blowing parallel to a coast, the solution to a problem in which the surface stress is of square wave form was examined. A boundary layer was found which for strong stratifications is thicker than the buoyancy layer. Later investigations have shown this thickness to be almost independent of the wavelength of the square wave. Further work is being carried out to determine the exact nature of this layer.

DOUBLE KELVIN WAVES

Michael S. Longuet-Higgins

It was shown in a recent paper (J.Fl.Mech. 31: 417) that a discontinuity in depth in a rotating shallow sea is capable of supporting a novel kind of wave motion. The wave energy is propagated along the discontinuity, and falls off exponentially to either side. Such trapped waves have been called "double Kelvin waves" or "seascarp waves". It was found that for any given wavelength, just one such wave motion is possible, and its period always exceeds one pendulum-day.

A discontinuity in the ocean depth is, however, a special and possibly uncommon situation. It is natural to inquire whether trapped waves exist when the bottom profile has other forms, for example when there is a continuous transition from one depth to another. One may further ask whether such trapped waves will tend to double Kelvin waves as the width of the transition zone is reduced to zero.

An investigation of certain special cases has already been made both by Rhines (1967) and by Buchwald and Adams (1968). These authors, however, assumed that the divergence of the wave motion (associated with a vertical displacement of the free surface) was negligible.

If the divergence is assumed to be negligible then it is not hard to see intuitively that waves will tend to be propagated along the sloping transition zone with the shallower water to their right, just as on a sloping plane bottom, or on a β -plane. Those vertical filaments of fluid displaced up the slope are shortened and so have a negative relative vorticity, and those displaced down the slope have a positive relative vorticity. The combination of alternate positive and negative vorticities results in a phase velocity to the west on a β -plane, or with shallow water to the right on a sloping bottom in the northern hemisphere.

Outside the transition zone the above mechanism ceases to act, and one might therefore expect some types of wave in which the energy was mainly limited to the transition zone.

However, when the divergence is taken into account some stretching of the vertical filaments of water is caused also by the vertical displacement of the free surface, as well as by the bottom slope. At first sight it is not clear which of these effects will predominate.

In the present paper we take the divergence of the wave motion fully into account, and investigate the possibility of trapped wave motions being associated with continuous depth profiles of a rather general kind. The depth h is assumed to be a function only of the coordinate x normal to the escarpment. Moreover h is assumed to be monotonic in x and to tend to uniform values at large distances from the escarpment on either side. The possibility of trapped waves in such a configuration is investigated on the basis of the linearized theory of waves in shallow water.

It is shown that the trapped waves always travel along the transition zone with the shallower water to their right in the northern hemisphere and to their left in the southern hemisphere. The wave period must always exceed a pendulum-day. The period is also bounded below by a quantity depending inversely on the maximum bottom gradient.

By allowing the width W of the transition zone to vary, asymptotic forms for the trapped modes are obtained, both as $W \rightarrow 0$ and as $W \rightarrow \infty$. In the limit as $W \rightarrow 0$ the depth becomes discontinuous, and it is shown that the lowest mode then becomes a double Kelvin wave (Longuet-Higgins, 1968) propagated along the discontinuity. The periods of the higher modes, on the other hand, all tend to infinity; these modes become steady currents.

Numerical calculations of the trapped modes are presented for two different laws of depth in the transition zone. It is found that as $W \rightarrow 0$ the lowest mode is insensitive to the form of the depth profile. Higher modes depend on the details of the profile. Hence the lowest mode is the most likely to be observed in the real ocean.

The dispersion relation is also investigated. It is shown that the group-velocity of all modes must change sign at some point in the range of wavenumbers, if the divergence is taken into account. When the divergence was neglected the lowest mode appeared to be exceptional, in that the group-velocity was always in the same direction. This anomaly is now removed.

In order to calculate the mean mass flux past a given recording station it is necessary to know more than the mean velocity in a vertical section. One must add an additional term - the "Stokes" velocity which depends also on the time and distance scales of the fluctuating currents. In typical circumstances, where the fluctuations are larger than the mean current, the Stokes velocity may dominate the mass transport, and lead to the mass transport being opposite in direction to the mean current.

Some general expressions are given for the Stokes velocity, and these are studied in detail for the particular case of double Kelvin waves. It is shown that in the regions of small bottom gradient the Stokes velocity is in the same direction as the phase velocity, but in the region of large bottom gradient the sign of the Stokes velocity is reversed. The mean Stokes velocity at the surface is in the direction of wave propagation. However, the mean total transport (integrated with respect to the depth) is in the opposite direction.

These conclusions are discussed in relation to some recent observations of currents near the continental shelf in the Northeast Atlantic.

ON WAVE BREAKING AND THE EQUILIBRIUM SPECTRUM OF WIND-GENERATED WAVES

Michael S. Longuet-Higgins

(1) Recent observations of the growth of sea waves under the action of wind have established that the rate of growth is several times greater than has yet been accounted for. A new mechanism of wave generation is proposed, based on the idea of a maser-like action of the short waves on the longer waves.

It is shown that when surface waves decay they impart their momentum to the surrounding fluid. Short waves are readily regenerated by shear instability. But a longer wave passing through shorter waves causes the short waves to steepen on the long-wave crests. Hence the short waves impart more of their momentum to the crests of the long waves, where the orbital motion of the long waves is in the direction of wave propagation. If the short waves are decaying only weakly (under the action of viscosity), the effect on the long waves is slight. But when the short waves are forced to decay strongly by breaking on the forward slopes of the long waves the gain of energy by the latter is greatly increased.

Calculations suggest that the mechanism is capable of imparting energy to sea waves at the rate indicated by observation.

(2) A theoretical calculation is made of the loss of energy by wave breaking in a random sea state in terms of the spectral density function. In the special case of the equilibrium spectrum $F(\sigma) = \alpha g^2 \sigma^{-5}$ the proportion ω of energy lost per mean wave cycle is found to be given by

$$\omega \doteq e^{-\frac{1}{8\alpha}}$$

irrespective of the low-frequency cut-off in the spectrum.

Assuming that in the equilibrium state the loss of energy by breaking is comparable to that supplied by the wind, one can estimate the constant α in terms of the drag coefficient of the wind on the sea surface. It is found that

$$\alpha \doteq -\frac{1}{8} / \log \left[1600 C^{3/2} (\rho_{air} / \rho_{water}) \right]$$

Taking a representative value of C one finds $\alpha \doteq 1.3 \times 10^{-2}$, which falls within the range of observed values of α . The above equation for α is extremely insensitive to the various assumptions made in the analysis.

There is some evidence, derived from observation, that α may not in fact be quite constant but may decrease slightly as the wave age ($g t/U$) or the non-dimensional fetch ($g x/U^2$) is increased. It is suggested that the drag coefficient may behave similarly.

THE EFFECT OF SURFACE TENSION ON THE LIMIT FORM OF WAVES

Robert L. Miller

Experimental studies of run-up of undular and fully developed bores were carried out recently, Miller, 1968. These brought out an interesting sequence of events during the beginning of transition from undular to fully developed bores at Froude numbers approx. 1.24. The first breaking of the crest was preceded by a surface pattern of ridges normal to the crest, which later coalesced to form a pattern of cell-like indentations. It appeared that the breaking process in its earliest stages might in part be a surface phenomenon. Accordingly comparisons were made of the sequence of early breaking with surface tension normal (approximately 73 dynes/cm at 20 C.) and surface tension reduced to approximately 40 dynes/cm. The results appeared to indicate that the limit angle of the crest was sharper for surface tension reduced, and that for surface tension normal, the wave form progressed about 20% further down channel before breaking.

Accordingly an examination of the literature was made for predicted limit crest angles for various wave types. These are indicated in Table 1. An

TABLE I
EFFECT OF SURFACE TENSION ON LIMITING CREST ANGLE*

WAVE TYPE	THEORY	EXPERIMENTAL RESULTS		% difference
		Surface tension 35-40 dynes/cm (average of 3 lowest)	Surface tension 72-74 dynes/cm	
PROGRESSIVE PERIODIC	120 (Stokes, Michell)	116 (40 dynes)	129	10%
		122 (53 dynes)		
STANDING WAVES (n = 6)	90 (Penney & Price, G.I. Taylor)	80 (35 dynes)	102	22%
		87 (28 dynes)		
CLAPOTIS	90 (analogous to standing wave)	80	101	21%
UNDULAR BORE (1st undulation)	120 (assumed similar to solitary)	114 ($\gamma_1 = 7.5\text{cm}$)	137	17%
		113 ($\gamma_1 = 10\text{cm}$)	134	15%
IMPULSE REGION (Solitary)	120 (McCowan)	113	129	13%
"CONFUSED SEA"	?	66	98	33%

* ALL WAVES DEEP WATER OR CONSTANT DEPTH BOTTOM

experimental procedure was developed using high speed motion picture photography and a number of wave types were examined for crest angle with surface tension normal and surface tension reduced. The results are given in Table 1.

Some indication of the variation in surface tension in natural waters has been acquired by a series of measurements, as shown in Table 2.

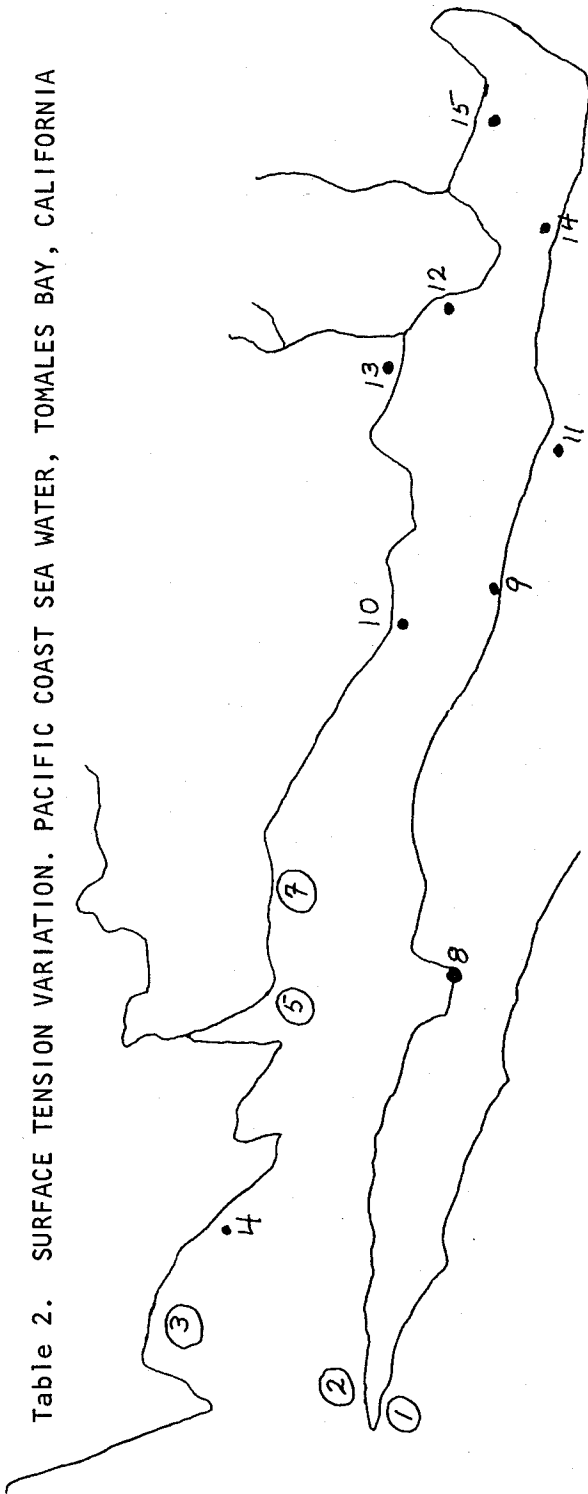
The study thus far should be considered as preliminary. It appears that a careful examination of the physical mechanisms operating just at the limit crest is needed. In addition, the method of reducing the surface tension by using a chemical additive, leaves doubt as to whether the results noted in Table 1 may not be due to surface effects of the type created by a soap film.

To resolve these difficulties, a small standing wave tank of the type described by G. I. Taylor will be used. Measurements will be attempted of 1) the accelerations at the limit crest angle, possibly to infer the "bursting" pressures, and 3) careful remeasurements of the gross limit crest angles. These experiments will be carried out for several frequencies. In addition, the experiments will be repeated for several homogeneous fluids other than water where the viscosity is low, and the surface tension is significantly lower than water. In this way the validity of the previous results for water with a surface tension reducing additive, can be checked.

Reference

Taylor, G.I. 1953. An experimental study of standing waves.
Proc.Roy.Soc.London, Ser.A, 218: 44-59.

Table 2. SURFACE TENSION VARIATION. PACIFIC COAST SEA WATER, TOMALES BAY, CALIFORNIA



SAMPLE NO.	DATE	SURFACE TENSION	REMARKS
1	1/8/68	70.4	open ocean coast
	1/12/68	74.0	
2 ₁	1/11/68	60.0	rapid channel flow
	1/12/68	67.0	
2 ₁₁	1/26/68	72.8* (heavy rain)	
	2/2/68	58.0	
2 ₁₁₁	3/11/68	72.8	
3 ₁	1/11/68	60.0	rapid channel flow
	1/12/68	70.0	
3 ₁₁	1/26/68	73.2* (heavy rain)	
3 ₁₁₁	3/11/68	62.3	
5 ₁	1/11/68	68.3	near creek entrance rapid flow
5 ₁₁	1/26/68	73.4* (heavy rain)	
5 ₁₁₁	3/11/68	61.2	
7 ₁	1/11/68	62.4	high organic content sewer outfall
7 ₁₁	1/23/68	73.4* (heavy rain)	
7 ₁₁₁	1/15/68	66.7	
	3/11/68	68.8	

All other samples approx. 72-74 dynes/cm with little variation.

MODELLING THERMALS WITH VORTEX RINGS

Bruce R. Morton

Atmospheric thermals consist of buoyant regimes of air ascending in a state of turbulent motion. Like all compact regions of fluid moving through like fluid environments, the mean motion of a thermal has the broad features of a vortex, and lies between the extremes of convective or ring vortices with mean vorticity and heat concentrated into a toroidal core, and diffusive or spheroidal vortices with both vorticity and heat distributed over the advancing fluid but with temperature maximum on the axis of propagation.

Although the gross properties of thermals and laboratory vortical (such as semi-angle of spread) appear to exhibit similarity there are likely to be departures from similarity in the turbulent structure. Thus as a convective vortex grows its core is stretched and can only expand with the vortex for a particular diffusivity, or a particular core geometry for given diffusivity. Sounders has observed that the relative size of visible surface elements in terms of the diameter of a thermal is a function of the Rayleigh number and hence differs in different thermals.

The principal properties of isolated convective and diffusive vortices in an extensive environment can be investigated using bulk equations obtained by integrating the continuity and Navier-Stokes equations over the environmental region. There proves to be no bulk mass conservation equation since the far-field disturbance due to a compact vortex is at most of doublet character, but simple equations are obtained for the impulse and buoyancy. In place of continuity a conservation equation is introduced for circulations, and this shows that the circulation is increased by buoyant generation and decreased by diffusion of

vorticity across the axis. Although a buoyant vortex ring suffers no change in circulation, its gross radius increases progressively with distance as positive vorticity is generated on its outer side and negative vorticity on the side nearer the axis. The system of bulk equations is completed by the Biot-Savart equation relating the propagation velocity and hence the gross displacement and time.

Typical features of vortex motion may be studied further by order-of-magnitude analysis of the equations to identify similarity structure, and three similarity regimes are identified for neutrally buoyant vortices with two for buoyant vortices. These solution types give useful information even though actual vortex behaviour will generally be intermediate in type. One class of neutral vortex is time-independent but all others develop with time and diffusive loss of mean vorticity is found to be specially important. In unsteady neutral vortices the circulation decreases steadily with time; but in buoyant vortices this diffusive loss is just balanced by buoyant generation and the circulation remains constant.

The treatment provides a basis for the formulation of vortex models, which may be developed approximately using the system of bulk equations.

NON-SIMILAR TURBULENT PLUMES

Bruce R. Morton

Entrainment models for buoyant plumes rising above steadily maintained sources of buoyancy in neutral or stably stratified environments have generally been based on similarity arguments, and have proved effective in the interpretation both of laboratory experiments and of observations at larger scale in the atmosphere. However, models in which entrainment is scaled in proportion to the local mean ascent velocity are based on a strict similarity relationship between the turbulent structure and mean flow, and hence cannot be expected to apply in source

neighbourhoods where the turbulent intensity (and entrainment of ambient fluid) may be expected to carry a strong imprint of the source. In such regions of developing flow the entrainment must be decoupled from the mean velocity field and scaled in terms of the local turbulent flow.

A modified entrainment model has been developed on the assumption of weak similarity in which the entrainment flux is related to the local Reynolds stress (averaged across the profile), and additional conservation equations are introduced for the flux of kinetic energy of fluctuating motion and for flux of temperature fluctuation intensity. The derivation of the new model has been based on an order-of-magnitude analysis of the full Navier-Stokes equations which provides an estimate of the errors involved in the neglect of various terms, and serves to identify the appropriate equations for the velocity and temperature fluctuation intensities. The analysis indicates that neglected terms in the momentum flux equation are likely to lead to errors amounting to ten per cent, and identifies a term representing the direct generation of turbulent (velocity fluctuation) intensity as a result of density fluctuations. The latter term is small in a hot jet, but is likely to play an important role in moist cumulus convection.

The model includes a parameter representing the effects of viscous dissipation and one for the conductive annihilation of temperature fluctuations. Neither of these can be deduced directly, and each has been evaluated by selecting appropriate levels of velocity and temperature fluctuation intensity in the asymptotic regime of flow far above the source; the values chosen prove to be of the anticipated order of magnitude.

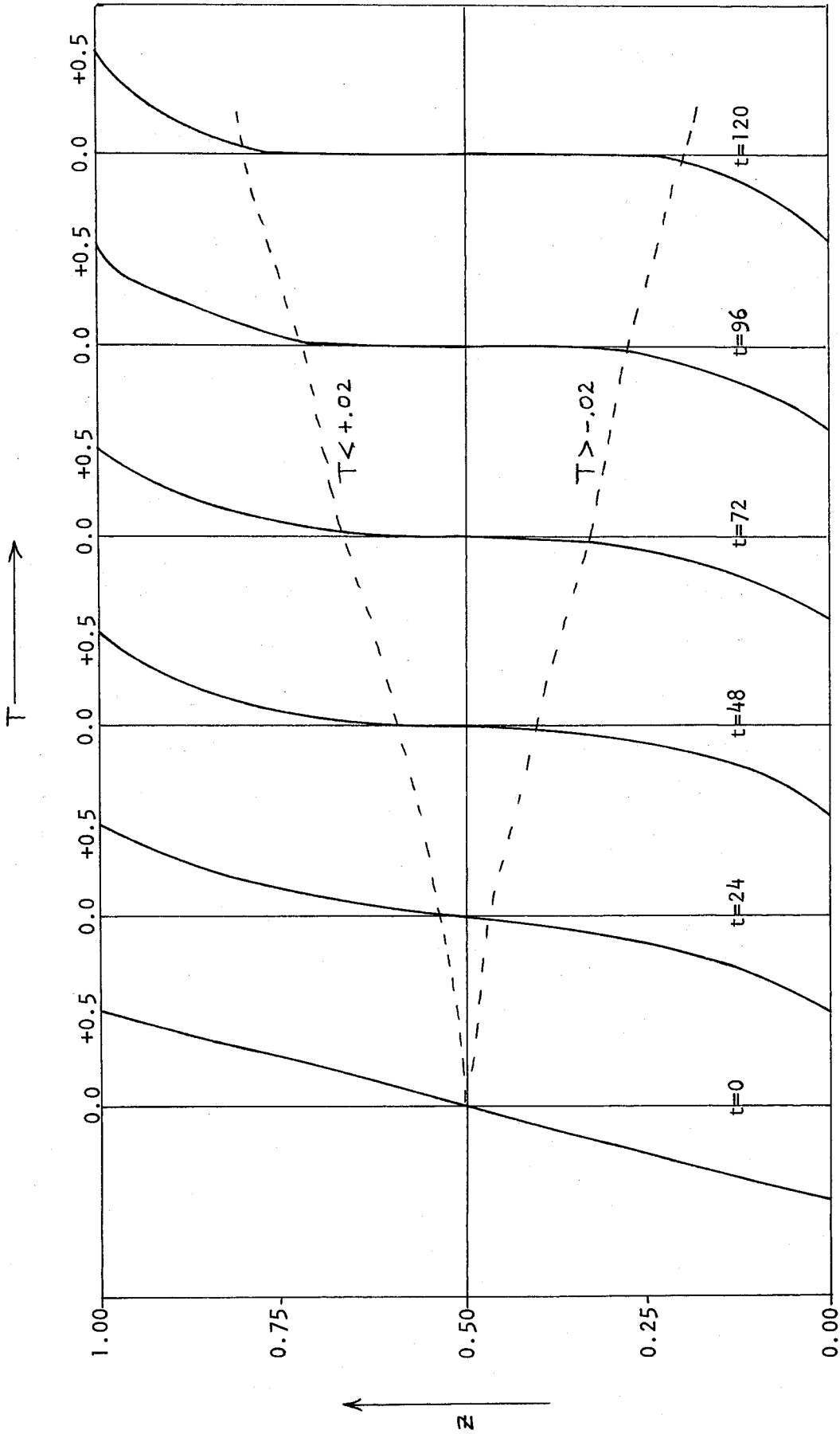
Numerical results have been obtained to illustrate the behaviour of a developing buoyant plume in a uniform environment and to determine the vertical extent of the development region. These show that for a wide range of input

conditions at source level the plume settles into an asymptotic state (and that this state is determined solely by the gross source conditions on momentum and buoyancy emissions) within a vertical ascent distance of between five and ten source diameters. In the development region the entrainment may depart appreciably from its asymptotic balance, and this departure may be expected to have a considerable influence in cumulus clouds where the release of latent heat depends in detail on the entrainment.

FINITE AMPLITUDE INTERNAL GRAVITY WAVES IN A CONTINUOUSLY STRATIFIED FLUID

Isidoro Orlanski and Kirk Bryan

In a fluid heated from above diffusive processes acting alone would tend to produce a uniform stratification. To determine the effect of mechanical stirring in modifying the density profile, the following problem is considered: a moving torque of the form $F_0 \sin(kx - \omega t) \cdot \sin \gamma z$ is applied to a body of fluid initially at rest. The frequency is chosen to be the resonant frequency of the internal wave of corresponding shape. The initial value problem is solved numerically using a 40×200 mesh, assuming cyclic continuity along the boundaries of a region, $0 < (kx, \gamma z) < 2\pi$. The self-interactions of the growing wave are also obtained analytically up to 3rd order in an expansion with respect to time. Agreement between theory and the numerical results is excellent for small amplitudes. Where the frequency is much less than the Brunt-Väisälä frequency, N_0 , and the Reynolds number is 10^4 , numerical experiments indicate breaking due to unstable folding of the density surfaces. Let Φ_{11} be the amplitude of the stream function for the primary mode.



Vertical temperature profiles corresponding to a point moving with the phase speed of the internal gravity wave. Time is given in units of $1/N_0$. Breaking occurs at $t = 45$ in this case.

Overtuning takes place when

$$1/Ri = \gamma^4 \bar{\Phi}_{||}^2 / N_o^2 \geq 2$$

The breaking is accompanied by the formation of a "step" structure in the vertical density profile.

It is concluded that in a continuously stratified fluid breaking due to convective overturning will take place for considerably smaller amplitudes than shear instability.

ENERGETICS OF THE GENERAL CIRCULATION

Melvin E. Stern

A theory of the main thermocline is advanced in which all of the work done by the wind on the mean Sverdrup circulation is used to increase the laterally available potential energy. The latter is transformed by large scale lateral motions and ultimately dissipated in small scale salt finger convection. Equating the rate of increase of mean potential energy by Ekman pumping to the rate of release due to salt fingers gives the following estimate of the typical lateral density gradient

$$\frac{1}{\rho_o} \nabla_2 \rho_m \sim \frac{f E^* S_o (1 - \gamma)}{\tau}$$

where E^* is the maximum evaporation rate, τ is the maximum wind stress,

S_o is the mean salinity of the ocean, f is the average coriolis parameter,

ρ_o is the average density, and $\gamma < 1$ is the ratio of the flux of thermal buoyancy (heat) to the flux of salt buoyancy.

A STABLE SALINITY GRADIENT HEATED FROM BELOW

J. Stewart Turner

When a linear stable salt gradient is heated strongly from below, it becomes unstable and convects in a series of layers, which form successively from the bottom up. In the past, there has been some doubt whether side-wall heating has affected the process of formation, and in particular the depth of the layers. The experiment discussed here has been designed to determine the relation between layer depth, h , initial salinity gradient, dS/dz , and heating rate H , by concentrating on the growth of the first layer, up till the time a second forms above it, and before spurious side-wall effects can be important.

It has been shown theoretically that the depth, and the temperature and salinity steps at the top of this first convecting layer, are all increasing as $t^{1/2}$. The way in which these quantities depend on dS/dz and H is also predicted, and the relations have been verified experimentally. Above the advancing turbulent front there is a diffusive boundary layer, whose depth is proportional to h and therefore also to $t^{1/2}$, so the whole shape of the temperature profile remains the same, but with an increasing scale. A stability criterion is developed to describe the breakdown of this region to form a second convecting layer. For large heating rates (in relation to dS/dz) a critical Rayleigh number based on the temperature distribution alone is relevant. The breakdown occurs in an oscillatory manner, consistent with the theoretical arguments which suggest overstability. The layer depth obtained in this way is proportional to $H^{3/4} (dS/dz)^{-1}$, and this form of dependence is confirmed by experiment. The numerical constant depends also on the molecular properties ν and χ and on the value of the critical Rayleigh number, which has so far not been determined theoretically for this time dependent case.

It is suggested that a similar argument could be used to discuss the formation of layers from a stable temperature gradient, when a flux of salt is provided at the top. In this case vertical transport can take place through the "salt finger" mechanism, but again a turbulent convecting layer will first form if the flux of salt is large enough. The front of this layer slows down in time, and the salinity and temperature step grows; the proposed criterion for the formation of a second layer is that the front velocity should become comparable with the individual finger velocity. This assumption leads to a prediction of layer depth of the same functional form as before, but with the roles of heat and salt just interchanged in the initial density gradient and buoyancy flux. Such a relation is not easy to test in the laboratory using heat and salt, because of the difficulty of maintaining large temperature gradients and the effects of side-wall cooling. Experiments carried out later in the summer with Melvin Stern have shown however that it is possible to produce convecting layers, separated by interfaces containing "fingers", using two diffusing substances (e.g. salt and sugar).

EFFECTS OF BOTTOM TOPOGRAPHY ON LARGE-SCALE OCEANIC FLOW

Pierre Welander

The effect of bottom topography has been studied for a two-layer frictional β -plane ocean driven by (a) a steady wind stress and (b) a concentrated source in the lower layer balanced by a slow upwelling through the interface.

In the model (a) the interface is a material surface, with no diffusive processes acting. The dynamics is linear (Ekman type). It turns out that interface stresses always are needed (except when the integrated wind-stress curl is non-zero). The circulation in the upper layer looks much the same as in the

one-layer solution with uniform depth derived by Stommel (1948). The motion in the lower layer is driven by interface stresses that are concentrated at the western side. When the lower layer is deep compared to the upper one, it can be shown that the motions in the lower layer are small, and the problems for the two layers decouple. One can first solve for the upper layer assuming the lower layer at rest, compute the interface stresses and then apply these to the lower layer. The lower layer problem then formally looks like the one-layer ocean, with a depth given by the distance from bottom to the (non-horizontal) interface, and with a wind stress driving in a narrow western strip. The lower layer circulation is confined to a recirculating boundary current when $\frac{\partial}{\partial y} (f/H)$, where f is the Coriolis parameter, H the lower layer depth and y a northward coordinate. If $\frac{\partial}{\partial y} (f/H) > 0$ there is a directly forced boundary current at the western side and a free boundary current at the eastern side, joined by an interior flow along f/H contours. If $\frac{\partial}{\partial y} (f/H) < 0$ changes sign in the basin these two solutions apply in their respective parts. Along the line $\frac{\partial}{\partial y} (f/H) = 0$ a free jet crosses over the basin.

In interior regions where closed f/H -contours occur, corresponding local gyres are added to the lower layer. In the North Atlantic such a region is found at the Azores and the theory predicts a local anticyclonic gyre in the deep water, but it is expected to be weak.

In the model (b) the lower layer shows the general poleward geostrophic drift and the equatorward deep boundary current, as predicted earlier by Stommel. It is shown how the calculation can be extended to basins of arbitrary geometry. The transport in the boundary currents can be simply related to the distribution function $A(f/H)$, where A is the horizontal area between a

standard contour (say, the equator), and an arbitrary contour for f/H . Different examples are worked out.

In particular, a model of the North Atlantic with realistic topography and deep water source in the northern part is considered. In this case a deep boundary current should run along the western edge, and another such current should run at the eastern slope of the Mid-Atlantic Ridge. These currents start both going southward from the northern end but as water leaks from the ridge current westward, the boundary current amplifies, while the ridge current diminishes. South of a certain latitude the ridge current will instead be fed by water flowing northward across the equator. Since the boundary and ridge currents are treated kinematically, and no dynamic model for them is used, the solution can only be sketched. Support can, however, be found from a simple laboratory experiment using a circular rotating basin with a ridge inserted. The geostrophic deep flow computed by Wüst and Defant for the 2000 db level in the North Atlantic shows also some general agreement with this proposed circulation.

References

- Welander, P. (1968) Wind-driven Circulation in One- and Two-layer Oceans of Variable Depth. Tellus 20: 1
- Welander, P. (1968) Effects of Planetary Topography on the Deep Sea Circulation; with an Application to the North Atlantic. Tech.Report No. 25 (ONR) and No. 28 (WB-ESSA). Mechanics Department, The Johns Hopkins University.

SEA LEVEL FLUCTUATIONS ACROSS THE STRAITS OF FLORIDA

Carl I. Wunsch and Donald V. Hansen

Sea level variations of less than inertial frequency are expected to be closely related to the surface current speed in highly geostrophic flows like the Florida Current. Power spectra and coherence were computed from simultaneous tide records at Miami, Florida and Cat Cay, Bahama Islands; at Key West, Florida and Havana, Cuba; and at Key West and Miami, Florida, as a measure of statistical variability of this contribution to the Gulf Stream. Diurnal and semi-diurnal tides account for over 80% of the power in sea level variations at all stations, and approximately half of the remaining power is in the annual variation. Power levels are generally higher on the left side of the current, but no significant power peaks were found between the annual and the tidal frequencies. Coherence is generally low between all stations, but where significant coherence is found, it occurs with essentially zero phase, indicating that sea level tends to rise or fall together on opposite sides of the Straits. Power in sea level difference is therefore intermediate between that at individual stations spanning the Straits. The zero-phase coherence suggests a common response to local weather events, so a multi-channel Wiener optimum filter was used to apply linear corrections for the effects of wind on sea level. Although very low coherence was found between atmospheric pressure and sea level, essentially an inverse barometer response was deduced for fluctuations of periods greater than ten days. At shorter periods the deduced response is direct barometric, for which we have no explanation. Coherence between vector wind and sea level was also low, so that removal of linear weather effects accomplished little reduction of total power, and does not materially influence coherence levels or phase. A sharp result is obscured by the general lack of coherence between

records, but major conclusions are that the Florida Current is very steady, r.m.s. modulation at all frequencies amounting to perhaps 10% of the mean, and that linear weather effects have only a minor influence on statistical sea level.

SUBTROPICAL COUNTERCURRENT

Kozo Yoshida

Recent observations appear to provide some convincing evidences of the presence of an eastward flow just to the north of 20°N in the western Pacific, which had first been suggested from the results of a theoretical computation of wind-driven transports (Yoshida et al., 1967 a, b) as well as of an earlier phase of the CSK (Cooperative Study of the Kuroshio) cruises. Although the detailed structure of this current-like feature is not yet known, an analysis of more recent data of CSK shows that the eastward flow, well separated from the Kuroshio, may appear to exhibit a form of multiple eastward streams of banded structure, with the most stable stream axis along latitudes between 21°N and 24°N .

Our earlier prediction from a wind-driven model was for the eastward transports associated with a singularity (a trough near the maximum of the negative wind stress curl) in the windstress field near the boundary between the Westerlies and the Trades. The origin of this singularity is, if at all real, suspected to be in the quadratic (or nonlinear) law of the wind stress function. If this interpretation may be valid despite the uncertainties in the computed values of the wind stresses, we may be led to a possibility that the eastward current may not be a local but a global phenomenon. The computations from winds indicate its occurrence also in other parts of the oceans, somewhat similar to the north and south Equatorial Countercurrents. In fact, similar eastward flows have been

observed in the mid-Pacific regions from VITYAZ cruises during 1957-8 and from the cruises of the Trade Wind Zone Oceanography Pilot Study near Hawaii Islands (Seckel et al., 1968), and by Voorhis and Hersey (1964) in the Sargasso Sea of the Atlantic.

On the other hand, a possible explanation may not necessarily require this singularity in the wind stress field. Stommel suggests a possibility of constructing a simple model which may yield a geostrophic eastward flow at these latitudes by some mechanism due to an interaction between the Ekman drift and the thermal structure of the mixed layer. In this case, the Subtropical Counter-current might be suggested to be a manifestation of one of the very basic features of the ocean circulation. The wind stress singularities might incorporate as well with such a mechanism.

Although further evidences with more systematic observations should obviously be needed to establish the reality of the new current, this curious feature as obtained would deserve some attention in view of ocean circulation theories.

References

- Seckel, Gunter R. 1968 A time-sequence oceanographic investigation in the North Pacific Trade-Wind Zone.
Trans.Amer.Geophys.Union, 49(1): 377-387.
- Voorhis, A.D. and J.B.Hersey 1964 Oceanic thermal fronts in the Sargasso Sea.
J.Geophys.Res. 69(18): 3809-3814.
- Yoshida, Kozo and Toshiko Kidokoro 1967a A Subtropical Counter-current in the North Pacific - an eastward flow near the Subtropical Convergence.
J.Oceanogr.Soc.Japan 23(2): 88-91.
- Yoshida, Kozo and Toshiko Kidokoro 1967b Subtropical Countercurrent (II) - a prediction of eastward flows at lower subtropical latitudes.
J.Oceanogr.Soc.Japan 23(5): 231-246.

ON THEORETICAL MODELS OF THE THERMOHALINE CIRCULATION

George Veronis

The thermohaline circulation of the oceans is modelled in terms of geostrophic dynamics and a heat equation which incorporates all of the convective terms plus vertical diffusion. This model has been the subject of several theoretical inquiries in the past. The present paper discusses some of the general features contained in the formulation and then goes on to summarize the significant results which have been derived analytically in earlier studies. The mathematical problem is formulated in terms of the pressure (Needler, 1967) rather than Welander's (1959) integrated density function. This allows the retention of the barotropic part of the pressure and velocity fields. All of the known, analytical, similarity solutions of the model are then derived by the method proposed by Kozlov (1966) in which the differential equation in terms of the similarity variable is divided into two parts each of which is satisfied by a common solution. The inverse power law solution of Fofonoff (1962) and the exponential solution of Blandford (1965) are special cases of the two solutions which emerge from the present approach. Since Blandford's solution with diffusion exhibits a remarkable similarity to Welander's non-diffusive solution, the two are compared in order to determine the role of vertical diffusion. It is found that Welander's model can satisfy all of the surface boundary conditions that Blandford's diffusive model satisfies. If Welander's model is extended to include barotropic velocities at great depth, a deep upwelling velocity is present also in his model. Hence, vertical diffusion in Blandford's solution is relegated to a role of secondary importance. The generalization of Fofonoff's solution is found to be applicable only to cyclonic gyres. With data from selected

stations to determine the scale depth of the thermocline region the value of the vertical diffusion coefficient is found to lie between 0.15 and $2.0 \text{ cm}^2 \text{ sec}^{-1}$. The corresponding upwelling velocity at great depths is about 4 cm day^{-1} which is higher than the maximum value deduced by Stommel and Arons (1960). The general exponential solution of Needler which is also closely related to Welander's solution is used to determine the effect of variable bottom topography on wind-driven circulation. It turns out that the upwelling velocity beneath the thermocline replaces the Ekman suction velocity in the determination of the abyssal flow. Finally, a simple model including horizontal diffusion of heat only in the east-west direction is shown to introduce an additional physical process which can balance vertical upwelling of cold water.